



Norwegian University of  
Science and Technology

# Wellhead platform subjected to accidental loads

**Anders Salberg Strand**

Marine Technology

Submission date: June 2016

Supervisor: Jørgen Amdahl, IMT

Norwegian University of Science and Technology  
Department of Marine Technology



# Preface

The Master thesis is written in the final semester of the Master's Degree program in Marine Technology at Norwegian University of Science and Technology (NTNU) and accounts for 30 credits. This thesis was inspired by having previously worked for Kvaerner, and their exciting new concept "Subsea On a Stick"'s media coverage. Having touched upon accidental actions in courses like "TMR4205 Buckling and Collapse of Marine Structures in steel and aluminium" and "TMR4195 Design of Offshore Structures" the interest was sparked.

The intention was early on to collaborate with Kvaerner, and hopefully use their existing structural design. It turned out that in such an early phase, still competing for contracts, they could not release any structural models, which is easy to understand. But though no official collaboration has been undertaken, tips and guidance was provided by Trond Granli in Kvaerner Jacket Technology Trondheim.

Automation of simulations has been of interest since a project work in the mentioned course TMR4195, where pushover analyses of a jacket structure were run for a large number of sea states and extreme waves. Seemingly, an extreme effectiveness can be obtained by the correct use of scripting techniques. This has, however taken up large amounts of time, and several weeks were spent understanding syntax and getting the programs to run. The result was a bad disposition of time, and too little time left over for evaluating the actual analysis results.

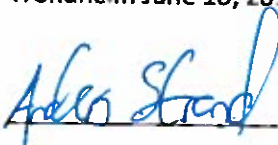
The work has been challenging and educational, as I had little to no knowledge of the fire process or background designing against fire scenarios. The learning outcome has been both theoretical in the field of fire and accidental actions, but just as much in acquiring knowledge about current practices and regulations.

I would like to thank my supervisor, Professor Jørgen Amdahl, for his guidance and patience. His ability to change thought process and give precise advice as soon as a confused student knocks on the door is astonishing.

Furthermore, I would like to thank Trond Granli in Kvaerner Jacket Technology, for tips and pointers on how to proceed throughout the semester. It has been a great motivation to get a small glimpse in to the offshore design industry.

Finally, I would like to thank my friend Andreas Andersen, for several hours of programming help and insightful discussions.

Trondheim June 10, 2016

A handwritten signature in blue ink that reads "Anders Strand". The signature is written in a cursive style and is positioned above a horizontal line.

Anders Strand



## MASTER THESIS 2016

for

Stud. Techn. Anders Strand

### **Fire resistance of unmanned wellhead platforms** *Brannmotstand til ubemannede brønnhodeplattformer*

Accidental fires are events with a severe consequence potential, demonstrated e.g. by the Piper Alpha catastrophe in 1986. Adequate design against fires is therefore essential in the offshore industry as well as in many other industrial sectors. Previously, fire design was based upon several assumptions, often of simplistic nature. Standard fire scenarios were typically used (standard temperature-time curves or heat flux histories), and the temperature evolution and the resistance of the load-carrying members with and without passive fire protection (PFP) were estimated by means of standard tables. Neither the fire nor the heat transfer and the mechanical response reflected the real processes in a fire. Consequently, the design often was overly conservative, notably with respect to excessive application of PFP.

In the period 1990-2002 SINTEF conducted a joint industry project entitled *Integrated Analysis of Steel and Aluminium Structures Exposed to Fire*. The objectives of the project were to develop modern and advanced tools for fire design, in which the governing phenomena were modelled by fundamental descriptions of the physical processes. This applied to all three steps of fire analysis and design: *the fire process, the heat transfer and the mechanical response*. The software KAMELEON FIREX (KFX) was developed to simulate the combustion process based on the actual amount of combustible material, air supply, ventilation etc. Based on the temperature- and flux histories obtained in the simulation of the fire process, the heat transfer into the structures was simulated in a time domain finite element software FAHTS. Any PFP was taken into account in an efficient manner. Finally, on the basis of the temperature evolution in the structure, the computer program USFOS was used to simulate degradation of the resistance of the structural. A key issue in the project was to develop efficient interfaces between the three analysis steps with respect to data transfer as well as finite element modelling. From year 2000 on the integrated program system has been used successfully in offshore projects around the world and has become more or less an industry standard. The experience from these projects is that significant cost savings with respect to PFP is often achievable without compromising fire safety. The improved prediction accuracy of the tools as well as more considerations of more realistic fire scenarios have sparked the development of efficient emergency shut down systems. Sometimes this allows leaving primary structural members unprotected.

1. Review of principles for analysis of the fire resistance of platforms. Reference is given to e.g. FABIG Technical Note 11 and draft revision DNV-GL RPC204 and Eurocode 3. The main principles for fire load and heat transfer and mechanical response shall be described.



2. A generic wellhead jacket platform shall be selected for the case study. The functional load case shall be described in some detail. Establish a finite element model of the jacket including relevant topside structures for FAHTS and USFOS analysis. If a relevant structure is not provided, one should be designed. Check that the structural utilisation is reasonable when exposed to functional loads only. Perform pushdown analyses in intact condition. The failure mode shall be described.
3. Establish characteristic fire scenarios for the platform. Perform modelling of the fires using available fire load modelling options in FAHTS. Conduct transient heat transfer analysis and generate equivalent fire loads for the beam elements in the USFOS model.
4. Perform mechanical response analysis with USFOS. The analyses shall be conducted in the load domain, the temperature domain and in the load-temperature domain for a few selected cases. The results obtained with the different methods shall be compared. Provided that the pushdown method is found to be sufficiently accurate, most analyses shall be conducted in the load domain using the so-called pushdown method. To the extent needed fire analysis of local models of connections shall be performed.
5. The need for passive fire protection (PFP) shall be investigated.
6. Conclusions and recommendations for further work

The work scope may prove to be larger than initially anticipated. Subject to approval from the supervisors, topics may be deleted from the list above or reduced in extent.

In the thesis the candidate shall present her personal contribution to the resolution of problems within the scope of the thesis work.

Theories and conclusions should be based on mathematical derivations and/or logic reasoning identifying the various steps in the deduction.

The candidate should utilise the existing possibilities for obtaining relevant literature.

#### **Thesis format**

The thesis should be organised in a rational manner to give a clear exposition of results, assessments, and conclusions. The text should be brief and to the point, with a clear language. Telegraphic language should be avoided.

The thesis shall contain the following elements: A text defining the scope, preface, list of contents, summary, main body of thesis, conclusions with recommendations for further work, list of symbols and acronyms, references and (optional) appendices. All figures, tables and equations shall be numerated.

The supervisors may require that the candidate, in an early stage of the work, presents a written plan for the completion of the work. The plan should include a budget for the use of computer and laboratory resources which will be charged to the department. Overruns shall be reported to the supervisors.

The original contribution of the candidate and material taken from other sources shall be clearly defined. Work from other sources shall be properly referenced using an acknowledged referencing system.

The report shall be submitted in two copies:

- Signed by the candidate
- The text defining the scope included
- In bound volume(s)
- Drawings and/or computer prints which cannot be bound should be organised in a separate folder.
- The report shall also be submitted in pdf format along with essential input files for computer analysis, spreadsheets, MATLAB files etc in digital format.

### **Ownership**

NTNU has according to the present rules the ownership of the thesis. Any use of the thesis has to be approved by NTNU (or external partner when this applies). The department has the right to use the thesis as if the work was carried out by a NTNU employee, if nothing else has been agreed in advance.

### **Thesis supervisors**

Prof. Jørgen Amdahl

Contact person at Kværner: Trond Granli

**Deadline: June 10. 2016**

Trondheim, January 15, 2015



Jørgen Amdahl

# Abstract

Cost reduction in the oil and gas industry forces new and innovative solutions. Unmanned wellhead platforms are alternative solutions for developing small fields which would normally be developed with subsea wellheads. For an installation to be approved to operate on the Norwegian Continental Shelf, it must be designed against accidental actions such as fire.

Current rules regarding design against fire loads has been reviewed, showing examples of heat transfer hand calculations, as well as material's strength degradation as function of temperature.

A generic wellhead platform has been designed, based on comparable structures, and simple hand calculations to have a reasonable model to work with. Conservativeness has been applied to end up with a tough structure and reduce the need for passive fire protection. The structure was tested against normal operational loads and were proven to have more than sufficient resistance.

Operational-, variable maintenance- and accidental loads has been established with help from Trond Granli in Kværner. Characteristic fire scenarios were provided and cases set up.

A shell script has been adapted for use on the heat transfer and response simulations. Trouble with multi- threading simulations prevented it from functioning perfectly, but it worked for single- threading.

A large amount of simulations has been run, resulting in the conclusion that loads relating to wireline well intervention operations in combination with moderate jet fires is survived by the structure. Reserve strength ratios in the range above 4.5 were exhibited. The case of accidental jack- up rig cantilever collapse was shown to be tolerated, and the case involving a large jet fire inside the platform also survived the duration of the characteristic fire scenario. But further simulations are recommended to confirm. Temperature- domain simulations has been run to validate a few of the pushdown simulations, with promising results.

A good pool fire model was not established, but was simulated with the standard hydrocarbon temperature curve. The results showed adequately strength after the duration of the fire.

# Sammendrag

Kostnadsreduksjoner i olje og gass- industrien tvinger fram nye og innovative løsninger. Ubemannede brønnhodeplattformer er et alternativ små feltutbygginger som ellers har måttet ty til dyre undervannsløsninger for brønnhoder. For at en installasjon skal få lov til å operere på den norske kontinentalsokkelen, må den beviselig være dimensjonert for å motstå uhellslaster som brann.

Gjeldende regler og standardverk om dimensjonering mot brannlaster har blitt gjennomgått, og eksempler på forenklede varmeoverføringsmodeller så vel som tap av bæreevne grunnet høye temperaturer er vist fram.

En generisk brønnhodeplattform har blitt dimensjonert, basert på sammenlignbare installasjoner samt forenklede håndberegningsetoder. Dette for å ha en rimelig virkelighetsnær struktur å jobbe med. Det har blitt lagt vekt på at strukturen skal ha robuste deler for å minske behovt av pasiv brannbeskyttelse. Plattformen ble utsatt for operasjonslaster og hadde beviselig mer enn høy nok kapasitet.

Operasjons-, variable vedlikeholds-, og ulykkeslaster har blitt definert med hjelp fra Trond Granli i Kværner. Karakteristiske brannlaster ble gitt, og lastkombinasjoner ble satt opp.

Et shell- program har blitt tilpasset bruk for simulering av varmeoverføring of strukturanalyser. Programmet hadde ikke optimal funksjon, da analyser ikke kunne kjøres i parallell, men med bruk av en prosessorkjerne av gangen fungerte programmet fint.

Store mengder simuleringer har blitt gjort, og de viktigste resultatene er gjennomgått. Laster tilknyttet brønnintervensjonsutstyr sammen med varmelaster fra en jetflamme ble overlevd med god margin. Laster opp over 4.5 ganger designlastene ble bært før sammenbrudd. Ulykkeslasta der et utkraget borretårn siger ned og hviler på dekk, ble tolerert uten store permanente skader. Denne ulykkeslasta i kombinasjon med en kraftig jetflamme ble også overlevd i den påkrevde tidsmengden, men simuleringer med videre tidssteg trengs for å bekrefte resultatet. Sammenligning av resultat fra simuleringer i lastdomenet og temperaturdomenet viste at lastdomenet predikerer forløpet godt.

En god model for sump-branner ble ikke etablert, men heller modellert ved hjelp av standard hydrokarbon temperaturkurve. Strukturen viste god kapasitet også i det tilfellet.

# Contents

<b>1</b>	<b>Introduction</b>	<b>1</b>
<b>2</b>	<b>Current design principles</b>	<b>3</b>
2.1	Limit state design . . . . .	3
2.2	DNV-GL Racommended practice . . . . .	6
2.2.1	General. . . . .	6
2.2.2	Combustion process . . . . .	7
2.2.3	Heat transfer analysis . . . . .	7
2.2.4	Mechanical response . . . . .	8
2.2.5	Thermal expansion . . . . .	9
2.2.6	Analysis methods . . . . .	10
2.2.7	Material modelling . . . . .	10
2.2.8	Cross-sectional capacities . . . . .	10
2.2.9	Equivalent imperfections . . . . .	10
2.2.10	Local cross sectional buckling . . . . .	11
2.2.11	Ductility limits . . . . .	11
2.2.12	Capacity of connections . . . . .	12
2.3	NORSOK . . . . .	13
2.4	Eurocode 3 1.2 . . . . .	15
2.4.1	Material properties . . . . .	15
2.4.2	Heat transfer . . . . .	19
2.4.3	Structural fire design . . . . .	21
2.5	FABIG technical note 11 . . . . .	23
2.5.1	Section 2, Estimating hydrocarbon fire loads . . . . .	23
2.5.2	Heat transfer and temperature development . . . . .	29
<b>3</b>	<b>Non-Linear Finite Element Method</b>	<b>35</b>
3.1	Problem formulation . . . . .	35
3.1.1	Geometrical non-linearity . . . . .	36
3.1.2	Material non-linearity . . . . .	38
3.1.3	Non-linearity associated to boundary conditions . . . . .	40
3.2	Solution procedures . . . . .	40
3.2.1	Load incremental methods . . . . .	41
3.2.2	Iterative methods . . . . .	42
3.2.3	Arc Length Methods . . . . .	43
<b>4</b>	<b>Simulation tools</b>	<b>45</b>

4.1	FAHTS . . . . .	45
4.1.1	Finite element approach . . . . .	46
4.1.2	Time domain integration . . . . .	48
4.1.3	Heat sources . . . . .	50
4.2	USFOS . . . . .	51
4.2.1	Beam element formulation . . . . .	52
4.2.2	Plasticity . . . . .	54
4.2.3	Load control . . . . .	56
<b>5</b>	<b>Early design of unmanned wellhead platform</b>	<b>57</b>
5.1	Comparable structures . . . . .	57
5.2	Load specification . . . . .	58
5.2.1	Functional loads . . . . .	58
5.2.2	Heat loads . . . . .	59
5.3	Quick dimensioning . . . . .	59
5.3.1	Deck plates . . . . .	60
5.3.2	Stiffeners . . . . .	63
5.3.3	Deck beams . . . . .	66
5.3.4	Girders . . . . .	67
5.3.5	Columns . . . . .	68
5.3.6	Dimensioning summary . . . . .	69
5.4	Finite element model . . . . .	70
5.4.1	Member groups . . . . .	71
5.4.2	Weight . . . . .	71
5.4.3	Operational condition . . . . .	72
<b>6</b>	<b>Simulations</b>	<b>75</b>
6.1	Automation . . . . .	76
6.1.1	Matlab input generator . . . . .	76
6.1.2	Bash script . . . . .	78
6.2	Cantilever collapse . . . . .	81
6.2.1	Fire on board jack- up rig . . . . .	82
6.2.2	Fire originating on topside . . . . .	84
6.3	Wireline operation . . . . .	92
6.3.1	Cold Pushdown Analysis . . . . .	93
6.3.2	250 $kW/m^2$ Jet Fire . . . . .	94
6.3.3	Pool fire . . . . .	99
6.4	Simulation summary . . . . .	100
<b>7</b>	<b>Conclusion</b>	<b>103</b>
<b>8</b>	<b>Further work</b>	<b>105</b>
<b>A</b>	<b>Web height of bulb flat steel</b>	<b>III</b>
<b>B</b>	<b>Girder grillage model</b>	<b>V</b>

<b>C</b>	<b>Matlab input generator</b>	<b>XI</b>
<b>D</b>	<b>Bash shell script</b>	<b>XVII</b>
<b>E</b>	<b>Simulation control files</b>	<b>XXV</b>

# List of Figures

2.1	Load( $f_S$ ) and resistance( $f_R$ ) probability density function . . . . .	3
2.2	(USFOSweb 2014). Degradation of ultimate resistance versus fire time(Pushdown analysis) . . . . .	9
2.3	(N-004 2013), partial safety to be used in (EC3-1-2 2005) . . . . .	13
2.4	(N-001 2012), table 1. Partial safety factors . . . . .	13
2.5	(N-003 2007), table 1. Variable deck actions . . . . .	14
2.6	(EC3-1-2 2005), figure 3.1. Stress-strain relationship for carbon steel at elevated temperatures . . . . .	16
2.7	(EC3-1-2 2005), table 3.1. Reduction factors . . . . .	17
2.8	(EC3-1-2 2005), figure 3.2. Reduction factors for the stress strain relationship of carbon steel at elevated temperatures . . . . .	17
2.9	(EC3-1-2 2005), figure 3.3. Relative thermal elongation of carbon steel as function of temperature . . . . .	18
2.10	(EC3-1-2 2005), figure 3.4. Specific heat of carbon steel as function of temperature . . . . .	19
2.11	(EC3-1-2 2005), figure 3.4. Thermal conductivity of carbon steel as function of temperature . . . . .	19
2.12	HC-fire curve. . . . .	21
2.13	(FABIG 2010), figure 2.2. Jet flame fire length . . . . .	24
2.14	(FABIG 2010), Table 2.2. Tabulated gas jet fire guidance . . . . .	25
2.15	(FABIG 2010), Table 2.3. Tabulated two-phase jet fire guidance . . . . .	26
2.16	(FABIG 2010), Table 2.4. Mass burning rates . . . . .	27
2.17	(FABIG 2010), figure 2.12. Model average SEP . . . . .	28
2.18	(FABIG 2010), table 2.6. Parameters for HC pool fires on land . . . . .	29
2.19	Derived multiple point source model . . . . .	31
2.20	Temperature development of engulfed object in jet fire . . . . .	32
2.21	Temperature development of engulfed object in a small pool fire . . . . .	33
3.1	Two-beam arch. Figure from Moan (2003) . . . . .	36
3.2	Equilibrium consideration. Moan (2003) . . . . .	37
3.3	Updating reference system. Moan (2003) . . . . .	37
3.4	Equilibrium function (rough sketch). Reproduced from Moan (2003) . . . . .	38
3.5	Idealized elasto-plastic yield criterion. (Moan 2003) . . . . .	39
3.6	Isotropic vs. kinematic hardening. (Moan 2003) . . . . .	39
3.7	Load incremental (Euler-Cauchy) method. (Moan 2003) . . . . .	41
3.8	Load incremental method with equilibrium correction. Moan (2003) . . . . .	42
3.9	Sketched illustration of the Newton-Raphson algorithm. . . . .	42



3.10	Pure Newton-Raphson procedure. (Moan 2003)	43
3.11	N - R without updating K. (Moan 2003)	43
3.12	USFOS arc length illustration. Skallerud & Amdahl (2005)	44
4.1	(SINTEF 1994). 2D heat transfer problem	47
4.2	(SINTEF 1994). Linear approximation of temperature in time domain	49
4.3	(SINTEF 1994). Line source model in FAHTS	51
4.4	Beam loaded with end moments and axial compressive force.	52
4.5	$\phi$ -functions expressed with normalized axial force. Amdahl (2005)	53
4.6	Example sketch of a yield surface. (Amdahl 2005)	55
5.1	(Lorentzen 2015). Early concept sketch of Kværner's UWP	58
5.2	Deck layout of one quadrant.	60
5.3	Beam theory figures	61
5.4	Post buckling stress distribution in a inter-stiffener plate field. (Amdahl 2005)	62
5.5	Bulb flat stiffener with plate flange	63
5.6	Assumed shear area of bulb flat	64
5.7	Checkpoints for stiffener stresses (upside down)	64
5.8	Moment diagram of deck beam. Assumed clamped at the inner girder due to symmetric load	66
5.9	From appendix B. Deck girder modelled as grillage system	68
5.10	Viewed from above	70
5.11	Viewed from "south side"	70
5.12	Viewed from "east side"	70
5.13	Tubular members in the topside, vertical column extended	73
6.1	FAHTS parameter data file generated by matlab program	77
6.2	USOFS parameter data file generated by matlab program	77
6.3	Load data for wireline distributed load	78
6.4	Group data for beams subjected to wireline load	78
6.5	Flow chart for matlab input generator	78
6.6	Flow chart for the shell script	80
6.7	Cantilever weight modelled as point loads	81
6.8	von Mises Stresses. JUR cantilever load. Load factor 1	82
6.9	Axial force in central column	83
6.10	Axial force in main column	83
6.11	Vertical displacement of central node, topside deck	83
6.12	Cold cantilever collapse. Contour lines. Buckling main column highlighted	84
6.13	Initial fire case. "Outer" position	85
6.14	Fire affecting the internal columns. "Inner" position	85
6.15	Temperature plot after the full 5 minute duration of the 350 [kW/m <sup>2</sup> ] fire	86
6.16	Updated yield strength for beam elements. JUR collapse "outer" case	87
6.17	Vertical displacement of topside deck central node. "Outer" position	88

6.18	Vertical displacement of heated girder. "Outer" position . . . . .	88
6.19	Bending moment in cellar deck girder. "Outer" position . . . . .	88
6.20	Vertical displacement of central topside node. "Outer" position . . . . .	88
6.21	Vertical displacement, last time step, temperature domain simulation.	89
6.22	Updated yield strength for beam elements. JUR collapse "inner" case	90
6.23	Fractured beams on mezzanine deck. "Inner" position . . . . .	90
6.24	Vertical displacement of fractured beam. "Inner" position . . . . .	91
6.25	Vertical displacement of central topside node. "Inner" position . . . . .	91
6.26	Vertical displacement in temperature domain of fractured beam. "Inner" position . . . . .	91
6.27	Different load configurations . . . . .	92
6.28	Wireline load configuration . . . . .	92
6.29	Buckling of diagonal truss member. Wireline load . . . . .	93
6.30	Vertical displacement of topside girder midpoint . . . . .	93
6.31	Vertical displacements before ultimate collapse shown as contour curves	93
6.32	Various flame directions. 108°, 45° and 342° in succession . . . . .	94
6.33	Low incident fire elevation. Displacement of topside girder . . . . .	95
6.34	Axial force curve for main column . . . . .	95
6.35	Vertical displacement of topside girder . . . . .	95
6.36	Vertical displacement, top of the main east column . . . . .	96
6.37	Collapse mechanism after column buckling . . . . .	97
6.38	Fracture due to reduced material strength . . . . .	97
6.39	Vertical displacement, top of the main east column during fracture . . . . .	98
6.40	Small HC fire . . . . .	99
6.41	Failure mode, 30 minutes local HC-fire . . . . .	100
6.42	Vertical displacement of topside girder node . . . . .	100

# List of Tables

5.1	Functional and accidental load specification . . . . .	59
5.2	Specified characteristic fire scenarios . . . . .	59
5.3	Stresses in deck plates due to distributed loads. . . . .	62
5.4	Section- and load data for the plate-stiffener system . . . . .	65
5.5	Bending and shear stresses in the plate-stiffener system [MPa] . . . . .	65
5.6	Stiffener and plate utilization table . . . . .	66
5.7	Deck beam utilization table . . . . .	67
5.8	Girder utilization table . . . . .	67
5.9	Column utilization table . . . . .	69
5.10	Chosen main structural components . . . . .	69
5.11	FE-model structural components . . . . .	71
5.12	Weight of the different structural components [tonn] . . . . .	72

## Abbreviations

ALS	Accidental Limit State
CFD	Computational Fluid Dynamics
FEA	Finite Element Analysis
FEM	Finite Element Method
FLS	Fatigue Limit State
GUI	Graphical User Interface
PFP	Passive Fire Protection
SEP	Surface Emissive Power
SLS	Servicability Limit State
ULS	Ultimate Limit State

# List of Symbols

Roman

$b$	$[m]$	distance from object to source
$c_p, c_a$	$[J/kgK]$	Specific heat
$c/t$		Width to thickness ratio, cross section
$d$	$[m]$	normal from object to jet fire
$d$	$[m]$	Diameter
$e_i$	$[kW/m]$	point source radiative power
$e^*$	$[m]$	Amplitude of initial imperfection
$f_y$	$[MPa]$	Yield strength
$h$	$[kW/m^{-2}K^{-1}]$	Convective heat transfer coefficient
$h$	$[m]$	height
$\dot{h}_{net}$	$[W/m^2]$	Net heat flux
$\dot{h}_{net,c}$	$[W/m^2]$	Net convective heat flux
$\dot{h}_{net,r}$	$[W/m^2]$	Net radiative heat flux
$i$	$[m]$	Radius of gyration
<b>k</b>		Conductivity matrix
$k$	$[W/mK]$	Conduction coefficient
$k$	$[m^{-1}]$	Measure of obtaining max burning rate
$k_{E,\theta}$		Stiffness reduction factor
$k_s h$		Correction factor for shadow effect
$k_{x,y,z}$	$[W/mK]$	Thermal conductivities in x,y and z directions
$\hat{k}_{y,\theta}$		Effective yield strength reduction factor
$l$	$[m]$	member length
<b>m</b>		Mass matrix
$\dot{m}_b$	$kg/s$	mass release rate
$\dot{m}_b$	$kg/m^2s$	Finite mass burning rate
$\dot{m}_\infty$	$kg/m^2s$	Maximum mass burning rate
$q$	$[kW/m^2]$	Radiation received
$q_a$	$[kW/m^2]$	Total heat absorbed by object per area
$q_c$	$[kW/m^2]$	Convective heat absorbed per area
$q_{loss}$	$kW/m^2$	Heat loss
$q_r$	$[kW/m^2]$	Radiative heat absorbed per area
$t_{fi,d}$	$[min]$	Dimensioning fire duration
$t_{fi,req}$	$[min]$	Required fire duration time
$\bar{q}$	$W/m^2$	prescribed heat flux
$q$	$[N/m]$	Line load
$u, v, w$	$[m]$	Diplacements
$v, \bar{v}$		Arbitrary functions
$w_i, w, j$		Weight functions
$z_0$	$[m]$	Distance, neutral axis to outer fibre

$A$	$[m^2]$	Cross-sectional area
$A, B$		General functions
$A_m$	$[m^2/m]$	Surface area per unit length
$A_{tot,pl,s}$	$[m^2]$	Cross section area of total, plate, stiffener
$E$	$[MPa]$	Elastic modulus
$E_{fi,d,t}$		Design effect of action at time t
$E_i$	$[kW]$	Total energy emittance
$E_t$	$[MPa]$	Tangential stiffness modulus
$F$		Fraction of heat radiated
$I_{tot,pl,s}$	$[m^4]$	Moment of inertia of total,plate,stiffener
$K(r)$		Stiffness at load increment r
$L$	$[m]$	Jet fire length
$M_{fi,Rd}$	$[Nm]$	Design bending resistance, elevated temperature
$M_p$	$[nm]$	Plastic bending moment capacity
$M_{Rd}$	$[N/m]$	Design bending moment, normal temperature
$M_{x,y,z}$	$[Nm]$	Bending moment about x,y,z-axis
$N$	$[N]$	Axial force
$\mathbf{N}$		Shape function vector
$N_p$	$[N]$	Plastic axial force capacity
$N a_{tot,pl,s}$	$[m]$	Neutral axis z-coordinate of total,plate,stiffener
$N_{x,y}$		Normal vectors in x and y direction
$Q$	$[MW]$	Net power of combustion
$\mathbf{Q}_g$		Surface heat flow vector
$\mathbf{Q}_q$		Edge heat flow vector
$Q_R$	$[kW]$	Rate of heat radiation
$Q_{y,z}$	$[N]$	Shear forec in y,z-direction
$R$		Structural resistance
$R$	$[m^2K/W]$	Thermal resistance
$R_c$		Characteristic resistance
$R_d$		Design resistance
$R_{fi,d}$		Design resistance at time t
$R_\theta$		Connection capacity at high temperatures
$R_0$		Connection capacity at normal temperature
$S$		Expected loads
$S_c$		Load
$S_d$		Design load
$\mathbf{T}$		Temperature vector
$\dot{\mathbf{T}}$		Temperature increase vector
$\bar{T}$	$[K]$	prescribed temperature
$T_i$	$[K]$	Temperature in an iterative step
$T_s$	$[K]$	Surface temperature
$T_f$	$[K]$	Flame temperature
$U$	$[W/m^2K]$	Heat transfer coefficient
$V$	$[N]$	Shear force
$V$	$[m^3/m]$	Volume per unit length
$W$	$[m^3]$	Elastic section modulus
$W_p$	$[m^3]$	Plastic section modulus

## Greek

$\alpha$		Diffusion coefficient
$\alpha$		Column curve factor
$\gamma_{tot}$		Total safety factor
$\gamma_{ULS}$		ULS design load factor
$\gamma_{M,0}$		Material factor, normal temperature
$\gamma_{M,fi}$		Material factor, elevated temperature
$\gamma_m$		Material factor
$\gamma_d$		Design load factor
$\varepsilon$		surface emissivity
$\varepsilon$		Emissivity coefficient
$\varepsilon$		Material strength parameter(cross-section classes)
$\varepsilon_{cr}$		Critical strain
$\varepsilon_f$		flame emissivity
$\varepsilon_m$		member surface emissivity
$\varepsilon^{true}$		True strain
$\theta_{cr}$	$[^{circ}C]$	Critical temperature
$\theta_d$	$[^{circ}C]$	Design temperature
$\theta$		Weight parameter
$\theta_{a,cr}$	$[^{circ}C]$	Critical temperature
$\lambda_a$	$[W/mK]$	Thermal conductivity
$\mu_0$		Utilization
$\mu_R$		Resistance mean value
$\mu_S$		Load mean value
$\rho$	$[kg/m^3]$	Specific gravity
$\sigma$	$[kW/m^2K^4]$	Stepha-Boltzmann's constant
$\sigma$	$[MPa]$	Stress
$\sigma_R$		Resistance standard deviation
$\sigma_S$		Load standard deviation
$\sigma_v$	$[MPa]$	von- Mises stress
$\sigma_{x,y,x}$		Stress x,y,z-direction
$\tau_{xz,yz,yx}$		Shear stresses
$\phi_{1...6}$		Functions used in the Livesly functions

$\Gamma$		Yield surface
$\Gamma_{q,T}$		Boundaries for flux and heat respectively
$\Delta$	$[m]$	displacement
$\Delta T$	$[K]$	Temperature rise
$\Delta t$	$[s]$	time interval
$\Delta l$	$[m]$	temperature induced elongation
$\Delta H_c$		net calorific value
$\Delta\theta_{a,t}$	$[^{circ}C]$	Temperature increase
$\Delta\Lambda$		Scalar factor
$\Theta_g$	$[^{circ}C]$	Gas temperature
$\Theta_m$	$[^{circ}C]$	Material temperature
$\Theta_r$	$[^{circ}C]$	Effective radiation temperature
$\Phi$		Configuration factor
$\Omega$		Natural domain



# Chapter 1

## Introduction

The oil and gas industry in Norway has realised that it's operating costs have been on an unhealthy level these last years, and is trying to cut down. One type of cost driver has been the use of subsea wellheads, as several of the maintenance tasks require large ships or drilling rigs. Unmanned wellhead platforms can help the industry reduce it's costs. Kværner was awarded a concept study by Statoil in August 2014, related to a standardised, unmanned platform for the Oseberg field (OffshoreEnergyToday 2014): "The concept is focused on minimisation of facilities, equipment and costs down to water depths of 150 meters and may be a cost effective solution compared to a conventional subsea tie-back solution."

All installations in the North Sea must be designed against accidental actions such as fire. Incidents like the Piper Alpha catastrophe where 167 people were killed and the more recent Deepwater Horizon accident where 11 persons lost their lives show just how serious fires on board offshore installations can be.

Passive Fire Protection (PFP) is a safety precaution often applied to primary and secondary structural elements on offshore structures. Besides having that protective quality, however, its use has several downsides. Application is both costly and poses a minor health risk to the operator. The possibility of inspection and Non Destructive Testing is very limited on a member that has PFP applied. Thus, there are several upsides to gain if it can be shown that safety is ensured without the use of PFP.



# Chapter 2

## Current design principles

When designing structures to withstand expected loads throughout their lifetime there will always be uncertainties. There could be flaws in the construction material, unexpected loads or fabrication errors to name a few.

### 2.1 Limit state design

The overall demand of a structure design is that the expected loads,  $S$  should not exceed the structure's resistance,  $R$ :

$$S \leq R \Rightarrow R - S \geq 0 \quad (2.1)$$

Treating both load and resistance as stochastic variables means that they can be modelled by probability density functions (figure 2.1), based on large amount of data gathered throughout the history of structural engineering.

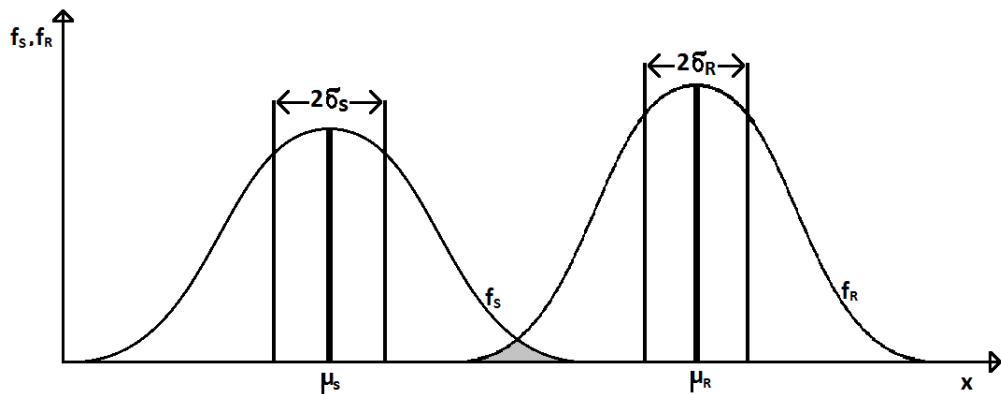


Figure 2.1: Load( $f_S$ ) and resistance( $f_R$ ) probability density function

If the probability density functions for the given structure and loading are known, its reliability could be calculated using statistical formulas. However, as each new structure would require a new and unique set of probability density functions, a simplified method is preferred. The approach involves finding the characteristic values for the resistance and load,  $R_c$  and  $S_c$ , depending on the limit state of interest. These characteristic values are set at a level giving a certain fractile of probability to be exceeded and not exceeded respectively. Given a limit state, the characteristic resistance and load are defined as:

$$R_c = \mu_R - C_R \cdot \sigma_R , \quad (2.2)$$

$$S_c = \mu_S + C_S \cdot \sigma_S \quad (2.3)$$

where  $\mu$  are the mean values,  $\sigma$  are standard deviations and the coefficients,  $C$  characterise the chosen fractile. A commonly used probability fractile is 5 %. Dimensioning values are obtained by adding safety factors to the characteristic values:

$$R_d = \frac{R_c}{\gamma_m} \quad (2.4)$$

$$S_d = \gamma_d \cdot S_c , \quad (2.5)$$

where  $\gamma_m$  is the material factor, meant to account for flaws in material or fabrication errors and  $\gamma_d$  is the design load factor. The total design requirement becomes:

$$S_d = \gamma_d \cdot S_c \leq \frac{R_c}{\gamma_m} = R_d \quad (2.6)$$

This simplified method is called "Load and Resistance Factor Design" (LRFD), also known as "Limit State Design" (LSD).

Four different limit states are considered:

- Ultimate Limit State (ULS)
- Accidental Limit State (ALS)
- Service Limit State (SLS)
- Fatigue Limit State (FLS)

**Ultimate Limit State** are the characteristic loads a structure is intended to withstand, and be able to function as normal without damages. An example is the "100 year wave". Offshore structures are required under ULS to withstand waves with annual probability of occurrence of 1 %, without structural damage.

**Service Limit State** ensure that a structure is able to fulfill functionality and not just be load bearing. The easiest examples are ship decks. They often fulfill a role as floor for crew and equipment performing daily operational tasks. This demands that the deck is reasonably flat, often more so than the ULS codes demand.

**Accidental Limit State** deals with loads under damaged condition, as well as extreme loads not covered by ULS. Local damage can often be accepted, as long as survivability of the installation is secured.

**Fatigue Limit State** prevents crack propagation beyond acceptable limits. Where ULS only take into account large loads and load combination, FLS accounts for the fact that cracks can grow in stress ranges well below the yield limit of a material.

## 2.2 DNV-GL Recommended practice

DNV-GL has a set of recommended practises for design of offshore structures. Among them is C204, Design Against Accidental Loads. The version referenced here (DNV-RP-C204 n.d.) is a pre-merger version from 2010, but the data is taken from a proposed revision, so the risk of being outdated is considered small. The overall goal of the recommended practice is to ensure that main safety functions of an installation is unimpaired during an accidental action. It is developed for use worldwide, though some countries have additional regulations that needs to be considered as well. Main subjects covered in RP-C204 are:

- Design philosophy
- Ship collisions
- Dropped objects
- Fire
- Explosions

Chapter 5 deals with fire, and is being revised at the moment. The information below is taken from the proposed revision.

### 2.2.1 General.

It is pointed out that the characteristic load in a fire is the member temperature rise, which is dependent on fire intensity, degree of member engulfment and insulation parameters. Internal stresses due to steel expansion is said to be of minor importance to the load bearing capacity and may often be omitted in analyses. The loss of strength and stiffness due to elevated temperature will cause redundant structures to redistribute loads from weakened members to colder and stronger members. The load bearing capacity of a single member or substructure is allowed to degrade substantially, if the overall global load bearing function of the installation is intact during the fire load.

Structural analyses may be performed on either individual members, substructures or the entire system. They are performed using simplified calculation methods on individual members, general calculation methods or a combination of the two. It is stated that simplified calculations yield overly conservative results, whereas general methods employ engineering to estimate more realistic behaviour of specific fire scenarios. Reference is made to Eurocode 3 part 1-2 (EC3-1-2 2005) for calculating structural response of singular members, and the present recommended practice gives guidance on more general calculation methods.

A separate assessment of ultimate strength for fire is said not to be needed if the maximum steel temperature is shown not to exceed  $400^{\circ} C$ , though checks with regard to deformation criteria may be needed to maintain safety functions. The three steps of design against accidental fire effects are:

- Combustion process
- Heat transfer
- Mechanical response.

### 2.2.2 Combustion process

Heat transfer analysis need input in the form of temperature- or temperature flux distributions through space and time, and these are the results from the combustion process. There are several standard temperature-time curves in the literature, but as these often are overly conservative, more accurate models are encouraged.

Computational Fluid Dynamics(CFD) software packages are able to simulate the combustion process, based on input as fuel type, burning rate, ventilation, soot production etc. As specific fire cases are simulated with CFD, the output often needs some generalization to account for uncertainties in fire location and direction.

### 2.2.3 Heat transfer analysis

The structure absorbs heat from the fire through radiation and convection. It will also transfer heat to the environment through irradiation and convection to cooler areas. The propagation through the structure is carried by conduction. These five contributions shall be included in heat transfer analysis.

Conduction is governed by the thermal diffusivity of the material. For steel this is a slow process and commonly only considered to have importance in the "through-thickness" direction of a member, though conduction through a joint may carry enough heat past a fire barrier to weaken an assumed cold member. Diffusivity is temperature dependent, as it is defined through a conduction coefficient  $k$ , specific weight  $\rho$  and specific heat of the material  $c_p$ :

$$\alpha = k/\rho c_p \quad (2.7)$$

Recommended practice is to use  $k = 45 [W/mK]$ . Specific heat is discussed in chapter 2.4.1.

Heat radiation is described by Stefan-Boltzmann's law. Surface properties of the material governs the emissivity coefficient,  $\varepsilon$ . Light, polished surfaces will have

lower emissivity coefficient than dark ones. Absorption of incident rays depends on an absorption coefficient, but assuming grey body conditions it can be set equal to  $\varepsilon$ .  $\varepsilon = 0.8$  is recommended for unpainted oxidized steel.

Convective heat transfer depends on the properties of the gas/fluid surrounding the structure. Parameters like flow conditions and boundary shapes makes the calculation complicated. Recommended convection coefficients are  $10[W/m^2K]$  for steel to calm air, and  $40 - 50[W/m^2K]$  for steel to strong wind. The case where the structure is enveloped in fire uses the same coefficient as the strong wind assumption.

Finite element methods carry out heat transfer analysis efficiently in time domain. Regular thin-walled objects are said to have moderate through thickness gradient, and are adequately modelled by quadrilateral elements(shells).

Passive fire protection (PFP) is common in offshore structures and can be dealt with by a resultant property (Thermal resistance). Modelling the PFP in the finite element model is not recommended due to numerical complexity. A heat transfer coefficient is defined as the inverse of the thermal resistance:

$$U = 1/R [W/m^2K] , \quad (2.8)$$

and typical values are presented:  $U = 5 [W/m^2K]$  for high protection demands and  $U = 10 [W/m^2K]$  for lower demands. The behaviour of an epoxy based PFP material is typical that the thermal resistance is initially low while expanding, followed by a high constant value until it burns off.

## 2.2.4 Mechanical response

Three different methods for calculating fire mechanical response:

1. The temperature-load domain. This is the most accurate representation of reality, but also the most complex and challenging numerically. Starting by applying the functional loads and then introducing the heat loads incrementally. As the element heat exceeds a members capacity, it can no longer carry its functional loads. Where reality would redistribute the loading and displace automatically, a static analysis has to carry out unloading of the element and reloading the system until equilibrium is reached. The temperature is then again increased in increments. If, however equilibrium can not be found when unloading the element, the temperature load is said to be critical for the system. Switching between temperature- and functional load control like this result in large computational costs, and though it demonstrates whether or not the system survives a given fire, it says nothing about the margin of which it survives.
2. The temperature domain method. Like the previous, the functional loads are applied first. The temperature loads are then incremented up to ultimate



collapse. Redistribution of loads is not performed, so the analysis will likely end at an earlier stage than a temperature-load domain analysis due to numerical ill conditioning. Survivability of the structure is evaluated, but in case of survival, information about the margins with respect to loss of load bearing function can not be obtained.

3. Load domain (Pushdown) method. Unlike the two previous methods, the temperature load is now applied first. At various stages of the fire, material properties corresponding to the temperature are updated for heat affected elements. The functional loads are then applied incrementally until collapse. This way, information about degradation of the ultimate strength of the system is obtained for each time step of a fire scenario, and a margin with respect to loss of load bearing function over fire time can be derived. When the ultimate resistance of the structure has degraded below the demands of the functional loads, the critical fire time is reached.

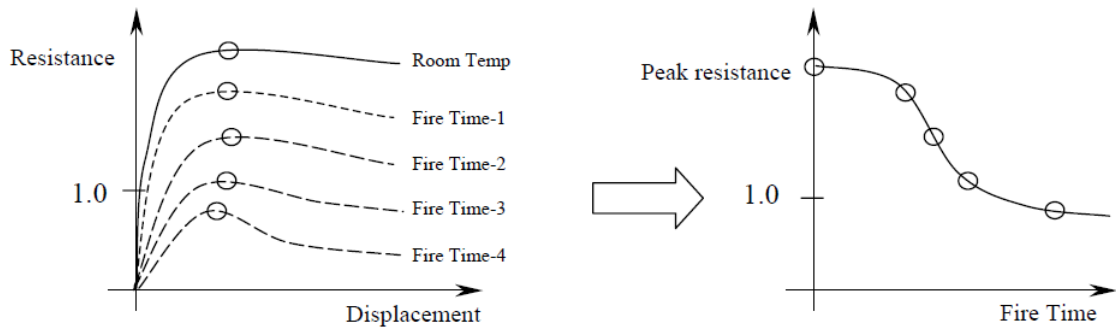


**Figure 2.2:** (USFOSweb 2014). Degradation of ultimate resistance versus fire time(Pushdown analysis)

As the Pushdown method is an easy and efficient way to document fire resistance, it is recommended to be the first analysis. If the mentioned margin is discovered to be critically small, the survivability of the structure can then be evaluated by means of one of the other methods.

The main focus of a structural response analysis is to ensure integrity of main load bearing components. Secondary components may be omitted from the model, as they may cause numeric ill conditioning due to extreme temperatures. Primary structural components experiencing extreme temperatures must be protected. In certain cases the use of PFP can be considered to force the "least critical" failure mode, rather than just to increase the time to collapse.

### 2.2.5 Thermal expansion

Thermal expansion of members subjected to heat loads result in compression and tension forces in the structure. They are similar to and treated the same way as fabrication residual forces, and they do not change the estimation of plastic capacity.

Even members experiencing tension forces in low temperature may buckle as result of thermal expansion, but the buckling is displacement controlled and not critical as it releases the expansion induced stresses. The effect of thermal expansion is normally small on a global system level and can be neglected. It is actually favourable for beams and girders restrained from axial motion as it reduces the need for plastic elongation.

### 2.2.6 Analysis methods

Non-linear ultimate strength assessment methods are classified in two groups:

**Stress-strain based methods**, where non-linear material behaviour is accounted for on a fiber level.

**Stress-resultant based methods**, where non-linear material behaviour is accounted for by stress resultants, based on closed-form solutions for cross-sectional forces.

### 2.2.7 Material modelling

Temperature dependent stress-strain relationship in stress-strain based methods are found in Eurocode 3 part 1-2 §3.2 (figure 2.6).

Stress-resultant based design uses the reduction factors  $k_{E\theta}$  and  $k_{y\theta}$  from §3.2 to obtain effective stiffness and yield strength respectively.

### 2.2.8 Cross-sectional capacities

Calculation of plastic capacities should be performed with the updated yield strength for elevated temperatures. Any large temperature gradients over a cross-section may significantly change the position of plastic neutral axis. Thus, axial forces may act as bending moments on the cross-section.

### 2.2.9 Equivalent imperfections

Lateral imperfections and residual stresses effect the buckling resistance of a compressive member. These effects are taken care of by equivalent imperfections. The formulation of imperfection for an elastic perfectly plastic material is proposed removed, so it will not be included here. Elasto-plastic material, however is included, and the definition of an equivalent imperfection is given as:

$$\frac{e^*}{l} = \frac{W_p}{W} \frac{1}{\pi} \sqrt{\frac{f_y}{E}} \frac{i}{z_0} \alpha = \frac{1}{\pi} \sqrt{\frac{f_y}{E}} \frac{W_p}{\sqrt{AI}} \alpha, \quad (2.9)$$

$\alpha$	0.5 for exposed members. Column curve c (EC3-1-1 2005).
$i$	radius of gyration
$z_o$	distance from neutral axis to outer fibre of the cross-section
$W_p$	plastic section modulus
$W$	elastic section modulus
$A$	Cross-sectional area
$e^*$	amplitude of initial imperfection
$l$	length of member

When using full length beam elements, the application is straight forward. If the member is modelled as multiple finite elements, the initial imperfection is modelled as displaced nodes. The imperfection has to be modelled in the same direction as deformations caused by heat loads.

### 2.2.10 Local cross sectional buckling

Special consideration is needed for dealing with local buckling. Shell modelling requires verification that the software is able to predict local buckling with satisfactory accuracy.

### 2.2.11 Ductility limits

It is known that Ductility increases with temperature, but quantitative information is limited.

**Beams in bending** may use the given requirements in section 3.10 of (DNV-RP-C204 n.d.), which is the same as for normal temperature. An example critical strain  $\varepsilon_{cr}$  for *S* 355 steel:  $\varepsilon_{cr} = 0.15$

**Beams in tension** assumes limiting criterion as failure to meet demand of axial resistance. For nearly uniform heating of a beam members that can carry membrane forces, a lateral displacement of 10 % is accepted. Conservativeness is assured by

using criteria from normal temperature codes.

### 2.2.12 Capacity of connections

Connection capacity at elevated temperatures  $R_\theta$  may be calculated as :

$$R_\theta = k_{y,\theta} R_0 , \quad (2.10)$$

where  $k_{y,\theta}$  is the effective yield strength reduction factor for maximum temperature in the connection, and  $R_0$  is the capacity at normal temperature.

## 2.3 NORSOK

NORSOK N-001 (N-001 2012) is the principal standard for offshore structures. It specifies guidelines and general principles for design assessment of offshore facilities. The part of most relevance to this thesis is chapter 6, about Actions and Action Effects. Partial safety factors for different limit states are listed here and reference is made to NORSOK N-003 (N-003 2007) for calculating actions and action effects. They are in turn covered by chapter 2.4 and 2.5. Reference is made to the NORSOK standards for the relevant material, and for steel design that is N-004 (N-004 2013). NORSOK N-004 chapter 9 and annex A deals with accidental actions, and besides referencing figure 2.4 a table of recommended material factors for using in Eurocode 3 part 1-2 (EC3-1-2 2005) is presented:

Type of calculation	Material factor 1)	Value
Resistance of Class 1,2 or 3 cross-sections	$\gamma_{M0}$	1.0
Resistance of Class 4 cross-sections	$\gamma_{M1}$	1.0
Resistance of member to buckling	$\gamma_{M1}$	1.0
Resistance of net section at bolt holes	$\gamma_{M2}$	1.1
Resistance of fillet and partial penetration welds	$\gamma_2$	1.1
Resistance of bolted connections	$\gamma_2$	1.1

1) Symbols according to NS-EN 1993-1-1 and NS-EN 1993-1-8.

Figure 2.3: (N-004 2013), partial safety to be used in (EC3-1-2 2005)

Limit state	Action combinations	Permanent actions (G)	Variable actions (Q)	Environmental actions (E) <sup>d</sup>	Deformation actions (D) <sup>e</sup>
ULS	a <sup>a</sup>	1,3	1,3	0,7	1,0
ULS	b	1,0	1,0	1,3	1,0
SLS		1,0	1,0	1,0	1,0
ALS	Abnormal effect <sup>b</sup>	1,0	1,0	1,0	1,0
ALS	Damaged condition <sup>c</sup>	1,0	1,0	1,0	1,0
FLS		1,0	1,0	1,0	1,0

<sup>a</sup> For permanent actions and/or variable actions, an action factor of 1,0 shall be used where this gives the most unfavourable action effect  
<sup>b</sup> Actions with annual probability of exceedance =  $10^{-4}$   
<sup>c</sup> Environmental actions with annual probability of exceedance =  $10^{-2}$   
<sup>d</sup> Earthquake shall be handled as environmental action within the limit state design for ULS and ALS (abnormal effect)  
<sup>e</sup> Applicable for concrete structures

Figure 2.4: (N-001 2012), table 1. Partial safety factors

Data worth noting is table 1 in NORSOK N-003, dealing with variable actions on deck structures. It is used when designing the platform model

Area	Local design		Primary design	Global design See NOTE 5
	Distribution action, p (kN/m <sup>2</sup> )	Point action, P (kN)	Apply factor given below to distributed action, p	Apply factor given below to distributed action, p
Storage areas	q	1,5 q	1,0	1,0
Laydown areas	q	1,5 q	f	f
Lifeboat platforms	9,00	9,00	1,0	may be ignored
Area between equipment	5,00	5,00	f	may be ignored
Walkways, staircases and platforms	4,00	4,00	f	may be ignored
Walkways and staircases for inspection and repair only	3,00	3,00	f	may be ignored
Roofs, accessible for inspection and repair only	1,00	2,00	1,0	may be ignored

NOTE 1 Wheel actions to be added to distributed actions, where relevant. Wheel actions can normally be considered acting on an area of 300 mm x 300 mm.

NOTE 2 Point actions to be applied on an area 100 mm x 100 mm, and at the most severe position, but not added to wheel actions or distributed actions.

NOTE 3 q is to be evaluated for each case. Storage areas for cement, wet or dry mud should be the maximum of 13 kN/m<sup>2</sup> and  $\rho g H$ , where H is the storage height in m. Laydown areas not normally to be designed for less than 15 kN/m<sup>2</sup>.

NOTE 4 f is the minimum of 1,0 and  $(0,5 + 3/A^{0,5})$ , where A is the action area in m<sup>2</sup>.

NOTE 5 Global action cases should be established based upon "worst case", representative variable action combinations, complying with the limiting global criteria to the structure. For buoyant structures these criteria are established by requirements to the floating position in still water and intact and damage stability requirements, as documented in the operational manual, considering variable actions on the deck and in tanks.

Figure 2.5: (N-003 2007), table 1. Variable deck actions

## 2.4 Eurocode 3 1.2

The eurocodes has a set of codes regarding design against fire scenarios. Eurocode 3 deals with steel dimensioning, and more specific, part 1-2 (EC3-1-2 2005) handles accidental fire situations. Three domains are assessed in eurocode 3:

**Time domain**, where fire resistance is stepwise assessed in terms of time duration. The requirement of fire resistance is formulated in terms of a required and dimensioning fire duration time,  $t_{fi,req}$  and  $t_{fi,d}$  respectively:

$$t_{fi,d} \geq t_{fi,req} \quad (2.11)$$

**Load resistance domain**, where the capacity is assessed at the end of the required fire duration. The design effect of action at the required time instant,  $E_{fi,d,t}$  can not exceed its corresponding design resistance,  $R_{fi,d,t}$ :

$$R_{fi,d,t} \geq E_{fi,d,t} \quad (2.12)$$

**Critical temperature domain**, where the element temperature after a required duration of time,  $\theta_{cr,d}$ , is evaluated against a design temperature  $\theta_d$ . The criterion is:

$$\theta_{cr,d} \geq \theta_d \quad (2.13)$$

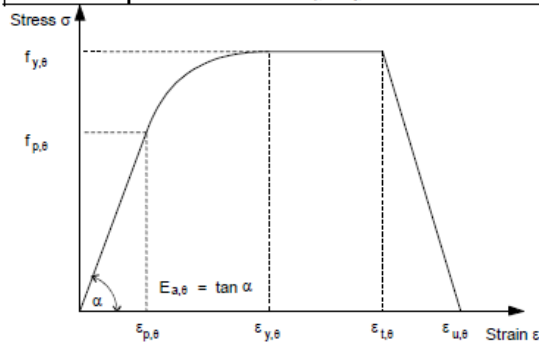
Global analysis and analysis of parts of a structure imply interaction between structural elements, e.g. redistribution of loads from hot to colder elements. This requires stepwise updates of the systems resistance and loading, thus the time domain is assessed using computer codes and programs. For evaluation of single elements, the two latter methods are applicable and these are discussed to some extent in the eurocode.

### 2.4.1 Material properties

The material properties of carbon steels are discussed in eurocode 3-1-2, chapter 3. Formulations for the stress-strain curves, thermal elongation, specific heat and thermal conductivity are listed as functions of temperature.

**The Stress-strain relationship** is shown in figure 2.6. Different temperature dependent reduction factors are listed in EC3-1-2, table 3.1 (figure 2.7), curves shown in figure 2.8.

Strain range	Stress $\sigma$	Tangent modulus
$\varepsilon \leq \varepsilon_{p,\theta}$	$\varepsilon E_{\lambda,\theta}$	$E_{\lambda,\theta}$
$\varepsilon_{p,\theta} < \varepsilon < \varepsilon_{y,\theta}$	$f_{p,\theta} - c + (b/a) [a^2 - (\varepsilon_{y,\theta} - \varepsilon)]^{0.5}$	$\frac{b(\varepsilon_{y,\theta} - \varepsilon)}{a [a^2 - (\varepsilon_{y,\theta} - \varepsilon)]^{0.5}}$
$\varepsilon_{y,\theta} \leq \varepsilon \leq \varepsilon_{l,\theta}$	$f_{y,\theta}$	0
$\varepsilon_{l,\theta} < \varepsilon < \varepsilon_{u,\theta}$	$f_{y,\theta} [1 - (\varepsilon - \varepsilon_{l,\theta}) / (\varepsilon_{u,\theta} - \varepsilon_{l,\theta})]$	-
$\varepsilon = \varepsilon_{u,\theta}$	0,00	-
Parameters	$\varepsilon_{p,\theta} = f_{p,\theta} / E_{\lambda,\theta}$ $\varepsilon_{y,\theta} = 0,02$ $\varepsilon_{l,\theta} = 0,15$ $\varepsilon_{u,\theta} = 0,20$	
Functions	$a^2 = (\varepsilon_{y,\theta} - \varepsilon_{p,\theta})(\varepsilon_{y,\theta} - \varepsilon_{p,\theta}) + c^2 / E_{\lambda,\theta}^2$ $b^2 = c (\varepsilon_{y,\theta} - \varepsilon_{p,\theta}) E_{\lambda,\theta} + c^2$ $c = \frac{(f_{y,\theta} - f_{p,\theta})^2}{(\varepsilon_{y,\theta} - \varepsilon_{p,\theta}) E_{\lambda,\theta} - 2(f_{y,\theta} - f_{p,\theta})}$	



- Key:
- $f_{y,\theta}$  effective yield strength;
  - $f_{p,\theta}$  proportional limit;
  - $E_{\lambda,\theta}$  slope of the linear elastic range;
  - $\varepsilon_{p,\theta}$  strain at the proportional limit;
  - $\varepsilon_{y,\theta}$  yield strain;
  - $\varepsilon_{l,\theta}$  limiting strain for yield strength;
  - $\varepsilon_{u,\theta}$  ultimate strain.

Figure 2.6: (EC3-1-2 2005), figure 3.1. Stress-strain relationship for carbon steel at elevated temperatures



Steel Temperature $\theta_a$	Reduction factors at temperature $\theta_a$ relative to the value of $f_y$ or $E_a$ at 20°C		
	Reduction factor (relative to $f_y$ ) for effective yield strength	Reduction factor (relative to $f_y$ ) for proportional limit	Reduction factor (relative to $E_a$ ) for the slope of the linear elastic range
	$k_{y,\theta} = f_{y,\theta}/f_y$	$k_{p,\theta} = f_{p,\theta}/f_y$	$k_{E,\theta} = E_{a,\theta}/E_a$
20°C	1,000	1,000	1,000
100°C	1,000	1,000	1,000
200°C	1,000	0,807	0,900
300°C	1,000	0,613	0,800
400°C	1,000	0,420	0,700
500°C	0,780	0,360	0,600
600°C	0,470	0,180	0,310
700°C	0,230	0,075	0,130
800°C	0,110	0,050	0,090
900°C	0,060	0,0375	0,0675
1000°C	0,040	0,0250	0,0450
1100°C	0,020	0,0125	0,0225
1200°C	0,000	0,0000	0,0000

**NOTE:** For intermediate values of the steel temperature, linear interpolation may be used.

Figure 2.7: (EC3-1-2 2005), table 3.1. Reduction factors

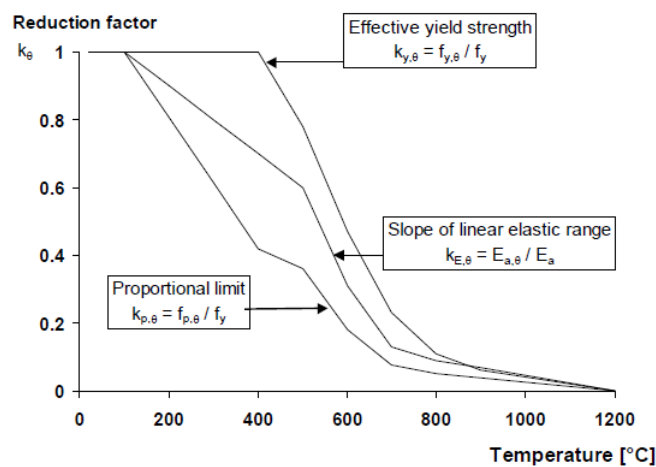
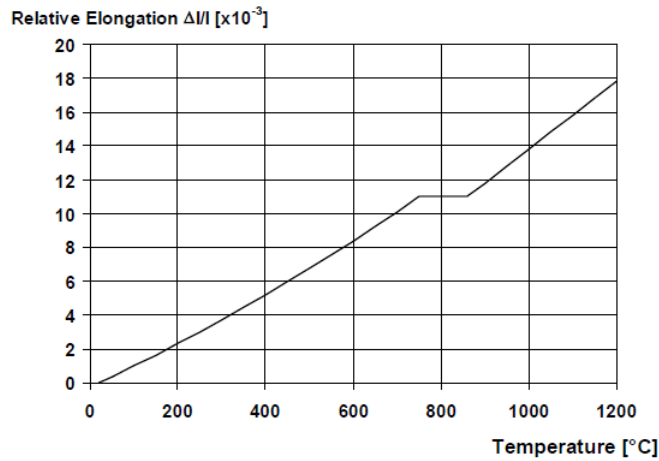


Figure 2.8: (EC3-1-2 2005), figure 3.2. Reduction factors for the stress strain relationship of carbon steel at elevated temperatures

**Relative thermal elongation** of steel at elevated temperatures is defined as:

$$\Delta l/l = \begin{cases} 1.2 \cdot 10^{-5} \cdot \theta_a + 0.4 \cdot 10^{-8} \cdot \theta_a^2 - 2.416 \cdot 10^{-4}, & \text{for } 20^\circ C \leq \theta_a < 750^\circ C \\ 1.1 \cdot 10^{-2}, & \text{for } 750^\circ C \leq \theta_a \leq 860^\circ C \\ 2 \cdot 10^{-5} \cdot \theta_a - 6.2 \cdot 10^{-3}, & \text{for } 860^\circ C < \theta_a < 1200^\circ C, \end{cases} \quad (2.14)$$

where  $l$  is the length at temp  $20^\circ C$ ,  $\Delta l$  is the temperature induced elongation and  $\theta_a$  is the steel temperature. The resulting curve is shown in figure 2.9.



**Figure 2.9:** (EC3-1-2 2005), figure 3.3. Relative thermal elongation of carbon steel as function of temperature

**Specific heat**,  $c_a$  [ $J/kgK$ ] is determined by the following formulae:

$$c_a = \begin{cases} 425 + 7.73 \cdot 10^{-1} \theta_a - 1.69 \cdot 10^{-3} \theta_a^2 + 2.22 \cdot 10^{-6} \theta_a^3, & \text{for } 20^\circ C \leq \theta_a < 600^\circ C \\ 666 + \frac{13002}{738 - \theta_a}, & \text{for } 600^\circ C \leq \theta_a < 735^\circ C \\ 545 + \frac{17820}{\theta_a - 731}, & \text{for } 735^\circ C \leq \theta_a < 900^\circ C \\ 650, & \text{for } 900^\circ C \leq \theta_a \leq 1200^\circ C, \end{cases} \quad (2.15)$$

$\theta_a$  still representing the steel temperature. These equations gives the curve:

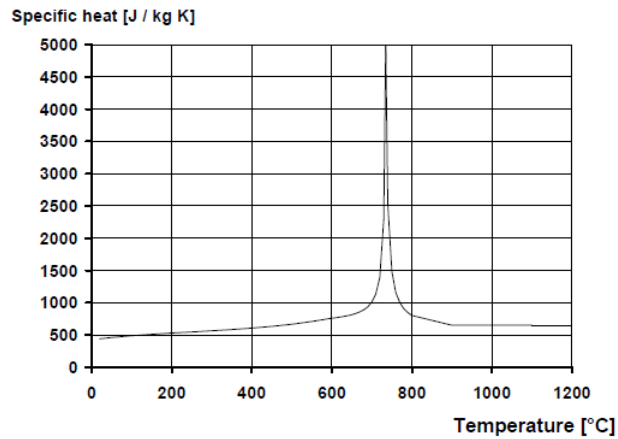


Figure 2.10: (EC3-1-2 2005), figure 3.4. Specific heat of carbon steel as function of temperature

Thermal conductivity,  $\lambda_a$  [ $W/mK$ ] of steel has formulation:

$$\lambda_a = \begin{cases} 54 - 3.33 \cdot 10^{-2} \theta_a, & \text{for } 20^\circ C \leq \theta_a < 800^\circ C \\ 27,3, & \text{for } 800^\circ C \leq \theta_a \leq 1200^\circ C, \end{cases} \quad (2.16)$$

giving the curve:

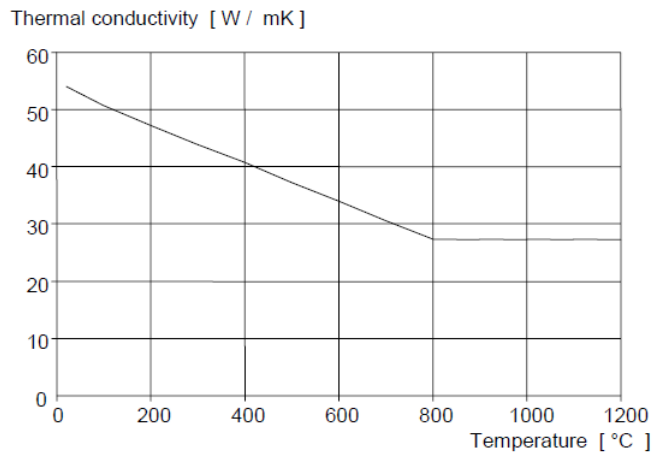


Figure 2.11: (EC3-1-2 2005), figure 3.4. Thermal conductivity of carbon steel as function of temperature

## 2.4.2 Heat transfer

In order to calculate the capacity of structural members, with data from the previous section, the steel temperature must be found. Heat transfer to unprotected steelwork and the resulting temperature increase,  $\theta_{a,t}$  in a time interval  $\Delta t$  is determined by:

$$\Delta\theta_{a,t} = k_{sh} \frac{A_m/V}{c_a \rho_a} \dot{h}_{net} \Delta t \quad (2.17)$$

The different symbols are explained in the following.

**Section factor for unprotected steel members,  $A_m/V$ .** Relationship between surface area per unit length,  $A_m$  and volume per unit length,  $V$ . A derivation of this is the box value of the section factor,  $[A_m/V]_b$

**Correction factor for shadow effect,  $k_{sh}$ ,** takes into account the fact that some parts of a profile may not be subjected to the full amount of radiation. For an I-section, parts of the web is in the shadow of the flanges. It is defined as:

$$k_{sh} = \begin{cases} 0.9[A_m/V]_b/[A_m/V], & \text{For I-sections} \\ [A_m/V]_b/[A_m/V], & \text{for all other cases} \end{cases} \quad (2.18)$$

**Specific heat of steel,  $c_a$ ,** as defined in chapter 2.4.1.

**Steel density,  $\rho_a$ ,** set to be  $7850 \text{ kg/m}^3$ .

**Net heat flux,  $\dot{h}_{net}$**  is obtained by referencing another eurocode standard, NS-EN 1991-1-2 (EC1-1-2 2002) chapter 3.1, and is an iterative method as the heat fluxes are temperature dependent:

$$\dot{h}_{net} = \dot{h}_{net,c} + \dot{h}_{net,r} \quad (2.19)$$

The convective heat flux component  $\dot{h}_{net,c}$  is defined as:

$$\dot{h}_{net,c} = \alpha_c \cdot (\Theta_g - \Theta_m), \quad [W/m^2] \quad (2.20)$$

where  $\alpha_c$  is the coefficient of heat transfer by convection  $[W/m^2K]$ ,  $\Theta_g$  and  $\Theta_m$  are the gas and material temperatures respectively  $[^\circ C]$ . In the iterative procedure,  $\Theta_m$  will be the material temperature found in the previous step.  $\Theta_g$  has different expressions, depending on the type of fire. Multiple standard formulations are listed. The hydrocarbon temperature-time curve is:

$$\Theta_g = 1080(1 - 0.325e^{-0.167t} - 0.675e^{-2.5t}) + 20, \quad [^\circ C] \quad (2.21)$$

where  $t$  is the time in minutes. The curve demands  $\alpha_c = 50$ .

The radiative net heat flux is a little more cumbersome, following Stephan Boltzmann's law:

$$\dot{h}_{net,r} = \Phi \cdot \varepsilon_m \cdot \varepsilon_f \cdot \sigma \cdot [(\Theta_r - 273)^4 - (\Theta_m - 273)^4], \quad [W/m^2] \quad (2.22)$$

where  $\Phi$  is a configuration factor set equal to 1,  $\varepsilon_m$  is the member surface emissivity set to be 0.7 according to EC3-1-2 chapter 2.2,  $\varepsilon_f$  is the emissivity of the fire set equal to 1 and  $\sigma$  is Stephan Boltzmann's constant. The effective radiation temperature  $\Theta_r$  is set equal to  $\Theta_g$  for engulfed elements. Figure 2.12 shows the steel temperature development where a HE500B beam is fully engulfed in flames. The steel specific heat is simplified to a constant  $600 \text{ [J/kgK]}$ .

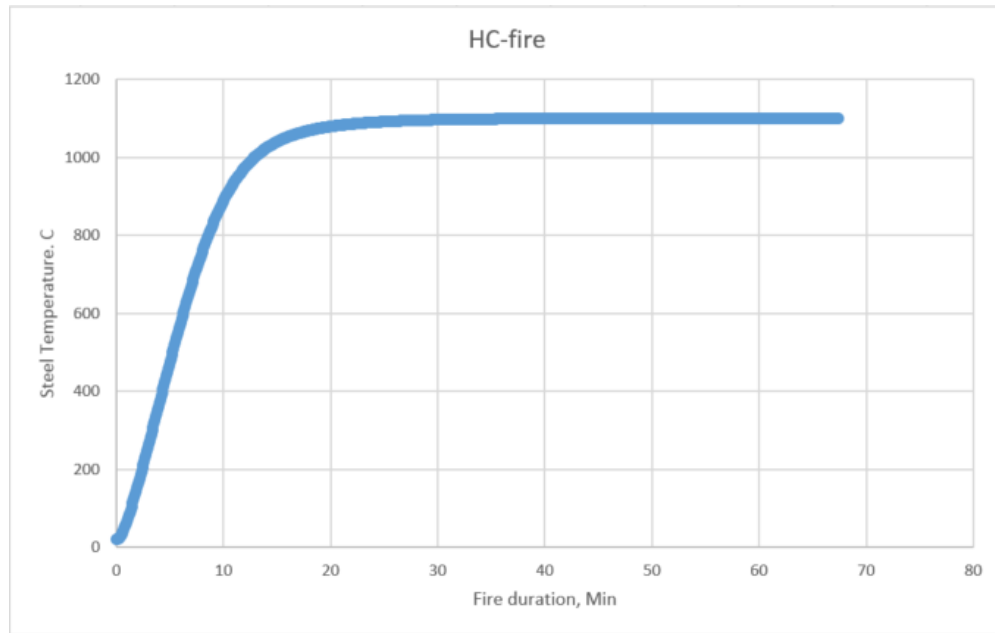


Figure 2.12: HC-fire curve.

### 2.4.3 Structural fire design

With the temperature known for a given time instant, the capacity can now be calculated. Depending on the loading situation, cross sections are divided into classes representing how they behave in the plastic range. Eurocode 3 part 1-1 (EC3-1-1 2005) chapter 5 deals with classification of cross sections. The criteria of cross section classes depends on a dimensionless parameter  $\varepsilon$  as well as a width to thickness ratio  $c/t$ . Example; cross section class 1 in bending:

$$c/t \leq 72\varepsilon, \quad \text{where} \quad \varepsilon = \sqrt{235/f_y} \quad (2.23)$$

The addition when working with elevated temperatures is a reduction factor to  $\varepsilon$ :

$$\varepsilon = 0.85\sqrt{235/f_y} \quad (2.24)$$

For the aforementioned HE500B beam with yield strength 355 MPa,  $c/t = 27.6$  and  $72 \cdot \varepsilon = 72 \cdot 0.85\sqrt{\frac{235}{355}} = 57.4$ . Hence it is a class 1 cross section in bending action.

Having established the cross section class, there are formulas for resistance to different types of loading. Chapter 4.2.3.2 handles bending of class 1 and 2 cross sections:

$$M_{fi,Rd} = k_{y,\theta}[\gamma_{M,0}/\gamma_{M,fi}]M_{Rd}, \quad (2.25)$$

Where  $M_{fi,Rd}$  is the design moment resistance accounting for elevated temperature, both material factors  $\gamma$  is set equal to 1, and  $M_{Rd}$  is the plastic moment resistance

according to Eurocode 3 part 1-1 chapter 6. The reduction factor  $k_{y,\theta}$  is found in table 3.1 of Eurocode 3 part 1-2. It shows that after 10 minutes the steel temperature is  $890^\circ C$  (figure 2.12), which corresponds to a reduction factor of 0.06. The HE500B has lost 94 % of its bending capacity after 10 minutes engulfed in the HC-fire. Similar formulas are listed for the different load combinations.

**Critical temperature** can be used as an alternative. The utilization  $\mu_0$  is then calculated in advance:

$$\mu_0 = E_{fi,d}/R_{fi,d} , \quad (2.26)$$

where  $E_{fi,d}$  is the design action and  $R_{fi,d}$  is the design resistance at normal temperature. The critical temperature for a member with uniform temperature distribution is:

$$\theta_{a,cr} = 39.19 \ln \left[ \frac{1}{0.9674 \cdot \mu_0^{3.833}} - 1 \right] + 482 \quad (2.27)$$

If the HEB beam was 30 % utilized, its critical temperature would be  $664^\circ C$ , corresponding to a fire duration of 7 minutes (fig 2.12).

## 2.5 FABIG technical note 11

Following the Piper Alpha disaster in 1988, it was clear that the current understanding of hydrocarbon explosions and fires were lacking. Several joint industry projects were commissioned to uncover knowledge gaps. The Fire And Blast Information Group was created in 1992 as one such project, with the aim to “disseminate knowledge and best practice, and to develop guidance on the prevention and mitigation of fires and explosions and the protection of people and facilities from such hazards” (Fabigweb 2016).

FABIG technical note 11 (FABIG 2010) is named **Fire Loading and Structural Response** and provides guidance regarding design of steel structures’ resistance to hydrocarbon fires:

- Section 2 covers jet and pool fires
- Section 3, heat transfer and temperature development in steel
- Section 4, general principles of passive fire protection(PFP)
- Section 5, material data for steel and stainless steel at high temperatures
- Section 6 & 7 describes the basis of fire design in accordance with Eurocode 3

### 2.5.1 Section 2, Estimating hydrocarbon fire loads

**Jet fires** are produced by a pressurized release of some sort of fuel, be it gas, liquid or a two-phase mix of the two. The simplest case is the release of pure gas, and will be dealt with in the following, it is however noted that a two-phase jet fire is likely to produce some liquid drop-out, producing a pool. Hence, a combination of pool- and two-phase jet fire may be a likely case.

Depending on the pressure of the container, pipe or vessel, a pressurised gas release into the atmosphere can produce velocities around and over the speed of sound of the fluid. The flame only commences downstream in the expansion region, where the fluid has decelerated into subsonic velocities and burns with a blue color. The turbulent yellow main body of the jet flame is a product of further expansion and air entrainment. Lift-off is a term sometimes referring to the distance between release and the initiation of the blue flame, but as the yellow part is far more radiative, the term is often expanded to include the length of the blue flame.

A stable jet fire needs a certain combination of release hole size, geometry and surrounding geometry. Formula for calculating the blow-out velocity of the gas is

provided, but as the fire cases are given for this thesis, it will not be elaborated here. Calculating the jet fire length  $[m]$  is of more interest, and an estimation formula is given:

$$L = 2.8893 \cdot Q^{0.3728} , \quad (2.28)$$

where  $Q$  is the net power of combustion  $[MW]$ , defined by release rate times calorific value of the fuel. Set the release rate equal to the lowest standard case,  $0.1 [kg/s]$ . The calorific value of natural gas is given as  $1.25 \cdot 10^4 [kcal/kg]$  on CNG Europe's websites (CNGEurope 2014). Using a conversion of  $1 [kcal] = 4.184 [kJ]$ , the flame length becomes:

$$L = 2.8893 \cdot \left[ 0.1 \cdot 4.184 \cdot 1.25 \cdot 10^4 \cdot \frac{1 \text{ MW}}{1000 [kW]} \right]^{0.3728} = 5.35 [m] , \quad (2.29)$$

so the given length of  $10 [m]$  seems a bit conservative. Flame lengths for a range of fuels are plotted against combustion power in figure 2.13, see that the flame of  $Q = 5.23 [MW]$  is not likely to reach  $10 [m]$  for any of the tested fuels.

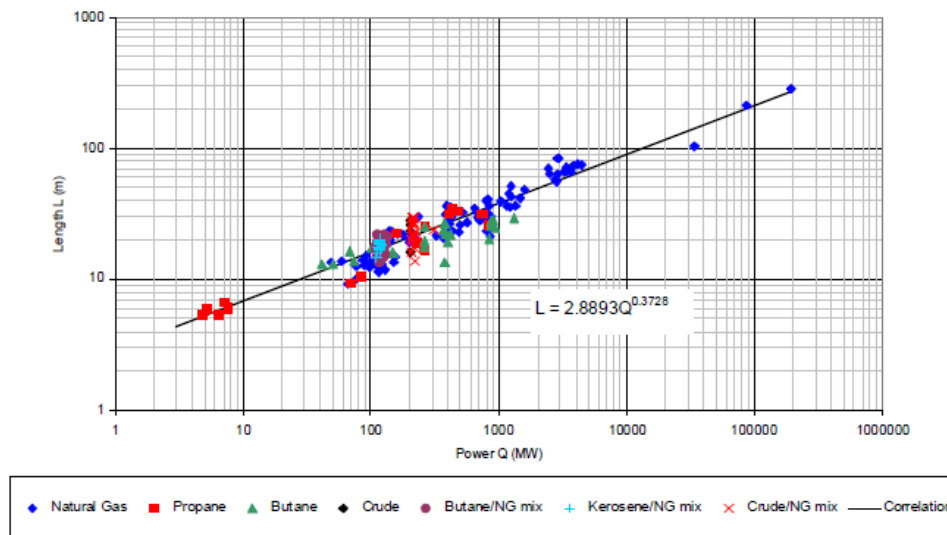


Figure 2.13: (FABIG 2010), figure 2.2. Jet flame fire length

The effect of soot formation is discussed, and a correlation between the radiated fraction  $F$  of the combustion power and carbon number of the gas is shown.

As compartmentalization is not likely to occur on such an open platform, and water deluge systems are not considered in this thesis, their effects are not shown here. A group of lessons from the experimental work studied by FABIG is listed, mentioning sound design of compartments, ventilation, extinguishing equipment and piping layout to minimize the consequence of a fire.

The tabulated guidance on behaviour of gas jet fires is shown in figure 2.14. These are used to estimate steel temperature development during gas jet fires. 2.15 is a



similar table regarding two-phase jet fires. It is seen that lower exit velocities will result in less air entrainment, thus giving the rise to soot formation. Hence, the radiated heat flux is significantly higher for a to-phase jet, while the corresponding convective flux is not.

**Table 2.2 Guidance on the behaviour of gas jet fires**

Mass release rate ( $\text{kg s}^{-1}$ )	0.1	1.0	10	>30	Effect of confinement
Flame length $L$ (m), 1% flame	5	15	40	65	Affected by enclosure shape and openings
Fraction of heat radiated, $F$	0.05	0.08	0.13	0.13	
CO level (% v/v) and smoke concentration ( $\text{g m}^{-3}$ )	CO < 0.1 Soot ~0.01	CO < 0.1 Soot ~0.01	CO < 0.1 Soot ~0.01	CO < 0.1 Soot ~0.01	Increased CO up to about 5% v/v at a vent prior to external flaming, but after external flaming <0.5 % v/v exiting the flame. Soot levels depend on equivalence ratio from about 0.1 $\text{g m}^{-3}$ at $\phi=1.3$ to 2.5 $\text{g m}^{-3}$ at $\phi=2.0$
Initial total heat flux on engulfed object ( $\text{kW m}^{-2}$ )	180	250	300	350	For ventilation controlled jet fires, up to 400 $\text{kW/m}^2$ in the impingement zone for large fires but typical values are around 300-350 $\text{kW/m}^2$ . For fuel controlled jet fires with flowrates up to $10\text{kg s}^{-1}$ , use values for open jet fires with flowrates $10\text{kg s}^{-1}$ or greater due to deflected hence thicker flames. Outside the impingement zone, heat flux is nearly 100% radiative.
Radiative flux on engulfed object ( $\text{kW m}^{-2}$ )	80	130	180	230	280
Initial convective flux on engulfed object ( $\text{kW m}^{-2}$ )	100	120	120	120	120 in the impingement zone
Flame temperature, $T_f$ (K)	1560	1560	1560	1560	1600
Flame emissivity, $\epsilon_f$	0.25	0.4	0.55	0.7	0.75
Convective heat transfer coefficient, $h$ ( $\text{kW m}^{-2} \text{K}^{-1}$ )	0.08	0.095	0.095	0.095	0.09
Effect of deluge	No effect on heat loadings to engulfed objects. In far field, take $F_1=0.8F$ for 1 row of water sprays, $F_1=0.7F$ for 2 rows, $F_1=0.5F$ for >2 rows at 12 litres $\text{m}^{-2} \text{min}^{-1}$ . May improve combustion efficiency and reduce CO levels within flame.				Risk of extinguishment and explosion hazard if deluge activated in later stages.

**Figure 2.14:** (FABIG 2010), Table 2.2. Tabulated gas jet fire guidance

**Table 2.3 Guidance on the behaviour of two-phase jet fires**

Mass release rate ( $\text{kg s}^{-1}$ )	0.1	1.0	10	30	Effect of confinement
Flame length $L$ (m)	5	13	35	60	Affected by enclosure shape and openings
Fraction of heat radiated, $F$	See below				
CO level (% v/v) and smoke concentration ( $\text{g m}^{-3}$ )	CO < 0.1 Soot ~0.01	CO < 0.1 Soot ~0.01	CO < 0.1 Soot ~0.01	CO < 0.1 Soot ~0.01	Increased CO up to about 5% v/v at a vent prior to external flaming, but after external flaming < 0.5% v/v exiting the flame. Soot levels depend on equivalence ratio from about $0.1 \text{ g m}^{-3}$ at $\phi = 1.3$ to $2.5 \text{ g m}^{-3}$ at $\phi = 2.0$
Initial total heat flux ( $\text{kW m}^{-2}$ )	200	300	350	400	For flashing and pressurised multi-component two-phase jet fires such as live crude or gas dissolved in liquid, take values as per $30 \text{ kgs}^{-1}$ two-phase jet fire in the open (see Important Note 2 below). For evaporating jets such as condensate, up to $250 \text{ kWm}^{-2}$ for ventilation controlled fires and $170 \text{ kWm}^{-2}$ for fuel controlled fires. Up to $280 \text{ kW m}^{-2}$ at the smoke/air interface for horizontal jets pointing away from the vent. All two-phase confined jet fires are considered optically thick. Outside the impingement zone, heat flux is nearly 100% radiative.
Initial radiative flux ( $\text{kW m}^{-2}$ )	100	180	230	280	
Initial convective flux ( $\text{kW m}^{-2}$ )	100	120	120	120	
Flame temperature (K)	1560	1560	1560	1560	
Flame emissivity, $\epsilon_f$	0.3	0.55	0.7	0.85	
Convective heat transfer coefficient, $h$ ( $\text{kW m}^{-2} \text{K}^{-1}$ )	0.08	0.095	0.095	0.095	
Effect of deluge	Some benefit to engulfed objects but temperature may still rise although at a slower rate. Combined area and dedicated deluge may prevent temperature rise if effectively applied. Take $F_1$ as per gas jet fires.				Risk of extinguishment if the compartment is already hot and potential formation of pool and explosion hazard. Effective cooling of compartment if deluge applied early.

**Figure 2.15:** (FABIG 2010), Table 2.3. Tabulated two-phase jet fire guidance

**Pool fires** are formed when non-pressurised containers experience leakage, and the resulting pool of fluid catch fire. They can also be formed as a result of a two-phase jet fire, if the liquid fraction is not sufficiently atomised. Listed physical aspects determining a pool fire's harm potential:

- Pool spread and shape
- Rate of flame speed
- Mass burning rate
- Flame size and shape

- Thermal radiation field
- Properties of any formed smoke, gases and thermal plumes
- Temporal variation of all above

Pool fire models often assume circular pools of uniform depth and constant shape throughout the duration of the fire. Note that it is not the liquid itself that is burning, but the vapour rising up from the pool. Hence, ignition may be dependent of some external heat source, e.g. a nearby jet fire. When the vapour has caught fire, the flame radiates heat that in turn causes more vapour formation sustaining the fire. It follows that the mass burning rate of a pool fire is dependent on the vapour evolution rate. It is also dependent on the fuel type, shown in FABIG tn11's table 2.4 (figure 2.16)

**Table 2.4 Pool fire mass burning rate coefficients on solid substrates at ambient temperature**

Fuel	$\dot{m}_\infty$ (kg m <sup>-2</sup> s <sup>-1</sup> )	$k$ (m <sup>-1</sup> )	Approximate boiling temperature range, K
LNG	0.141	0.136	112
LPG	0.13	0.271	231-273
Propane	0.13	0.271	231
Butane	0.078	0.5	273
Gasoline	0.055	2.0	313-483
Kerosene	0.06	2.6	423-523
Diesel	0.044	1.15	438-633
Diesel – ventilation controlled	0.031	-	438-633

**Figure 2.16:** (FABIG 2010), Table 2.4. Mass burning rates

The mass burning rates on a finite sized pool  $\dot{m}_b$  is given as:

$$\dot{m}_b = \dot{m}_\infty (1 - e^{-kD}) \quad , \quad (2.30)$$

where  $\dot{m}_\infty$  is the maximum mass burning rate and  $k$  is a measure of how quickly the maximum burning rate is achieved as the pool diameter  $D$  increases.

Soot formation is considerable in a pool fire and increases with pool size, as the availability of air is less in the centre of the flame. The soot may in some cases reduce the radiant heat. Hence the surface emissive power SEP and the fraction of heat radiated,  $F$  will first increase with pool diameter, and then decrease as the soot starts shielding some of the radiation. Figure 2.17 shows variation of average surface emissive power as function of pool diameter. Average SEP is used in simple geometric pool fire models, and not necessarily the measured values in reality. Model

flames will often have a larger surface area, as fires in reality tend to narrow with height.

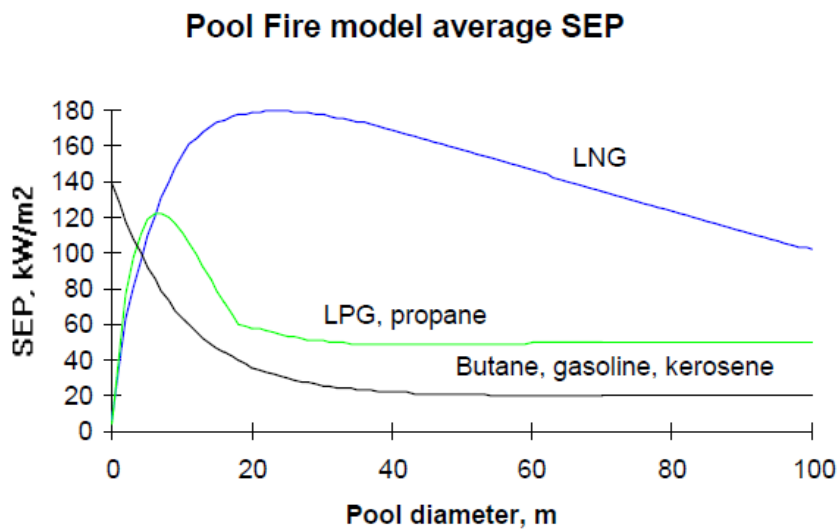


**Figure 2.17:** (FABIG 2010), figure 2.12. Model average SEP

The effects of deluge or confinement will not be discussed here, as there will be no compartments on the unmanned wellhead platform. The formation of a pool on the sea surface is of interest, and though it will not be investigated here it is noted that it would behave as a non-confined pool. There would be less probability of ignition, and if ignited the flame would be shorter, cooler and less radiant than the case of a pool fire on land. The consequence of a sea surface pool fire could be loss of capacity in jacket legs and braces.

Guidance on parameter data for hydrocarbon pool fires on land is given in FABIG tn 11 table 2.6 shown in figure 2.18. Similar tables are given for methanol pool fires as well as pool fires on the sea surface.

**Table 2.6** Guidance on hydrocarbon pool fires on land

Type	Small hydrocarbon pool	Large hydrocarbon pool	Effect of confinement
Typical pool diameter (m)	<5	>5	Any
Flame length $L$ (m)	Twice pool diameter	Up to twice pool diameter	Take values as per large hydrocarbon pool fire for worst case. If confinement is severe then mass burning rate will decrease to match available air flow and large external fire at vent expected.
Mass burning rate ( $\text{kg m}^{-2} \text{s}^{-1}$ )	Crude: 0.045-0.06 Diesel: 0.055 Kerosene: 0.06 Condensate: 0.09 C3/C4s: 0.09	Crude: 0.045-0.06 Diesel: 0.055 Kerosene: 0.06 Condensate: 0.1 C3/C4s: 0.12	
Fraction of heat radiated, $F$	0.25	0.15	
CO level (% v/v) and smoke concentration ( $\text{g m}^{-3}$ )	CO < 0.5 Soot 0.5 – 2.5	CO < 0.5 Soot 0.5 – 2.5	Increased CO up to about 5% v/v at a vent prior to external flaming, but after external flaming about 0.5 % v/v at the end of the flame. Soot levels up to $3 \text{ g m}^{-3}$ .
Initial total heat flux ( $\text{kW m}^{-2}$ )	125	250	Take values as per large hydrocarbon pool fire.
Radiative flux ( $\text{kW m}^{-2}$ )	125	230	
Initial convective flux ( $\text{kW m}^{-2}$ )	0	20	
Flame temperature (K)	1250	1460	
Flame emissivity, $\varepsilon$	0.9	0.9	
Convective heat transfer, $h$ coefficient ( $\text{kW m}^{-2} \text{K}^{-1}$ )	-	0.02	
Effect of deluge	<p>Considerable fire control and potential extinguishment can be achieved. Expect a reduction in flame coverage (and hence flame size) of up to 90% within 10 minutes. Rapid extinguishment with AFFF.</p> <p>Up to 50 % reduction in radiative heat flux to engulfed objects.</p> <p>In far field take <math>F_1 = 0.8F</math> for 1 row of water sprays, <math>F_1=0.5F</math> for 2 rows and <math>F_1=0.4F</math> for &gt;2 rows at <math>12 \text{ litres min}^{-1} \text{ m}^{-2}</math>.</p>		<p>Expect reduced flame temperatures and reduced or no external flaming.</p> <p>Mass burning rate reduces to match available air flow.</p> <p>Fire does not extinguish but continues to burn at much reduced rate.</p>

**Figure 2.18:** (FABIG 2010), table 2.6. Parameters for HC pool fires on land

## 2.5.2 Heat transfer and temperature development

Chapter 3.1 of FABIG tn 11 explains simple methods for calculating heat transfer from fires to steel members. The heat transfer is said to happen by radiation for a non-impinging fire, and by a combination of radiation and convection for an impinging(engulfing) fire. Heat loss happens by radiation from the outside surface for an impinging fire, and by both radiation and forced convection (wind) for the non-impinging case. Two assumptions are made to simplify the predictions of temperature rise:

- The side of an object not facing the fire is assumed insulated, so that all absorbed heat goes into heating the object. This is a conservative assumption, as the "backside" will radiate a fraction of the absorbed heat.
- Conduction is assumed so slow that the conduction problem is one dimensional. The heat gradient will be non-zero only across a plate's thickness.

Two different cases are, as mentioned, impinging (engulfed objects) and non-impinging (surrounding objects).

### Heat transfer to surrounding objects.

Three approaches are common for the case of external radiation from jet and pool fires:

- The point source model
- Multiple point source model
- Idealised flame shape with a given surface emissive power

The last method will not be evaluated in this thesis.

**Point source model.** Assuming fire emanating from a single point in space, most common the estimated midpoint of the visible fire. The radiation received outside the fire  $q$  [ $kW/m^2$ ] is given as:

$$q = \frac{Q_R \tau}{4\pi d^2}, \quad (2.31)$$

where  $\tau$  is the atmospheric transmissivity set equal to 0.8, but in reality dependent on atmospheric conditions like humidity.  $d$  is the distance from the point source to the object.  $Q_R$  is the rate of heat radiated from the flame:  $Q_R = FQ$ , where  $F$  is the fraction of combustion heat release and  $Q$  is the net combustive power:

$$Q = \dot{m}_b \Delta H_c, \quad (2.32)$$

$\dot{m}_b$  being either gas release rate or mass burning rate depending on the fire type, and  $\Delta H_c$  is the net calorific value of the fuel.

**Multiple point sources** can be used with the same model, where the point sources contributes with a given power per length. References are made in FABIG tn 11 to tested models, but the author failed to locate that source. Thus, a model is derived from the point source model.

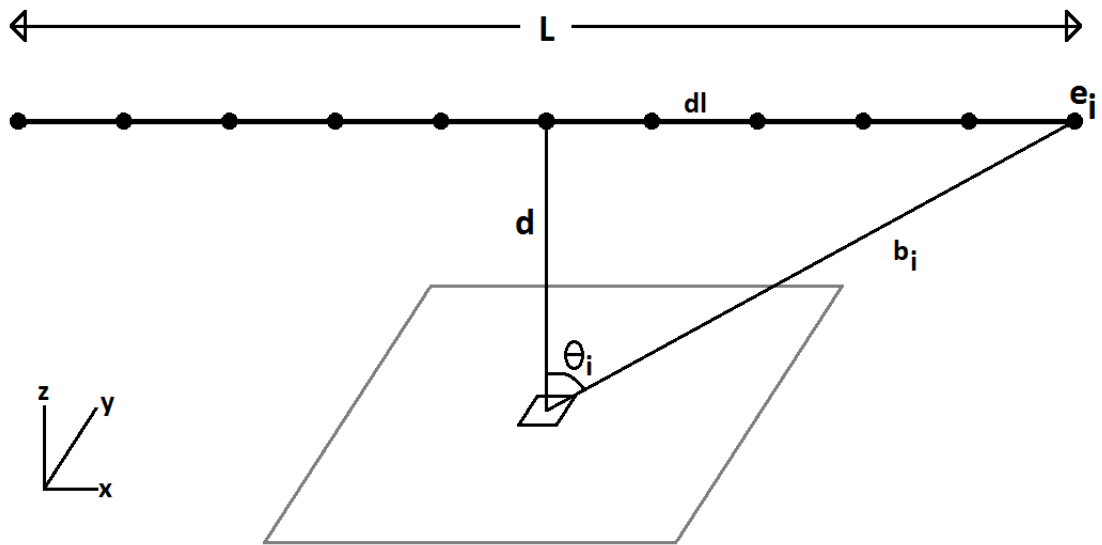


Figure 2.19: Derived multiple point source model

Here, each point source have a power of  $e_i$  [kW/m]. The total received radiation becomes:

$$\sum_{i=1}^n \frac{e_i \tau}{4\pi b_i^2} \cos(\theta_i) \quad (2.33)$$

The cosine factor accounts for view factor between source and object. Defining the origin of the local model in the measuring point, the angle,  $\theta_i$  between the heat ray and the surface normal is obtained by  $\theta_i = \tan^{-1}(\frac{x_i}{d})$ , giving the distance from point source to object,  $b = \frac{d}{\cos(\theta)}$ . It is not recommended to use the multiple point source method within one flame length from the fire.

**Heat transfer to engulfed objects** is a complicated problem as it is dependent on temperature, velocities and distribution of chemical compounds. The expression for total heat flux including both radiation and convection in a flame is dependent on emissivities,  $\varepsilon$  and temperatures,  $T$  of both the flame,  $f$  and the object surface,  $s$ :

$$q_a = q_r + q_c = \varepsilon_s \sigma (\varepsilon_f T_f^4 - T_s^4) + h(T_f - T_s) , \quad (2.34)$$

$\sigma = 5.67 \cdot 10^{-11}$  [kW/m<sup>2</sup>K<sup>4</sup>] is the Stefan-Boltzman constant.  $q_a$  is the total heat load,  $q_r$  and  $q_c$  are radiative and convective heat respectively. The surface emissivity,  $\varepsilon_s$  is set equal to 0.9, but is found to be 0.65 for carbon steel inside the fire impingement zone. Flame emissivity,  $\varepsilon_f$  and the convective heat transfer coefficient,  $h$  are both found in figure 2.14 and figure 2.18.

As mentioned, several parameters inside a fire may vary and equation 2.34 should be summed over the area of the object. As the convective heat load is inversely

proportional to the object temperature, the parameters  $T_f$ ,  $h$  and  $\varepsilon_f$  should be updated for each temperature step to obtain the most accurate transient solution.

The temperature rise,  $\Delta T$  over a time increment,  $\Delta t$  for an engulfed object can be estimated by:

$$\Delta T = \frac{\Delta t}{\rho c l} (q_a - q_{loss}) , \quad (2.35)$$

where  $\rho$  is the specific gravity of the material,  $c$  is the specific heat capacity,  $l$  is the wall thickness,  $q_a$  is the absorbed heat flux and  $q_{loss}$  is the heat loss (zero for engulfed object). For many profiles the wall thickness is substituted by the section factor  $A_m/V$  as described in chapter 2.4.2. The heat transfer problem can now be solved by iteration:

$$T_{i+1} = T_i + \Delta T_i , \text{ for } i \geq 0 \quad (2.36)$$

$$\Delta T_i = \frac{\Delta t}{\rho c l} \cdot q_{ai} \quad (2.37)$$

$$q_{ai} = \varepsilon_s \sigma (\varepsilon_f T_f^4 - T_{si}^4) + h(T_f - T_{si}) \quad (2.38)$$

On the basis of values from table 2.2 and 2.6 (figures 2.14 and 2.18), the iteration process was performed in a spreadsheet for a jet fire of  $\dot{m} = 1.0$  and a small hydrocarbon pool fire:

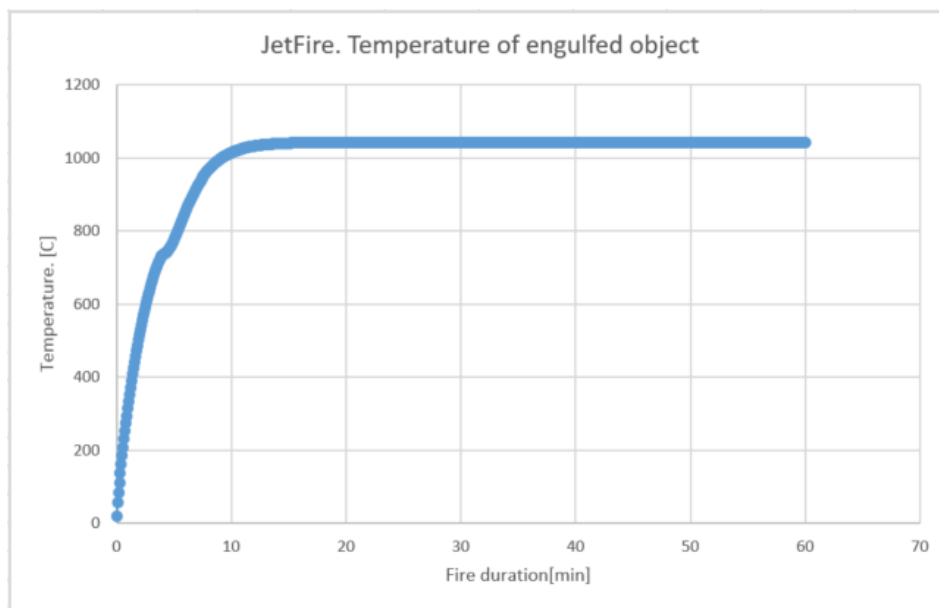


**Figure 2.20:** Temperature development of engulfed object in jet fire



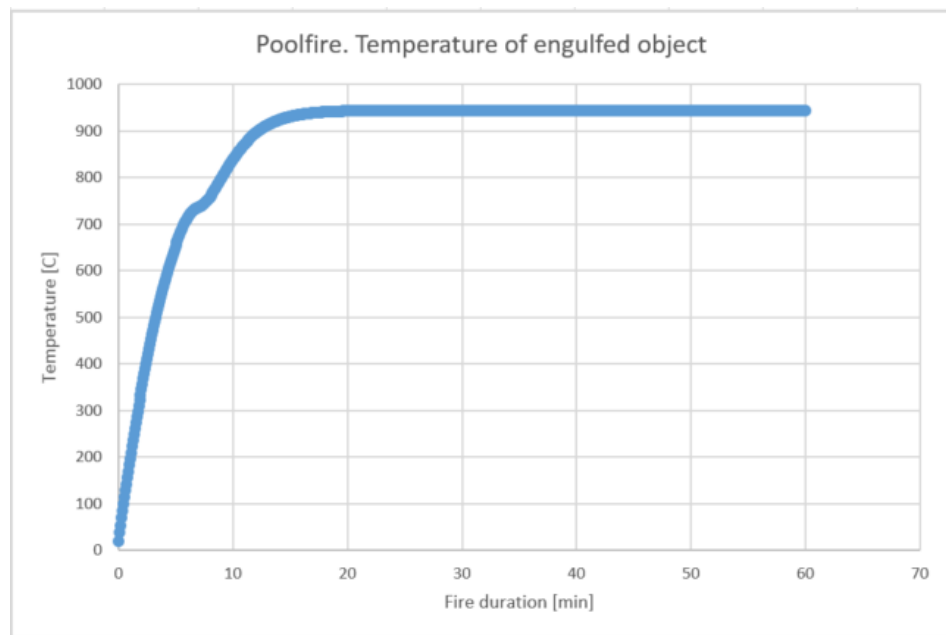


**Figure 2.21:** Temperature development of engulfed object in a small pool fire



# Chapter 3

## Non-Linear Finite Element Method

The following chapter explains some features of non-linear finite element analysis. For structures exposed to fire, the requirements in chapter 2 should be applied in the running of analyses.

### 3.1 Problem formulation

Three main principals forms the basis of linear finite element analysis in structural engineering:

- *Equilibrium* between internal and external forces.
- *Kinematic compatibility*. Adjacent elements/components should stay together.
- A *material law*, so that stresses and strains are proportional.

Displacements are assumed small, thus the material is acting linearly elastic,  $\varepsilon_x = \frac{\partial u}{\partial x}$ , and Hooke's law is commonly used. A useful effect of all this is that equilibrium can be established in relation to the original position.

When working with accidental actions, failures such as buckling, fracture, and global collapse might occur. These are non-linear issues, and so the assumptions from linear analysis may no longer be valid. The relation between load and displacement may no longer be proportional as the stresses exceeds the material's yield stress.

Non-linear behaviour in marine structures is often divided into three main effects Moan (2003):

- *Geometrical non-linearity* as the displacements become large, equilibrium can no longer be associated with the initial configuration. The reference frame will then need to be updated
- *Material non-linearity* when moving beyond the elastic range of a material, the stress-strain relationship may exhibit non-linear behaviour. As discussed in section 2.4.1, the temperature also influence material properties.
- *Non-linearity associated to boundary conditions.* Often an issue in contact problems. As contact between two bodies occurs, the boundary conditions change.

Analysis of these types of problems are often complex, and models can be difficult to set up. As computational power has become less expensive, the actual running time of the analyses are now of less importance. It should be mentioned, however, that analyses of both local and global action effects may prove time consuming, and thus it is important to ensure correct modelling.

### 3.1.1 Geometrical non-linearity

As small displacements are assumed in linear analysis, the load carrying mode is unchanged throughout the load history. When surpassing the range of small displacements, the load actions are may be carried by a combination of modes, or be completely transferred to another one. A relevant example is the intersection between girders in the platform deck. If elevated temperatures cause one of them to fail, the bending moment in the other may cause a plastic hinge. The load now has to be carried by membrane forces.

One classical example often used to illustrate geometrical non-linearity, is the two-beam arch (forces, stresses and strains positive in compression).

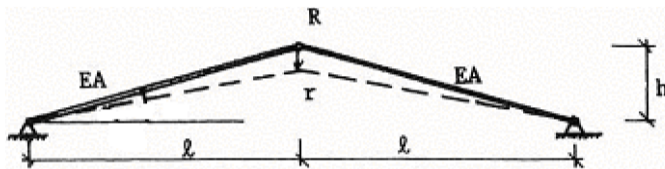


Figure 3.1: Two-beam arch. Figure from Moan (2003)

All three connections are hinged, so the load is carried as membrane stresses. The assumption is that the bars to experience elastic longitudinal deformation,  $\Delta = \varepsilon l$ , as the axial forces,  $S$  must balance the external vertical load,  $R$  see figure (fig3.2).

$$R = 2S \sin\alpha_0 = 2EA\varepsilon \sin\alpha_0 = \frac{2EA}{l} \sin^2\alpha_0 \cos\alpha_0 \cdot r \quad (3.1)$$

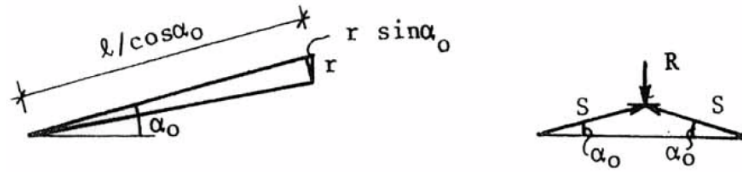


Figure 3.2: Equilibrium consideration. Moan (2003)

See that the stiffness is constant, and related to the original configuration. If, however, the deflection becomes large, the reference system needs to be updated. Now both shortening and displacement in question are finite:

$$\Delta = \frac{l}{\cos\alpha_0} - \frac{l}{\cos\alpha}, \quad (3.2)$$

as shown in figure 3.3.

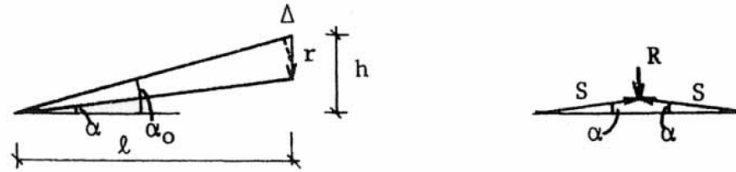


Figure 3.3: Updating reference system. Moan (2003)

The updated axial strain then becomes

$$\varepsilon = \frac{\Delta}{l/\cos\alpha_0} = 1 - \frac{\cos\alpha_0}{\cos\alpha} \quad (3.3)$$

And the updated equilibrium equation can be written as

$$R = \frac{2EA}{l} \left( \frac{h}{r} - 1 \right) \left( \frac{l}{\sqrt{l^2 + (h-r)^2}} - \frac{l}{\sqrt{l^2 + h^2}} \right) \cdot r \quad (3.4)$$

where

$$\sin\alpha = \frac{h-r}{\sqrt{l^2 + (h-r)^2}}, \cos\alpha = \frac{l}{\sqrt{l^2 + (h-r)^2}}, \cos\alpha_0 = \frac{l}{\sqrt{l^2 + h^2}} \quad (3.5)$$

Hence, the stiffness is no longer constant, and the force-displacement relationship is non-linear. If the applied load is plotted against the relationship between displacement and distance to a horizontal configuration, equilibrium is seen to have multiple solutions. As  $r$  moves towards  $h$  (figure 3.4), the two bars have no vertical components to counter the applied load, and the system snaps through, resulting in tensile restoring forces. Trying to solve this problem analytically will be futile, and thus incremental or iterative methods are needed (section 3.2).

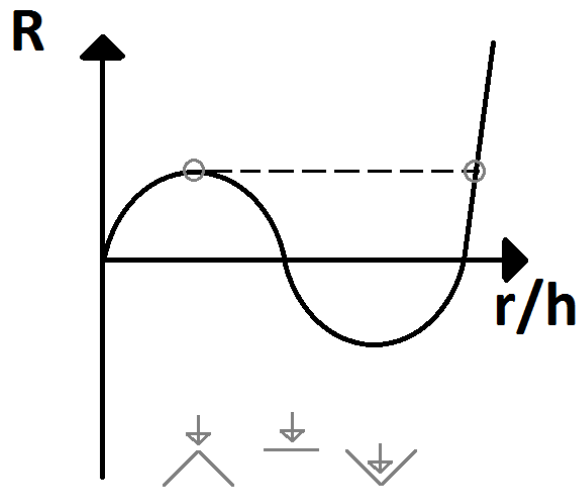


**Figure 3.4:** Equilibrium function (rough sketch). Reproduced from Moan (2003)

### 3.1.2 Material non-linearity

Besides the material properties described in section 2.4.1, there are some other non-linear effects that can change the properties of a material.

The elastic range of material behaviour is not sufficient to describe ultimate strength, buckling and accidental action effects. As the material is strained beyond the elastic range, we end up with permanent plastic strains. In simplified plastic analyses such as plastic mechanism calculations, materials are often assumed linear elastic - perfectly plastic, which means we assume no stresses exceeds the yield limit. In more complicated Finite Element analyses, however, strain hardening is accounted for. Now, both stresses and strains are dependent on the actual strain. Making the problem complex is the fact that the strain is not known in advance.

”A material is called nonlinear if stresses  $\sigma$  and strains  $\varepsilon$  are related by a strain-dependent matrix rather than a matrix of constants.” (Moan 2003)

In order to deal with elastic-plastic actions, three rules are applied:

- *Yield criterion*, defining the point where stresses exceed the elastic range.
- *Hardening rule*, describing the changes of the yield criterion, caused by plastic flow
- *Flow rule*, defining the relation between stress and strain.

### 3.1.2.1 Yield criterion

This states that first yield occurs when the stress,  $\sigma$ , either in compression or tension, reach the yield strength,  $\sigma_Y$  (tensile yield strength most commonly used). If the material is not linear-elastic perfectly-plastic, further yield will then require higher stresses, as hardening effects occur (figure 3.5).

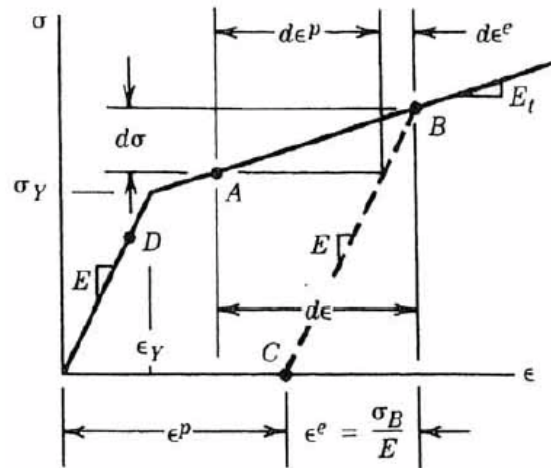


Figure 3.5: Idealized elasto-plastic yield criterion. (Moan 2003)

### 3.1.2.2 Hardening rule

As, mentioned, the yield criterion changes if a material has experienced plastic flow. If, for example the material is loaded to a point  $B > \sigma_Y$  and unloaded down to a point  $C$  (figure 3.5), further yielding will not be achieved until stresses above point  $B$  are experienced. Two different hardening rules usually describe what happens if the material is subsequently loaded in the reverse direction.

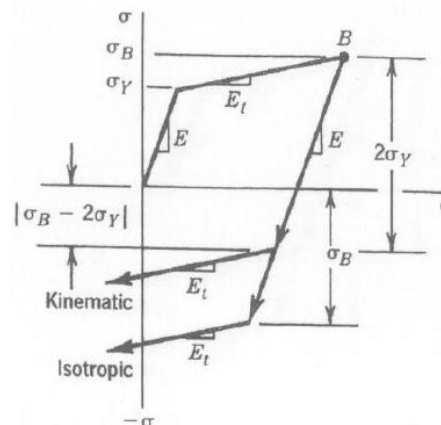


Figure 3.6: Isotropic vs. kinematic hardening. (Moan 2003)

For the most common metals, the **kinematic hardening** rule is applied. This states that when unloading from B, the material acts linearly down a "distance"  $2\sigma_Y$  from point B (figure 3.6).

If, however the material acts linearly down a "distance"  $2\sigma_B$  from point B, an **isotropic** hardening rule is more suiting.

### 3.1.2.3 Flow rule

Material tests have shown that linearity does not apply beyond a proportionality limit,  $\sigma_P$ . As elasto-plastic behaviour is experienced, the Young's modulus will likely change and the strain rate is altered. As the elastic strain rate is already well known, it is convenient to superimpose the elastic and plastic contributions:  $d\varepsilon^e + d\varepsilon^p = d\varepsilon^{true}$ . By using that stress is defined as  $\sigma = E\varepsilon$ , the stress rate can be written as:

$$d\sigma = Ed\varepsilon^e = E(d\varepsilon^{true} - d\varepsilon^p); d\sigma = E_t d\varepsilon^{true}; d\sigma = H' d\varepsilon^p, \quad (3.6)$$

where H' is the plastic tangent modulus,  $\partial\sigma/\partial\varepsilon^p$ , and  $E_t$  is the tangent modulus:

$$E_t = E \left( 1 - \frac{E}{E + H'} \right) \quad (3.7)$$

### 3.1.3 Non-linearity associated to boundary conditions

Most common example is the contact problem. When two objects collide in high energy impacts, the contact area is not constant. Deformation of one object increase the contact area, making further penetration more energy demanding. Friction and soil structure interactions are also examples worth mentioning.

In fire scenarios, large deformations may lead to contact between main structure and equipment, outfitting or piping. If a pipe were to make contact with the main structure, non-linearities of the pipe's boundaries could occur. Another example is joints where several elements meet. If one of them were to fail due to elevated temperature, the boundary for the rest of the elements would change.

## 3.2 Solution procedures

As the simplified analyses in this thesis are of static nature, solution of dynamic problems will not be discussed here.



Figure 3.4 illustrated the fact that the solution needn't be unique for non-linear problems, as opposed to linear analyses where the solution is always unique. Thus, the result of an analysis may not be the correct one. To overcome this, there are several procedures of solving structural problems and they mainly divide in to three groups:

- Incremental procedures
- Iterative procedures
- Combinations of the two above

In order to get a solution, two conditions need to be fulfilled. These are the *total equation of equilibrium*:

$$\Sigma(a^i)^T S^i = R \quad (3.8)$$

and the *incremental equation of equilibrium*:

$$K_i(r)dr = dR \quad (3.9)$$

### 3.2.1 Load incremental methods

To find a unique displacement for a given load, the external load is applied incrementally. The Euler-Cauchy method does exactly that. For each load increment, the displacement increment is found by eq.3.9. The stiffness,  $K$  is kept constant through one load increment, and updated before the next step. Though the stiffness is updated and correct at the beginning of each step, a large step (coarse definition) will cause the result to drift off the exact solution (figure 3.7).

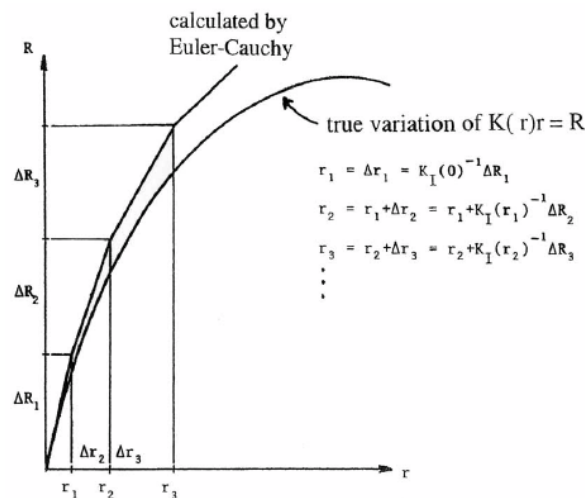


Figure 3.7: Load incremental (Euler-Cauchy) method. (Moan 2003)

To avoid large drift-off, there are procedures to automatically set an appropriate step length in computer programs. A more accurate way, however, is to modify the method by equilibrium correction. The difference between the calculated result for each step and the exact solution is the found and added before the next step. This way, eq. 3.8 is fulfilled before each step (figure 3.8).

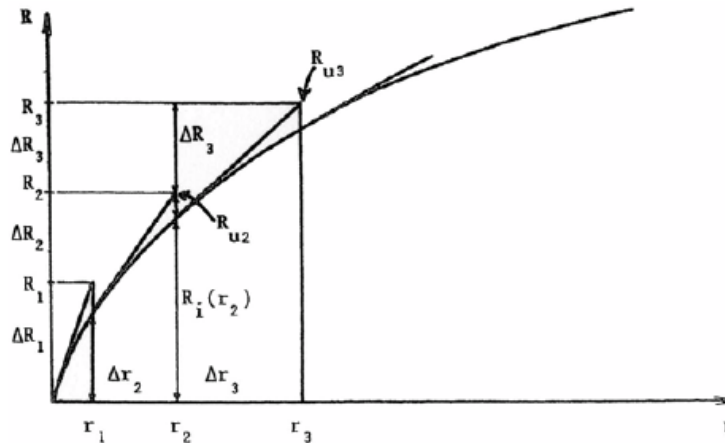


Figure 3.8: Load incremental method with equilibrium correction. Moan (2003)

### 3.2.2 Iterative methods

A common iterative method is the Newton-Raphson method. It is also the one used in USFOS ((Skallerud & Amdahl 2005)), so it will be explained in this section.

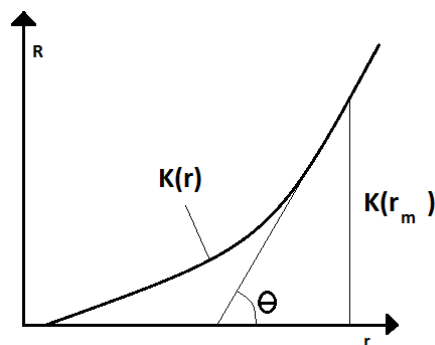


Figure 3.9: Sketched illustration of the Newton-Raphson algorithm.

Newton-Raphson initiates with a increment load value, and utilize tangential stiffness to determine the approximate response. The difference between internal and external forces is then corrected for, and the tangential stiffness is updated. The analysis is complete when the distance between result and exact solution satisfy a convergence criterion. As it is time consuming to update the stiffness for each step, it may be

beneficial to update only after the first step, less frequent, or not at all (figure 3.11) even though more steps are likely needed to get convergence. USFOS, however runs a pure Newton-Raphson procedure (though with arc length control, explained in section 3.2.3), updating the stiffness after every step.

The algorithm for a case solved for  $K(r) = 0$  is:

$$r_{m+1} = r_m - \frac{K(r_m)}{K'(r_m)} \quad (3.10)$$

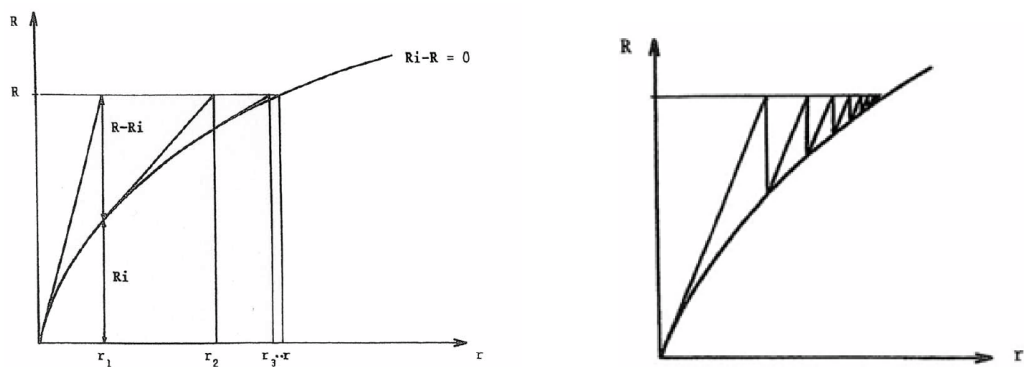


**Figure 3.10:** Pure Newton-Raphson procedure. (Moan 2003) **Figure 3.11:** N - R without updating K. (Moan 2003)

Efficiency can sometimes be improved by using a combination of load a incremental method and an equilibrium iteration method. An example is to first apply an increment load, and then iterate to reach convergence before applying the next load increment.

### 3.2.3 Arc Length Methods

As illustrated in fig. 3.4, information about the load-displacement equilibrium may "get lost" along a load history. In those cases the methods described above will diverge. Another example is when a structure buckles. Tangential stiffness becomes zero, singularity occurs, and the analysis will break down.

Displacement increment control instead of load increments could help avoid some of the problems, but it would fail in so-called snap-back points. Arc length methods will, on the other hand, ensure results in any of these cases.

The arc length method aims to find "a single equilibrium path" defined by a reference load,  $R_{ref}$ , the nodal displacement,  $r$ , and a loading parameter,  $\lambda$ . Both incremental and iterative approach are required to get a solution. It was originally introduced

by Wempner(1971) and Riks(1972)

In USFOS the iterations are made with reference to a normal plane. Thus, external load and displacement vectors are varied along a prescribed function.

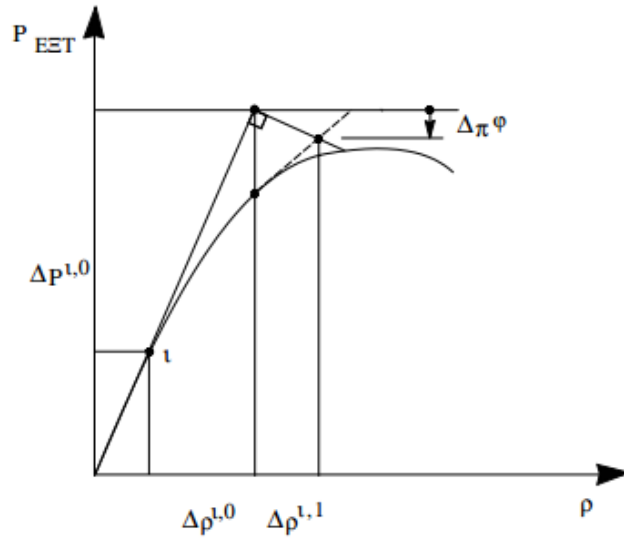


Figure 3.12: USFOS arc length illustration. Skallerud & Amdahl (2005)

The convergence of this method is defined as:

$$\begin{aligned} \delta r_{it}^j &= \frac{|\Delta r^{i,j}|}{|\Delta r^{i,0}|} \\ \delta R_{it}^i &= \frac{|\Delta R^{i,j}|}{|\Delta R^{i,0}|}, \end{aligned} \quad (3.11)$$

where  $i$  and  $j$  are iteration and step respectively. The actual convergence is tested on displacement only:

$$\delta r_{it} \leq \varepsilon_{it} \quad (3.12)$$

# Chapter 4

## Simulation tools

This chapter describes the simulation software used for simulating fire loads and structural response. The documentation files of the programs are briefly discussed, as they provide more understanding about the physics of the problems.

### 4.1 FAHTS

FAHTS is a Finite Element program designed to work effective in connection with USFOS (SINTEF 1994). It uses the same structural model file as USFOS, but as the heat transfer problem requires 3D elements the beam elements are automatically re-meshed. The temperature results are then written as beam element temperatures, to fit USFOS analysis. Fahts was originally written as a link between the computational fluid dynamics software Kameleon FireEx and USFOS, but has simplified fire scenario models built in. These simplified models are used for the heat transfer simulations in this thesis.

The governing equation for heat flow used in FAHTS is Fourier's law for heat flow through a medium:

$$\rho c \frac{\partial T}{\partial t} = \frac{\partial}{\partial x} \left( k_x \frac{\partial T}{\partial x} \right) + \frac{\partial}{\partial y} \left( k_y \frac{\partial T}{\partial y} \right) + \frac{\partial}{\partial z} \left( k_z \frac{\partial T}{\partial z} \right) + q \quad (4.1)$$

$\rho$  Specific weight of the medium [ $kg/m^3$ ]

$c$  Specific heat of the medium [ $J/kgK$ ]

$T$  Temperature [ $K$ ]

$t$  Time [ $s$ ]

$x,y,z$  Spatial coordinates [ $m$ ]

$k_{x,y,z}$	Thermal conductivities in x, y and z direction [ $W/mK$ ]
$q$	Heat input to the system [ $W/m^3$ ]

As this is not possible to solve analytically for the general case, discrete models are applied.

#### 4.1.1 Finite element approach

As mentioned, simplifications are necessary to solve the transient heat transfer problem. The first step is to transform the problem into two dimensions, taking care to define the heat input as the heat exchange between medium and surroundings. Note also that  $\mathbf{q}$  does not represent a true boundary condition, but will rather act as  $q = q_s/d$ , meaning the intermedium cross heat flow,  $\mathbf{q}_s$  across the thickness,  $\mathbf{d}$  of the medium:

$$\rho c \frac{\partial T}{\partial t} = \frac{\partial}{\partial x} \left( k_x \frac{\partial T}{\partial x} \right) + \frac{\partial}{\partial y} \left( k_y \frac{\partial T}{\partial y} \right) + q \quad (4.2)$$

For this to be true, the prescribed heat flow across the true boundaries,  $\bar{\mathbf{q}}$  across the true boundaries and temperature,  $\bar{T}$ , must equal the calculated values  $\mathbf{q}$  and  $\mathbf{T}$ . At any point of the boundary,  $\Gamma$  either flux or temperature must be prescribed, but at no point can they be prescribed simultaneously. They are denoted  $\Gamma_{\mathbf{q}}$  and  $\Gamma_{\mathbf{T}}$ , and the following relation applies:

$$\Gamma_q \cup \Gamma_T = \Gamma, \quad \Gamma_q \cap \Gamma_T = 0 \quad (4.3)$$

This yields the boundary conditions:

$$T - \bar{T} = 0 \quad \text{on } \Gamma_T \quad (4.4)$$

$$k_x \frac{\partial T(x, y)}{\partial n_x} + k_y \frac{\partial T(x, y)}{\partial n_y} - \bar{q} = 0 \quad \text{on } \Gamma_q \quad (4.5)$$

where  $\mathbf{n}_{x,y}$  are the in plane surface normals, normal to the boundary,  $\Gamma$ .

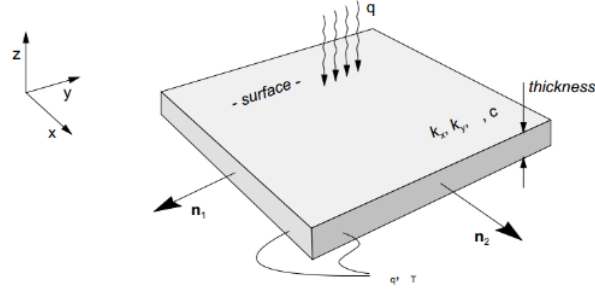


Figure 4.1: (SINTEF 1994). 2D heat transfer problem

The weak form of the problem is obtained by use of the Galerkin method of weighted residuals. Arbitrary functions  $v$  and  $\bar{v}$  are applied, and general functions,  $\mathbf{A}(\mathbf{u})$  and  $\mathbf{B}(\mathbf{u})$  linearly dependent on  $u \equiv T$  are put in for the differential equations above. The natural domain,  $\Omega$  is reduced to a sub-domain,  $\bar{\Omega}$  where the time variable is left out. Time dependent solutions are obtained in a next step by means of a time stepping algorithm. From equations 4.4 and 4.5, the boundary conditions have to be zero at each point:

$$\int v A(T) d\bar{\Omega} + \int \bar{v} B(T) d\Gamma = 0 \quad (4.6)$$

The temperature is defined at each point in  $\Omega$  with the use of shape functions:

$$T(x, y, t) = \sum_{i=1}^n N_i(x, y) T_i(t) = \mathbf{N}\mathbf{T} \quad (4.7)$$

To fulfill equation 4.6, it is obvious that the arbitrary functions  $v$  and  $\bar{v}$  are not sufficient. Thus, they are replaced by a set of weight functions  $w$  and  $\bar{w}$ , and the differential equations become:

$$\int_{\bar{\Omega}} w_j A(\mathbf{N}\mathbf{T}) d\bar{\Omega} + \int_{\Gamma} \bar{w}_j B(\mathbf{N}\mathbf{T}) d\Gamma = 0, \quad j = 1, n \quad (4.8)$$

Note that the residual may be non-zero in certain points, but equation 4.8 ensure the integrated average residual is zero. The Galerkin approach is then to set the weight functions equal the shape functions. As they can be defined arbitrarily,  $w_j = \bar{w}_j$  is a possibility. Choosing shape functions can be done on an element level and summed over all elements in  $\Omega$ , hence the Finite Element method is obtained. Already established equations and boundary conditions, for the transient problem:

$$A(t) = \frac{\partial}{\partial x} \left( k_x \frac{\partial T}{\partial x} \right) + \frac{\partial}{\partial y} \left( k_y \frac{\partial T}{\partial y} \right) + Q - c \frac{\partial T}{\partial t} = 0 \quad (4.9)$$

$$B(T) = T - \bar{T} = 0, \quad \text{on } \Gamma_T \quad (4.10)$$

$$k_x \frac{\partial T}{\partial x} k_y \frac{\partial T}{\partial y} - \bar{q} = 0, \quad \text{on } \Gamma_q \quad (4.11)$$

These are put into equation 4.8, with the proposed use of shape functions as weight functions and the use of the identity in equation 4.3. The resulting heat flow balance on element level is:

$$\mathbf{m}\dot{\mathbf{T}} + \mathbf{k}\mathbf{T} = \mathbf{Q}_g + \mathbf{Q}_q = \mathbf{Q} \quad (4.12)$$

where the element conductivity matrix,  $\mathbf{m}$ , specific heat matrix,  $\mathbf{m}$ , surface heat flow vector,  $\mathbf{Q}_g$  and edge heat flow vector,  $\mathbf{Q}_q$  are expressed:

$$\mathbf{k} = \int_{A_e} \left[ \frac{\partial N_j}{\partial x} k_x \frac{\partial N_i}{\partial x} + \frac{\partial N_j}{\partial y} k_y \frac{\partial N_i}{\partial y} \right] dA = \int_{A_e} \mathbf{N}_{,x}^T \mathbf{k} \mathbf{N}_{,x} dA \quad (4.13)$$

$$\mathbf{m} = \int_{A_e} \rho c N_j N_i dA = \int_{A_e} \rho c \mathbf{N}^t \mathbf{N} dA \quad (4.14)$$

$$\mathbf{Q}_g = \int_{A_e} N_j Q dA = \int_{A_e} \mathbf{N} Q dA \quad (4.15)$$

$$\mathbf{Q}_q = \int_{L_B} N_j \bar{q} dl = \int_{L_B} \mathbf{N} \bar{q} dl \quad (4.16)$$

For the whole system, at time instant  $i$ , the equation reads:

$$\mathbf{M}_i \dot{\mathbf{T}}_i + \mathbf{K}_i \mathbf{T}_i = \mathbf{Q}_i \quad (4.17)$$

### 4.1.2 Time domain integration

As both conductance, heat capacity and heat load vector tends to be temperature dependent, non- linearity will occur for the transient heat flow problem:

$$\mathbf{M}(T)\dot{\mathbf{T}} + \mathbf{K}(T)\mathbf{T} = \mathbf{Q} \quad (4.18)$$

Starting with a known temperature  $\mathbf{T}_{i-1}$ , numerical integration is applied over a time interval  $\Delta t = t_i - t_{i-1}$  assuming linear temperature variation (figure 4.2):

$$\mathbf{T} \approx \mathbf{T}(\tau) = \mathbf{T}_{i-1} + \frac{\tau}{\Delta t} (\mathbf{T}_i - \mathbf{T}_{i-1}) \quad (4.19)$$

where  $\tau = t - t_{i-1}$



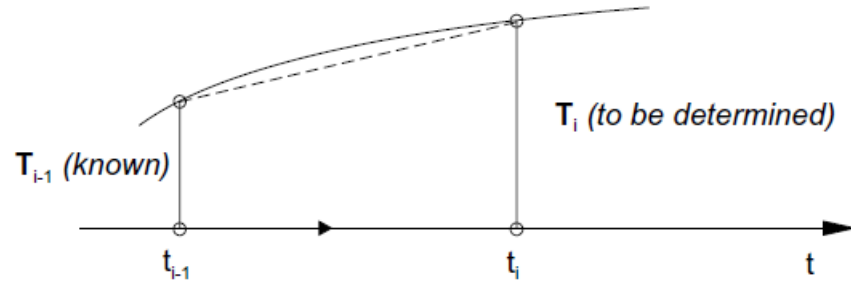


Figure 4.2: (SINTEF 1994). Linear approximation of temperature in time domain

The weighted residual principle is applied to equation 4.18, the heat flow in a time interval  $\Delta t$  becomes:

$$\int_0^{\Delta t} w \left( \mathbf{M}\dot{\mathbf{T}} + \mathbf{K}\mathbf{T} - \mathbf{Q} \right) d\tau = 0 \quad (4.20)$$

A small time interval provides the assumption that  $\mathbf{K}$  and  $\mathbf{M}$  are constant. By introducing an average heat load vector,  $\bar{\mathbf{Q}}$  and a weight parameter  $\theta$ :

$$\mathbf{M}(\mathbf{T}_i - \mathbf{T}_{i-1}) \frac{1}{\Delta t} + \mathbf{K}[\mathbf{T}_{i-1} + \theta(\mathbf{T}_i - \mathbf{T}_{i-1})] = \bar{\mathbf{Q}}, \quad (4.21)$$

where the weight parameter is defined as:

$$\theta = \frac{1}{\Delta t} \frac{\int_0^{\Delta t} w\tau d\tau}{\int_0^{\Delta t} w d\tau} \quad (4.22)$$

On incremental form, equation 4.21 can be written:

$$\mathbf{M}_i \frac{\Delta \mathbf{T}}{\Delta t} + \mathbf{K}_i \mathbf{T}_{i-1} + \theta \mathbf{K}_i \Delta \mathbf{T} = \bar{\mathbf{Q}} \quad (4.23)$$

If  $\mathbf{Q}$  is assumed linear over  $\Delta t$ :

$$\begin{aligned} \bar{\mathbf{Q}} &= \mathbf{Q}_{i-1} + \theta(\mathbf{Q}_i - \mathbf{Q}_{i-1}) \\ \Rightarrow (\mathbf{K}_i + \frac{1}{\theta \Delta t} \mathbf{M}_i) \Delta T &= \mathbf{Q}_i + \frac{1-\theta}{\theta} \mathbf{Q}_{i-1} - \frac{1}{\theta} \mathbf{K}_i \mathbf{T}_{i-1} \end{aligned} \quad (4.24)$$

In FAHTS, a weight parameter of  $\theta = 1/2$  is used. As  $\mathbf{K}$  is assumed constant during the time step the last term,  $\mathbf{K}_i \mathbf{T}_{i-1}$  can be replaced by  $\mathbf{K}_{i-1} \mathbf{T}_{i-1}$  and the incremental equation becomes:

$$(\mathbf{K}_i + \frac{2}{\Delta t} \mathbf{M}_i) \Delta T = \mathbf{Q}_i + \mathbf{Q}_{i-1} - 2\mathbf{K}_{i-1} \mathbf{T}_{i-1} \quad (4.25)$$

Solving this is done with an incremental procedure with equilibrium correction. The correction is done on last step's heat load:

$$\mathbf{Q}_{i-1} = \mathbf{M}_{i-1}\dot{\mathbf{T}}_{i-1} + \mathbf{K}_{i-1}\mathbf{T}_{i-1} , \quad (4.26)$$

and the equation ends up in the form:

$$\mathbf{A}\Delta\mathbf{T}_i = \mathbf{B} \quad (4.27)$$

Solved for  $\Delta\mathbf{T}_i$ :

$$\Delta\mathbf{T}_i = \mathbf{A}^{-1}\mathbf{B} , \quad (4.28)$$

where:

$$\mathbf{A} = \left( \mathbf{K}_i + \frac{2}{\Delta t}\mathbf{M}_i \right) \quad (4.29)$$

$$\mathbf{B} = \mathbf{Q}_i - \mathbf{K}_{i-1}\mathbf{T}_{i-1} + \mathbf{M}_{i-1}\dot{\mathbf{T}}_{i-1} \quad (4.30)$$

And, finally, the temperature in at time  $t_i$  can be found before the next step:

$$\mathbf{T}_i = \mathbf{T}_{i-1} + \Delta\mathbf{T}_i \quad (4.31)$$

### 4.1.3 Heat sources

Radiation and convection energy balance is described in the theory manual. The method is already covered in section 2.4.2 and will not be repeated here. But some of the simplified heat transfer functions used are described.

**Time dependent Concentrated source**, defined by its coordinates and energy emittance. Heat radiating equally in all directions, giving heat flux in an element located a distance,  $r$  from the source:

$$q_i = \frac{E}{4\pi r_i^2} \cos(\theta_i) \quad (4.32)$$

- $q_i$  Heat flux received by the element
- $E$  Total energy emittance from the source
- $r_i$  Distance between source and element midpoint
- $\theta_i$  Angle between surface normal and incident ray

The source energy emittance can be made time dependent, simulating a variable heat input.

**Time dependent Line Source** Defining a size, shape and energy emittance, a line source can be specified. This is done by adding contributions from several concentrated sources along a line. The shape is limited to a cylinder, but the end diameters does not need do be equal so a cone is obtainable. The same goes for the energy emittance; different intensities can be specified for each end. The total heat flux received by an element, using equation 4.32 becomes:

$$Q = \sum_{i=1}^n q_i(E_i, r_i, \theta_i) \quad (4.33)$$

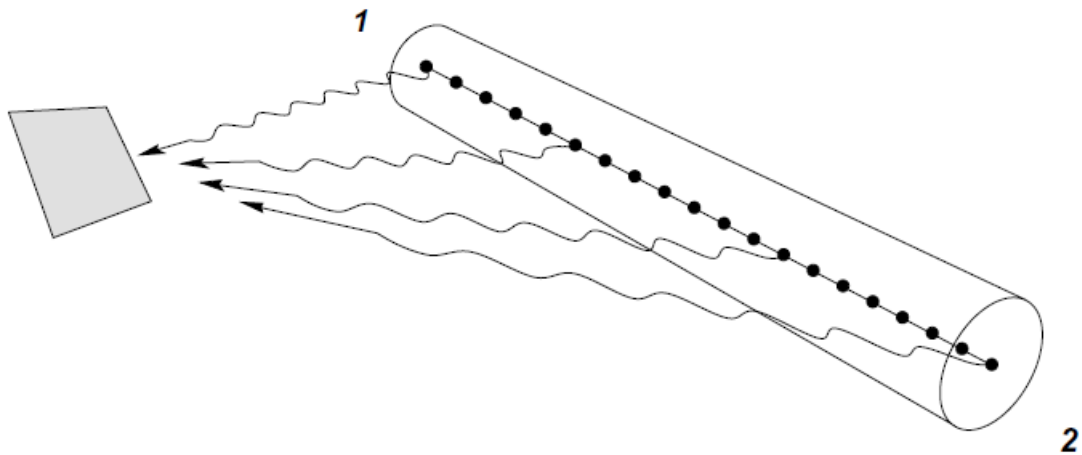


**Figure 4.3:** (SINTEF 1994). Line source model in FAHTS

The end forces are given a weight factor of 1/2,

**HC-fire.** FAHTS has the standard temperature curves HC-fire (figure 2.12) and ISO-fire built in. All outside surfaces in a given volume are assumed exposed to the temperature load. The surrounding gas emissivity coefficient is set to be 1.

## 4.2 USFOS

USFOS is a numerical tool for ultimate strength and progressive collapse analysis of space frame structures. (SINTEF 2001)

This section will give a short explanation of a few key features about USFOS, the program which was used for structural response simulations. It is preferred by many for conducting ultimate strength analysis on offshore frame structures due to

it's sophisticated beam element formulation. Since it is developed locally, there is also a little prestige in using it on thesis work. As the simplified calculations done in this thesis are of a static nature, dynamic issues will not be addressed.

### 4.2.1 Beam element formulation

As mentioned, USFOS is often preferred for frame analysis as its original main purpose was beam and frame calculation. Using the Green strain formulation, the USFOS' beam element is valid for large displacements:

$$\varepsilon_x = u_{,x} + \frac{1}{2}u_{,x}^2 + \frac{1}{2}v_{,x}^2 + \frac{1}{2}w_{,x}^2 \quad (4.34)$$

Tangent and secant stiffness matrices are obtained from shape functions,  $\phi$  to the displacements:

$$\begin{aligned} u(x) &= \phi^T q_u \\ v(x) &= \phi^T q_v \\ w(x) &= \phi^T q_w \end{aligned} \quad (4.35)$$

These are recognized as the Livesly stability function, and give the exact solution to the 4<sup>th</sup> order differential equation for beams with end loading. As this closed form solution is obtained, the discretization of a frame structure can be very coarse. In fact, one element per structural member gives satisfactory results, thus making the analysis very effective.

An example in the use of Livesly's stability functions is a beam with axial loading (chapter 2.8. Amdahl (2005)):

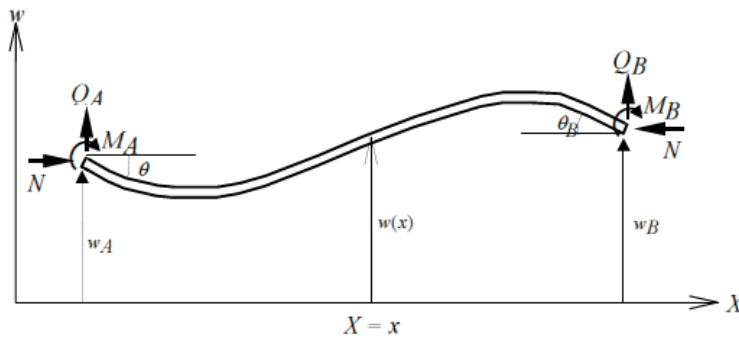


Figure 4.4: Beam loaded with end moments and axial compressive force.

Considering the virtual work done by internal and external moments:

$$\begin{aligned} M_i &= -EIw_{,xx} \\ M_e &= M_A + Q_A X - N(w - w_A), \end{aligned} \quad (4.36)$$

equilibrium becomes (with  $k^2 = \frac{N}{EI}$ ):

$$\begin{aligned} M_i + M_e &= 0 \\ \Rightarrow w_{,xx} + k^2 w &= \frac{1}{EI}(M_A + Q_A + Nw_A), \end{aligned} \quad (4.37)$$

The solution of the differential equation (homogeneous and particular):

$$w(x) = C_1 \sin(kx) + C_2 \cos(kx) + \frac{1}{N}(M_A + Q_A x + Nw_A), \quad (4.38)$$

together with the boundary conditions:

$$\begin{aligned} w(0) &= w_A, \quad w_{,x}(0) = -\theta_A \\ w(L) &= w_B, \quad w_{,x}(L) = -\theta_B, \end{aligned} \quad (4.39)$$

gives the stiffness matrix:

$$\begin{bmatrix} Q_A \\ M_A \\ Q_B \\ M_B \end{bmatrix} = \begin{bmatrix} \frac{12EI}{l^3} \phi_5 & -\frac{6EI}{l^2} \phi_2 & -\frac{12EI}{l^3} \phi_5 & -\frac{6EI}{l^2} \phi_2 \\ & \frac{4EI}{l} \phi_3 & \frac{6EI}{l^2} \phi_2 & \frac{2EI}{l} \phi_4 \\ & & \frac{12EI}{l^3} \phi_5 & \frac{6EI}{l^2} \phi_2 \\ \text{symm} & & & \frac{4EI}{l} \phi_3 \end{bmatrix} \begin{bmatrix} w_A \\ \theta_A \\ w_B \\ \theta_B \end{bmatrix} \quad (4.40)$$

In the referred chapter, the stability functions are expressed in terms of the axial force normalized to the Euler buckling load:

$$\beta = \frac{\pi}{2} \sqrt{\frac{N}{N_E}}, \quad N_E = \frac{\pi^2 EI}{l^2}$$

Compression	Tension
$\phi_1 = \frac{\beta}{\tan \beta}$	$\phi_1 = \frac{\beta}{\tanh \beta}$
$\phi_2 = \frac{1}{3} \frac{\beta^2}{(1 - \phi_1)}$	$\phi_2 = \frac{1}{3} \frac{\beta^2}{(\phi_1 - 1)}$
$\phi_3 = \frac{1}{4} \phi_1 + \frac{3}{4} \phi_2$	$\phi_3 = \frac{1}{4} \phi_1 + \frac{3}{4} \phi_2$
$\phi_4 = -\frac{1}{2} \phi_1 + \frac{3}{2} \phi_2$	$\phi_4 = -\frac{1}{2} \phi_1 + \frac{3}{2} \phi_2$
$\phi_5 = \phi_1 \phi_2$	$\phi_5 = \phi_1 \phi_2$

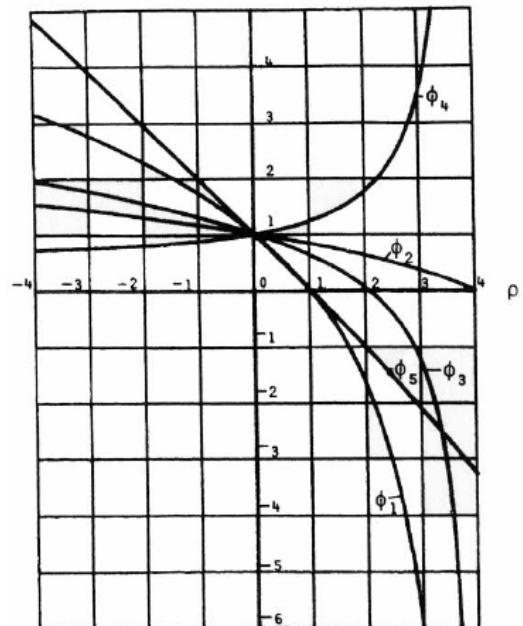


Figure 4.5:  $\phi$ -functions expressed with normalized axial force. Amdahl (2005)

## 4.2.2 Plasticity

Material non-linearities are modelled as plastic hinges in USFOS. They are inserted in the element midspan or at the ends. When the element hinges at midspan, it is automatically sub-discretized into two elements.

As mentioned in the section about material non-linearity (3.1.2), plasticity calculations need three rules.

### 4.2.2.1 Yield condition

The yield condition in USFOS is represented by a yield surface (sketched in figure 4.6) for stress resultants. For tubular cross-sections, neglecting shear and torsion, this surface is defined as:

$$\begin{aligned} \Gamma &= f\left(\frac{N}{N_P}, \frac{M_y}{M_P}, \frac{M_z}{M_P}\right) - 1 \\ &= \cos\left(\frac{\pi}{2} \frac{N}{N_P}\right) - \frac{\sqrt{M_y^2 + M_z^2}}{M_P} = 0 \end{aligned} \quad (4.41)$$

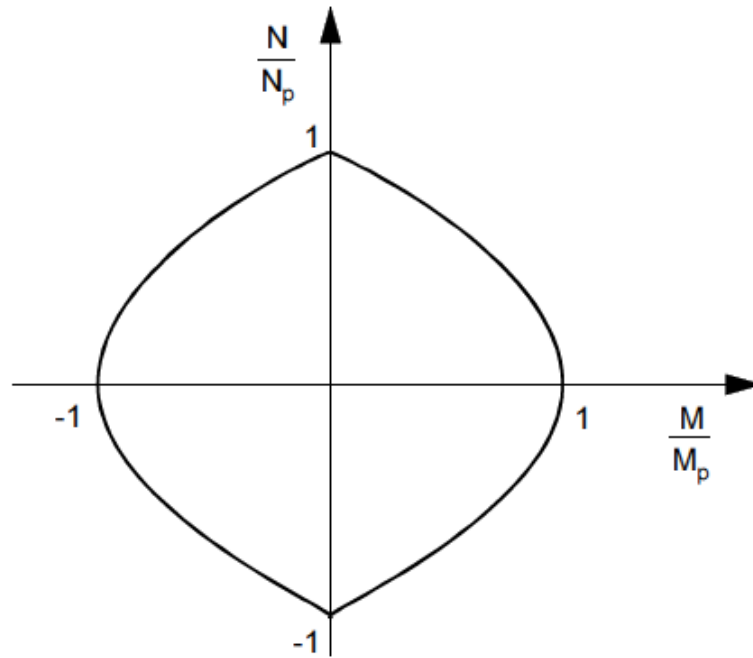


**Figure 4.6:** Example sketch of a yield surface. (Amdahl 2005)

$\Gamma$  is defined to be zero for a combination of forces giving full plasticity. In other words; with no forces (origin)  $\Gamma = -1$ , and  $\Gamma$  is not allowed to have positive values (can not go outside the yield surface).

#### 4.2.2.2 Flow rule

The relation between plastic strain and stress is called the flow rule, and in USFOS it states that the plastic displacements,  $\Delta v^P$  are normal to the yield surface,  $\Delta g$  at end  $i$  of the beam:

$$\Delta v^P = \begin{bmatrix} g_1 & 0 \\ 0 & g_2 \end{bmatrix} \begin{bmatrix} \Delta \lambda_1 \\ \Delta \lambda_2 \end{bmatrix} = G \Delta \lambda \quad (4.42)$$

$$g_i^T = \frac{\partial \Gamma}{\partial S_i} = \left[ \frac{\partial \Gamma}{\partial N}, \frac{\partial \Gamma}{\partial Q_y}, \frac{\partial \Gamma}{\partial Q_z}, \frac{\partial \Gamma}{\partial M_x}, \frac{\partial \Gamma}{\partial M_y}, \frac{\partial \Gamma}{\partial M_z} \right]_i$$

The scalar factor,  $\Delta \lambda$  give us the magnitude of the plastic displacement.

#### 4.2.2.3 Hardening rule

The hardening rule determines how the state of plasticity changes. When for example plastic hinges are formed, extra loads cannot be carried by bending action, but membrane action is mobilized. Thus the state of plasticity is moved along the

yield curve (up towards  $\frac{N}{N_P} = 1$  in figure 4.6). Mathematically, for a linear elastic perfectly plastic material, it is expressed:

$$\begin{aligned} \Delta\Gamma &= \frac{\partial\Gamma}{\partial N}\Delta N + \frac{\partial\Gamma}{\partial Q_y}\Delta Q_y + \frac{\partial\Gamma}{\partial Q_z}\Delta Q_z + \frac{\partial\Gamma}{\partial M_x}\Delta M_x + \frac{\partial\Gamma}{\partial M_y}\Delta M_y + \frac{\partial\Gamma}{\partial M_z}\Delta M_z \\ &= g^T \Delta S_i = 0 \end{aligned} \tag{4.43}$$

### 4.2.3 Load control

As mentioned in section 3.2.2, USFOS uses pure Newton-Raphson iteration with arc length control. This is to some extent controlled by the user, as the load stepping is defined in the header file. The user defines a reference load, number of post-collapse steps, load factor, max load and number of steps of the analysis. If the step length is too large, USFOS scales it down, so that the load state does not exceed the yield surface.



# Chapter 5

## Early design of unmanned wellhead platform

This chapter deals with design of the platform. Dimensions of a few key structural elements are picked out based on quick assumptions of the operating and accidental loading situation. The philosophy is that the structural elements should be reasonably robust, so as to try to avoid the use of passive fire protection. The resulting finite element model is presented and evaluated.

### 5.1 Comparable structures

In order to make a reasonable and realistic model of an unmanned wellhead platform some considerations need to be taken. A tradition in the maritime industry is to look at what already exists, and then modify for specific needs. This was done by looking at nearly unmanned platforms, and choosing one that operates in Norway. By looking at recent publications of Kværner's design, as well as regulations regarding strength requirements, a model was sketched and later modelled in FEM-software.

The unmanned wellhead platform concept is said to be unique as there is no living quarters on board, there are comparable unmanned platforms already operating. BP's platform Tambar is a generally unmanned wellhead platform, but with a heli-deck and accommodation for crew to live in during service work. It operates in 68 [m] of water depth, has a topside weight of 800 [tonn] and is resting on a tripod jacket structure weighing 1200 [tonn]. The available deck space on Tambar is 400 [m<sup>2</sup>].

Kværner has published images of their design, with the topside turned 45° in relation to a four-legged jacket. This will accommodate easier access to the topside edge for a jack-up drilling rig, as two of it's legs can move in line with one of the jacket

corners.

The chosen platform concept for this thesis is three decks of 20 [m] $\times$ 20 [m] turned 45° in relation to a jacket foundation. It will look similar to Kværner's concept.



**Figure 5.1:** (Lorentzen 2015). Early concept sketch of Kværner's UWP

## 5.2 Load specification

### 5.2.1 Functional loads

Even though a formal collaboration did not work out, some tips and guidance were given from Kværner's representative, Trond Granli. On the basis of comparable structures, he helped define reasonable functional loads. These have been the basis for design and applied loads for the unmanned wellhead platform. Intuitively, the steel and equipment weights adds up to the total topside weight of 800 tonnes. Note that wireline equipment on topside deck is a functional load, only applied in certain operational conditions. The case of cantilever collapse is an accidental load, in the event that a large fire should weaken the drilling rig's structural integrity enough for the cantilever to touch down on the topside deck. Operational and accidental load conditions are explained to detail in chapter 6.

Functional loads are presented below:

Anders Strand

<b>Permanent load</b>	
Steel weight	400 tonnes
Equipment, mezzanine deck	150 tonnes
Equipment, cellar deck	250 tonnes
<b>Variable load, maintenance</b>	
Wireline operation equipment distributed on half the deck area	150 tonnes
<b>Accidental load, JUR cantilever collapse</b>	
Two point loads on topside nodes	2 x 500 tonnes

**Table 5.1:** Functional and accidental load specification

### 5.2.2 Heat loads

A set of characteristic fire scenarios were provided by Kværner. They had run simulations on a very early version of their design. The fires are defined below.

Associated func. load	Initial heat flux	Release rate	Dimensions [m]	Dur [min]
Well int.+jet fire	250 [ $kW/m^2$ ]	> 0.1 [ $kg/s$ ]	10 x 2.5	60
Well int.+pool fire	150 [ $kW/m^2$ ]	> 0.1 [ $kg/s$ ]	10 x 10	30

**Table 5.2:** Specified characteristic fire scenarios

Two small notifications are made: The dimensions of the pool fire are set to be 10  $m^2$  of deck area times 10  $m$  height. The energy values are not necessarily the same as guidance values in section 2.5.1.

The durations are set to check against burn- out of the wells. It is estimated that the fuel supply runs dry in the tabulated time periods. Thus, the requirement is that the platform should maintain structural stability throughout the fire duration, as opposed to just ensuring evacuation.

## 5.3 Quick dimensioning

As this thesis does not use a real structure, no time is spent dimensioning the structure in detail. The main structural elements needs to be reasonable, however, in order to investigate the degradation of structural integrity due to fire. Thus, a rough estimation of a few of the profiles is carried out, to ensure close to realistic capacity. The partial safety factors from NORSOK N-001 (N-001 2012) are used in combination with material factor (figure 2.4). As no environmental load conditions are considered in this work, ULS-a is chosen:  $\gamma_{ULS} = 1.3$  and  $\gamma_{M_0} = 1.15$ . Giving a total safety factor:

$$\gamma_{tot} = \gamma_{ULS} \cdot \gamma_{M_0} \sim 1.5 \quad (5.1)$$

NORSOK N-003 (N-003 2007), table 1 (figure 2.5) regulates the minimum intensity of deck area actions. A dimensioning distributed deck load should be no less than  $15 [kN/m^2]$ .

The layout of one quadrant ( $10 [m] \times 10 [m]$ ) a deck is sketched below. Stiffener spacing of  $0.6 [m]$  is chosen, as that is a common measure. Deck beam spacing is set to  $2.5 [m]$ . Heavy girders goes on the diagonals between jacket legs (centre lines) and around the perimeter of the deck. It follows that both deck beam- and girder length will be  $10 [m]$ .

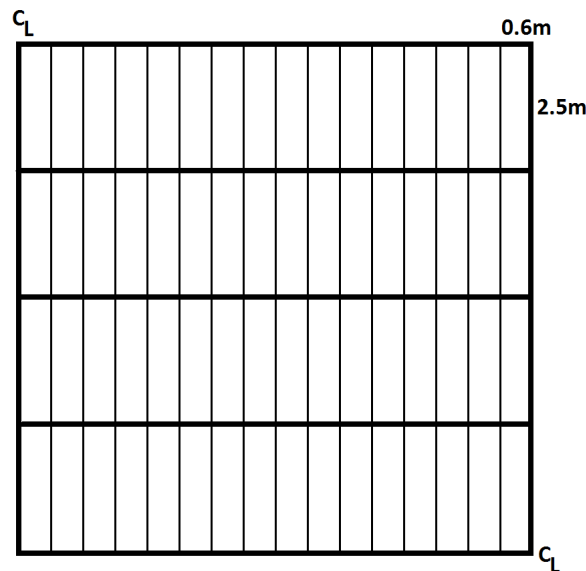


Figure 5.2: Deck layout of one quadrant.

### 5.3.1 Deck plates

Topside- and cellar deck have plate decks. Using plate strip theory and the loads from table 5.1, the stresses of the plate field are estimated quickly. Though shear stresses are distributed as a parabola over a rectangular cross section, a conservative mean shear stress is considered to interact with the axial stresses from bending action in the outer fibre when calculating von Mises stresses (figure 5.3a).

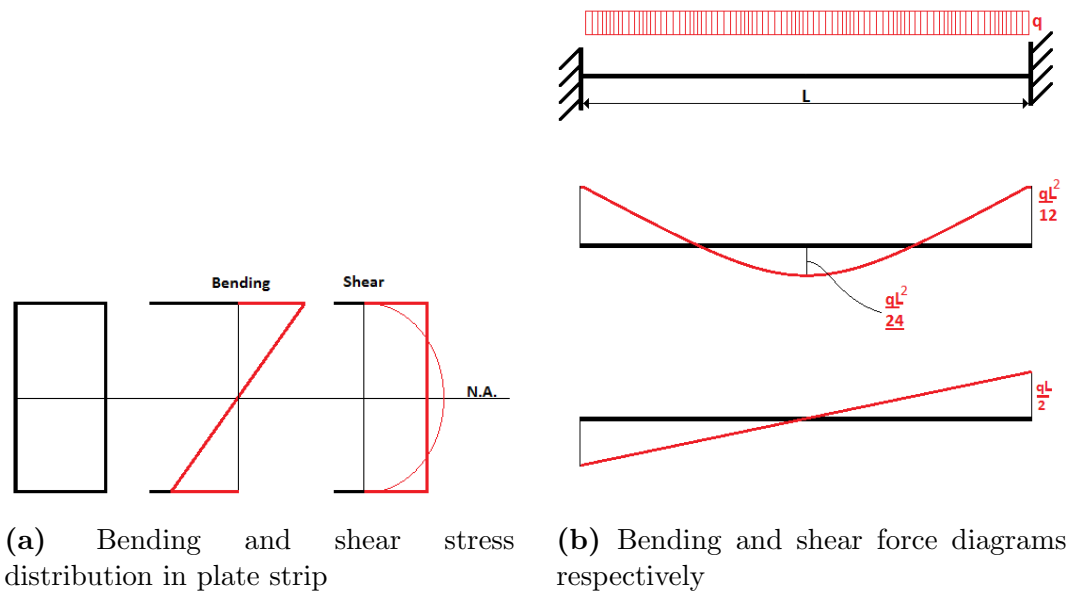


Figure 5.3: Beam theory figures

Other than the aforementioned simplification, classical beam theory is applied on the plate strip, giving moment and shear force distribution as shown in figure 5.3b. The plate strip length is set to be 0.6 [m], as that is the stiffener spacing.

The line load applied is calculated by assuming the equipment weight is smeared over the plate field and that the plate weight is negligible compared to the functional load.

$$deck\ pressure = \frac{250 \cdot 10^3 [kg] \cdot 9.81 [N/kg]}{400 [m^2]} = 6131.3 [N/m^2] \quad (5.2)$$

Unit width plate strip:

$$q = deck\ pressure \cdot 1 [m] = 6131.3 [N/m] \quad (5.3)$$

See that the minimum load from NORSOK N-003 is well above the calculated load level, and will be used for stress calculations.

The stress calculations now needs three additional formulas. Section modulus of the rectangle cross section:

$$W = \frac{bt^3}{6} \quad , \quad (5.4)$$

axial stress due to bending moment:

$$\sigma_x = \frac{M}{W} \quad , \quad (5.5)$$

and simplified mean shear stress:

$$\tau_{xz} = \frac{V}{A} \quad . \quad (5.6)$$

- b "unit width" of the cross section.
- t plate thickness.
- q distributed load a plate strip is subjected to.
- W section modulus of the rectangular plate strip.
- M bending moment at end point of plate strip.
- V shear force at end point of plate strip.
- A cross sectional area of plate strip.

Three plate thicknesses are investigated in a spreadsheet, before choosing one to use in the model for analyses.

Thickness [mm]	$\sigma_x$ [MPa]	$\tau_{xz}$ [MPa]
6	75	0.75
8	42.2	0.56
10	27.0	0.45

**Table 5.3:** Stresses in deck plates due to distributed loads.

More stresses will be accumulated in the plates, as they function as flanges for stiffeners and some cases girders. Thus, it is too soon to make a choice of plate thickness yet.

The failure mode of a stiffened plate field will determine where the most concentrated stresses are located (figure 5.4). And though these stress concentrations will be dimensioning for the plate thickness, the strip theory result is used for the deck plates in this early design phase. Local plate yielding is not deemed critical for the structure if it is satisfactory supported.

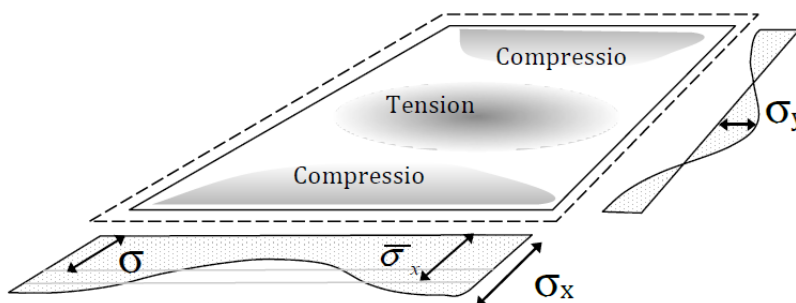


**Figure 5.4:** Post buckling stress distribution in a inter-stiffener plate field. (Amdahl 2005)

### 5.3.2 Stiffeners

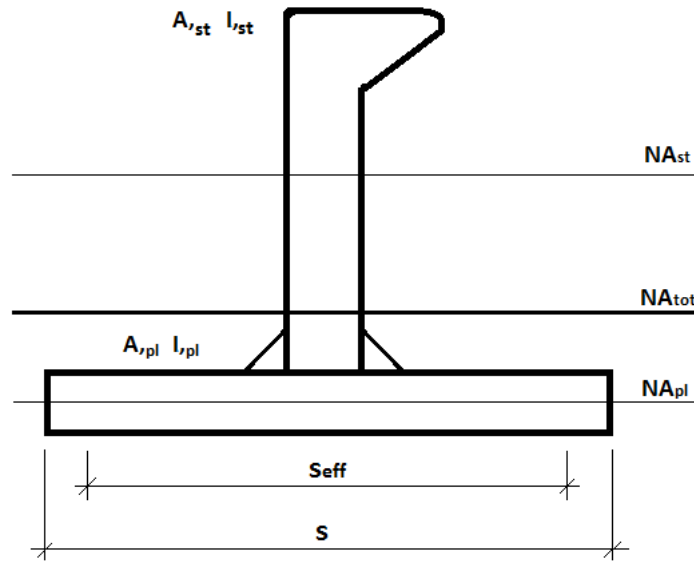


Figure 5.5: Bulb flat stiffener with plate flange

Profile data from a supplier's catalogue is used when dimensioning stiffeners and girders (DentSteel 2016). The stiffener length is 2.5 [m], as it fits well with platform dimensions of 20 x 20 [m<sup>2</sup>]. As bulb flat profiles, or Holland profiles, are commonly used in offshore structures and ships, three types are checked for this platform:

- HP80x6
- HP100x6
- HP120x6

To treat the plate and stiffener as a single beam, cross section parameters for the plate-stiffener system must be calculated.  $\mathbf{Na}$ , when used is referred to as the z-coordinate of the neutral axis, measured from the bottom of the respective part (figure 5.5). The contributions from the fillet welds are neglected. Cross section area is then simply added:

$$A_{tot} = A_s + A_{pl} , \quad (5.7)$$

neutral axis is found by a weighted average:

$$Na_{tot} = \frac{A_{pl} \cdot Na_{pl} + A_s \cdot (t_{pl} + Na_s)}{A_{tot}} , \quad (5.8)$$

and lastly, the moment of inertia is found by use of Steiner's theorem:

$$I_{tot} = I_s + I_{pl} + A_s \cdot (Na_s - Na_{tot})^2 + A_{pl} \cdot (Na_{tot} - Na_{pl})^2 . \quad (5.9)$$

$A_{tot}, A_s, A_{pl}$  Cross sectional areas, total, stiffener and plate respectively

$Na_{tot}, Na_s, Na_{pl}$  Neutral axis z-coordinate. Same suffixes as before

$I_{tot}, I_s, I_{pl}$  Moment of inertia, with the same suffixes

The use of effective flange concept is not carried out in detail. It is just assumed that 80 % of the stiffener spacing is utilized to carry bending moment and axial force, so  $S_{eff} = 0.8S$ .

The moment- and shear force diagrams from figure 5.3b are still applicable, though the shear area needs a new definition. A common practice when working with beams is to use the web area. For bulb flats the equivalent will be the flat part of the profile, about 80 % of the profile height (figure 5.6). 80 % is based on calculations in Appendix A.

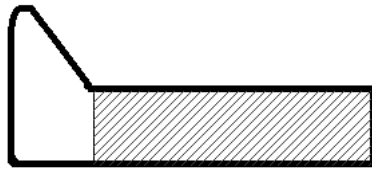


Figure 5.6: Assumed shear area of bulb flat

The line load  $\mathbf{q}$  is also changed:

$$q = \text{deck pressure} \cdot S = 15 \cdot 10^3 \text{ [N/m}^2\text{]} \cdot 0.6 \text{ [m]} = 9 \cdot 10^3 \text{ [N/m]} \quad (5.10)$$

Self-weight must now be considered as it amounts to more than 5 % of the functional load for the largest stiffener and thickest plate. The stiffener self weight per meter length is given in the profile tables. Assuming steel density to be  $\rho = 7850 \text{ [kg/m}^3\text{]}$  and the acceleration of gravity to be  $g = [9.81 \text{ N/kg}]$ , the self weight of the plate flange is calculated as:

$$p = t \cdot S \cdot \rho \cdot g \text{ [N/m]}. \quad (5.11)$$

The weight of both plate and stiffener is added to the line load  $q$  as the moments and shear forces are calculated.

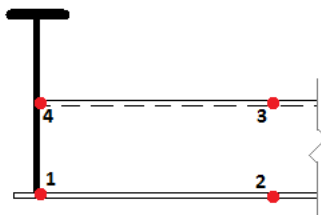


Figure 5.7: Checkpoints for stiffener stresses (upside down)



When Calculating stresses in the plate-stiffener system, four points are of interest (figure 5.7): The topmost fibre of the stiffener and bottom fibre of the plate flange at the end point (points 1 & 4) and in the centre of the stiffener (points 2 & 3). As the load now changes with the choice of profile, the stress table becomes a little more complicated than table 5.3, thus it is broken up into categories. In the presented result tables, a plate thickness of 10 [mm] is used for calculating self weight and section parameters in order to reduce space consumption.

Profile	$Na_{tot}$ [m]	$I_{tot}$ [m <sup>4</sup> ]	MidMom[Nm]	EndMom[Nm]	EndShear[N]
HP80x6	$1.10 \cdot 10^{-2}$	$1.44 \cdot 10^{-6}$	$4.954 \cdot 10^3$	$2.477 \cdot 10^3$	$1.189 \cdot 10^4$
HP100x6	$1.40 \cdot 10^{-2}$	$2.81 \cdot 10^{-6}$	$4.960 \cdot 10^3$	$2.480 \cdot 10^3$	$1.191 \cdot 10^4$
HP120x6	$1.75 \cdot 10^{-2}$	$4.88 \cdot 10^{-6}$	$4.967 \cdot 10^3$	$2.483 \cdot 10^3$	$1.192 \cdot 10^4$

**Table 5.4:** Section- and load data for the plate-stiffener system

The resulting stresses are presented in table 5.5 [MPa].

Profile	$\sigma_x$ point 1	$\sigma_x$ point 2	$\sigma_x$ point 3	$\sigma_x$ point 4	$\tau_{xz}$ point 1 and 4
HP80x6	72.2	-36.1	135.5	-271.1	31.0
HP100x6	42.3	-21.2	84.6	-169.3	24.8
HP120x6	28.0	-14.0	57.2	-114.5	20.7

**Table 5.5:** Bending and shear stresses in the plate-stiffener system [MPa]

Under the assumptions made about role of the plate, both in the field and as a plate flange, the stresses calculated in table 5.3 are taken into account. The local coordinates from the plate calculations will need to be transformed to fit with beam coordinates. Hence, x becomes y and vice versa.

The simplified von Mises yield criterion can be written as

$$\sigma_v = \sqrt{\frac{1}{2} [(\sigma_x - \sigma_y)^2 + (\sigma_y - \sigma_z)^2 + (\sigma_z - \sigma_x)^2] + 3\tau_{xy}^2 + 3\tau_{yz}^2 + 3\tau_{zx}^2} \quad (5.12)$$

Setting  $\sigma_z = \tau_{xy} = 0$  yields:

$$\sigma_v = \sqrt{\frac{1}{2} (2\sigma_x^2 - 2\sigma_x\sigma_y + 2\sigma_y^2) + 3\tau_{yz}^2 + 3\tau_{zx}^2} = \sqrt{\sigma_x^2 - \sigma_x\sigma_y + \sigma_y^2 + 3\tau_{yz}^2 + 3\tau_{zx}^2} \quad (5.13)$$

Defining utilization as  $\mu_0 = \gamma_{tot}\sigma_v/\sigma_y$ , and setting the yield stress  $\sigma_y = 355$  [MPa] the utilization table becomes:

	Checkpoint 1			Checkpoint 2			Checkpoint 4		
	PL6	PL8	PL10	PL6	PL8	PL10	PL6	PL8	PL10
HP80x6	0.37	0.33	0.35	0.45	0.35	0.32	1.08	1.12	1.16
HP100x6	0.33	0.25	0.24	0.41	0.29	0.25	0.69	0.71	0.74
HP120x6	0.31	0.33	0.19	0.38	0.36	0.21	0.48	0.49	0.51

**Table 5.6:** Stiffener and plate utilization table

Point 3 is not checked as the bending moment is half that of point 4 and there are no interactions with plate stresses.

From this consideration, a plate thickness of **10 [mm]** is chosen. This is to have some extra resistance with regards to denting on the topside deck, where containers will be lifted on board and sat down. The chosen stiffener is **HP100x6**.

### 5.3.3 Deck beams

The deck beams are assumed to carry shear stress in the web and bending moment in its own flanges, thus effective flange is overlooked. As the load is not symmetric around the outer main girders, the deck beam can not be assumed clamped at that end. A new moment diagram with end shear forces included is shown in figure 5.8. The weight of deck actions, deck plates, stiffeners and its own weight is included when calculating the line load, in the same manner as before. The difference is that the deck action is now updated to the realistic load case. As the cellar deck experience the heaviest deck loads, 250 tonnes, it is considered. Four different broad flange profiles are considered, and the utilization table is presented below.

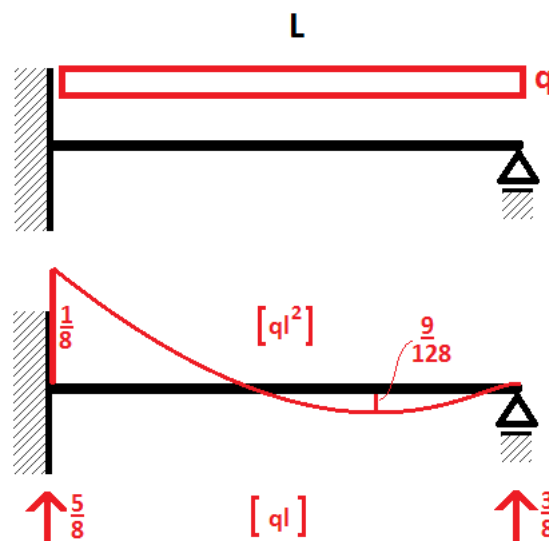


**Figure 5.8:** Moment diagram of deck beam. Assumed clamped at the inner girder due to symmetric load

Profile	Utilization
HEA400	0.82
HEB400	0.66
HEA500	0.46
HEB500	0.46

**Table 5.7:** Deck beam utilization table

See that relatively light beams are satisfactory for the operating condition. The chosen profile is **HEA500**.

### 5.3.4 Girders

The deck load is assumed to be transferred through the beams onto the heavy main girders. That way, all of the deck load rests on the girders going in one direction who are in turn supported by the orthogonal girders. This is illustrated by figure 5.9 cropped from appendix B. As seen in figure 5.8,  $\frac{5}{8}$  of the load is transferred in to the central girder (AB), making the line load on that girder 63 % of the total deck weight.

The end moments and shear forces from appendix B are used, and as they are largest for beam AB, only that one is considered. The utilization for two sections are tabulated below

Profile	Utilization
HEB800	0.78
HEB1000	0.57

**Table 5.8:** Girder utilization table

Though it is a little on the heavy side, HEB1000 is chosen for the main girders. Its importance for the structural integrity of the deck and knowing there will be quite a bit of strength reduction due to temperature makes some extra strength attractive. HEB800 will be considered for the two higher decks, as the loading is less intense there.

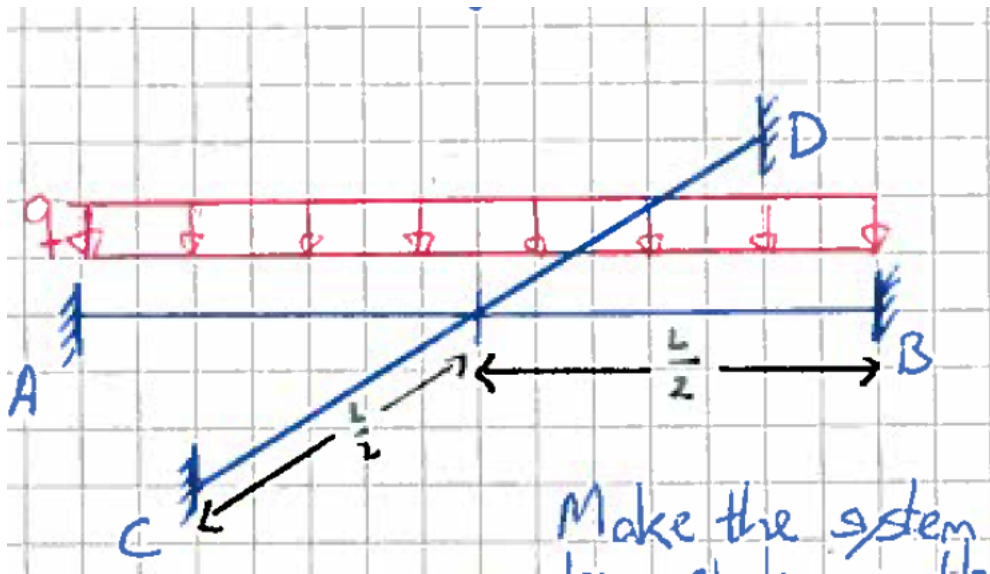


Figure 5.9: From appendix B. Deck girder modelled as grillage system

### 5.3.5 Columns

As seen in figure 5.1 there are a number of vertical columns and diagonal braces. The vertical columns connecting with the jacket legs are considered here. A conservative assumption about the loads in these four columns is that each of them carries 25 % of the topside weight subtracted equipment weights on cellar deck. That amounts to 110 tonnes on each column for the operating condition. For the case of cantilever collapse, an additional weight of 500 tonnes is considered. Interaction with bending moment from the main girder is considered in Eurocode 3 (EC3-1-1 2005), equation 6.61:

$$\frac{N_{Ed}}{\frac{\chi_y N_{Rk}}{\gamma_{M1}}} + k_{yy} \frac{M_{y,Ed} + \Delta M_{y,Ed}}{\frac{\chi_{LT} M_{y,Rk}}{\gamma_{M1}}} + k_{yz} \frac{M_{z,Ed} + \Delta M_{z,Ed}}{\frac{\chi_{LT} M_{z,Rk}}{\gamma_{M1}}} \leq 1 \quad (5.14)$$

Since the deck is loaded symmetrically, there will most likely be only one bending moment contribution, but a secondary moment is applied, put equal to 5 % of the girder moment. Cantilever collapse will most likely be dimensioning, and it is an accidental load, so the material factor is set to be 1.0. As mentioned in section 2.2.9, column curve c is used for fire analysis. One end is assumed clamped, so the buckling length is  $0.7 \cdot 6 [m] = 4.2 [m]$ . All intermediate equations and factors are not presented here as the standard uses nested references between chapters and annexes, but the spreadsheet "deck\_design.xlsx" is in the attached files. Three different tubular sections are considered:

Profile	Utilization
400x20	0.83
500x20	0.62
600x20	0.50

**Table 5.9:** Column utilization table

The stability of the topside relies heavily on these column, thus largest section is selected. This may prove to be extremely conservative, as the loads are already assumed quite large. In the diagonal truss members and the corner columns a lighter section is assumed to be satisfactory.

### 5.3.6 Dimensioning summary

The chosen profiles are listed in table 5.10

Member	Profile
Plate thickness	10 [mm]
Stiffeners	HP100x6
Deck beams	HEA500
Girders	HEB1000
Main columns	600x20

**Table 5.10:** Chosen main structural components

As mentioned, some of the sections may prove to be on the heavy side, while the girders seems a little light at first glance. This is by no means an attempt to optimize the structure, only a quick estimation to get fairly reasonable strength. It should also be mentioned that several load situations may introduce whole other sets of loads to the structure. A few examples are: different stages of fabrication, load-out, transport, installation and extreme weather.

## 5.4 Finite element model

By help of Trond Granli in Kværner, the structure was modelled in the finite element analysis software GeniE. Granli was helpful in choosing the rest of the structural elements for the model including frames for the riser sleeves, keeping in mind that the structure should rather be simple and robust than optimized for operational conditions. A small part of the supporting jacket structure was included. The finite element model was then imported to USFOS, using the utility program StruMan. The resulting model is presented below. The need for distinguishing between directions and parts of the structure was apparent early on. Thus a north direction was defined as standing on the topside centre point, facing away from the riser sleeves.

The north direction will in this case be straight up on the page. See that the model is meshed with 0.5 [m] element size. This would for many cases be unnecessary fine in a regular USFOS model, but as there will be temperature loads a fine mesh helps capture the temperature gradient.

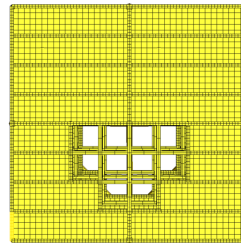


**Figure 5.10:** Viewed from above

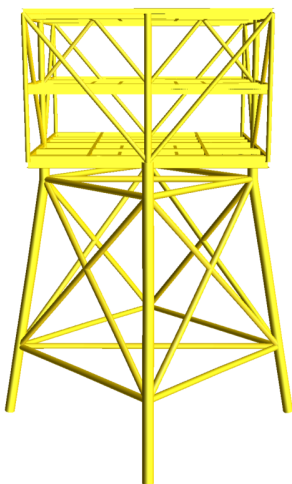


**Figure 5.11:** Viewed from "south side"

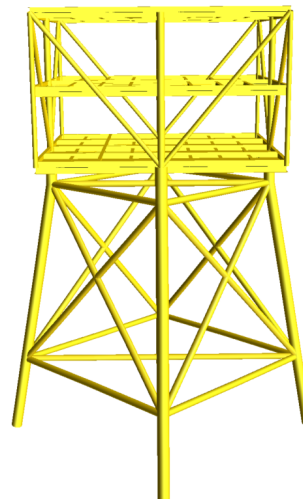


**Figure 5.12:** Viewed from "east side"

The total list of structural element profiles is presented in table 5.11

Member	Profile
Deck plates	10 [mm] shell
Deck beams	HEA500
Girders, cellar deck	HEB1000
Girders, mezzanine deck	HEB800
Girders, topside deck	HEB800
Main columns	600x20
Corner columns	400x15
Diagonal braces	400x15
Internal truss	400x15
Jacket legs	1000x30
jacket braces	600x20

**Table 5.11:** FE-model structural components

Note that the plate stiffeners are missing. They were left out to reduce the system size, and shorten modeling time. That means all loads need to be applied directly on the deck beams and girders, and the missing weight has to be accounted for (section 5.4.2)

### 5.4.1 Member groups

USFOS allows the user to specify subdivision of the structure into groups. The element or node numbers of members or nodal points sharing an attribute are specified in the model file and easily can be visualised in the graphical user interface (GUI) to make sure all elements or nodes are included. Figure 5.13 shows one such group, where only topside tubulars are rendered in the GUI.

The reason to make these groups is mainly for the user to have quick access to an element set of interest. Several groups were defined for the structural model, dividing the structure into deck beams, truss members and by material number. The east-west deck beams of each deck were also defined, to verify that the right beams were subjected to loads.

### 5.4.2 Weight

The finite element model includes only key structural elements. Among the features left out are: plate stiffeners, grating, personnel stairs, pipe supports, piping and other operational equipment. Deck loads are applied directly the the deck beams, so the plates are only carrying their own weight.

Leaving that many details out of the model reduces its weight which needs to be accounted for. To get an overview of the weights of different structure parts, six

different material types were defined. For each of them, a gravity analysis was run setting all but one of the material densities to be 0. The total reaction force was read in the .out result file that USFOS writes.

Material ID	Definition	Weight
1	Jacket members	192.2
2	Shell elements	53.0
3	Cellar beams and girders	72.7
4	Mezzanine beams and girders	52.9
5	Topside beams and girders	52.9
6	Columns and truss-work	43.7
	Total topside weight	275.1

**Table 5.12:** Weight of the different structural components [tonn]

See that 125 tonnes are missing from the design steel weight in table 5.1. For regular structural analysis this could have been dealt with by scaling the material density of some elements. Doing that for fire analysis is a bad idea, as the material density is a factor in the heat transfer (equation 2.17). The scaled elements would end up with large negative temperature values and the analysis would run in to numerical issues due to extreme temperature gradients.

The weight was corrected by using the X\_ELMASS routine in USFOS, which allows the user to add a uniform mass per length of beam elements. The extra mass was distributed on east-west beams and girders only, and a weighting was applied such that internal beams experiencing symmetrical loading was given twice the load intensity as the beams along the perimeter of the deck. Two different classes of extra mass was defined: grating and stiffener weight. The grating weight was set to  $60 [kg/m^2]$  by recommendation from Trond Granli, and applied only to mezzanine deck beams and girders. The rest of the missing weight was named stiffener weight and distributed equally between all three decks.

The equipment weights on cellar and mezzanine deck in table 5.1 were also applied as extra masses. This was chosen over distributed beamloads because they are permanently fixed to the structure. By doing this, the total topside weight is accounted for by gravitational acceleration in stead of needing extra load combinations.

### 5.4.3 Operational condition

As mentioned, an internal truss-work was added between mezzanine and topside deck to help carry the accidental loads from a cantilever collapse. Figure 5.11 show the truss going in the east-west direction. By stepwise increasing the gravitational acceleration in static analyses, it was evident that the capacity could be improved by a simple alteration. The vertical column in the internal truss was extended to



reach down to the cellar deck. This changed the failure mode from girder bending to buckling in the internal truss, and increased the capacity before first yield from 2.96 times gravity to 4.73. That 60 % increase was accepted, and the column was integrated for the rest of the analyses. Note that this gravity load factor has not taken the recommended load and material factors in to consideration, and so the ultimate strength capacity is found by dividing by  $\gamma_{design} = 1.5$  as explained in section 5.3 (equation 5.1). The tubular sections of the topside are shown in figure 5.13, including the extended vertical column. See that hanging the cellar deck up like this will increase tension in the innermost diagonals, thereby increasing the compression of the outermost diagonals. The collapse happens in those outer members.

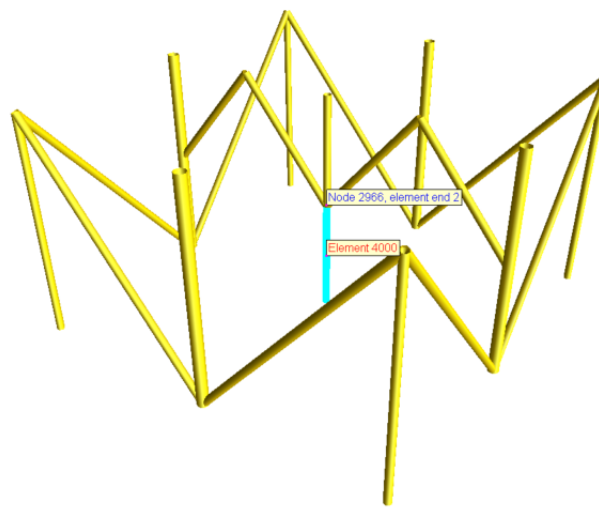


**Figure 5.13:** Tubular members in the topside, vertical column extended



# Chapter 6

## Simulations

This chapter will explain the procedure for running the different analysis performed for this thesis. As explained in section 2.2.4, the proposed revision for mechanical response analysis during fire, recommended practice is to start by running load-domain (Pushdown) analysis and then verify by temperature- or temperature-load domain analysis if the resistance margin is critically small. Thus, a large number of pushdown analyses are run for the various fire scenarios and a few temperature-domain simulations are run to confirm pushdown results. A reserve strength ratio above 1.0 means acceptance, if the pushdown results are trusted.

Fracture is as mentioned in section 2.2.11 not well understood for elevated temperatures. The criteria of  $\varepsilon_{cr} = 0.15$  will most likely be conservative as the ductility of steel increase with temperature. It is, however used for all analyses in this thesis, both for cold and fire simulations to have comparable results. When columns buckle, their strains may exceed the criteria, but they are not classified as "fractured", merely collapsed by buckling.

Such a large amount of simulations motivate the use of automated running procedures. Thus, a modification of a shell program used in the course "TMR4195 Design of offshore structures" (IMTsoftware 2012) was used to run analyses automatically. A considerable amount of time was spent making the program function for the heat transfer and following pushdown simulations. The program was run through the unix environment Cygwin, making it possible to work from a Windows operating system. Quite a few slight differences were noticed between working in a regular Linux terminal and Cygwin, and some time was spent getting familiar with the syntax.

The heat transfer problem, is as mentioned earlier a complicated one, with many variables. In real life, a wellhead platform will not be an empty shell. Equipment, pipe supports, piping, ladders and many more objects will in reality obstruct a flame. The simulations run below are by no means detailed in that sense, but the structural elements are loaded in a way that mimics reality. More sophisticated

models are needed for more accurate results. Using CFD software, the flow around obstructions can be modeled, and the heat loads obtained are more realistic.

## 6.1 Automation

**The heat transfer analysis** is done with FAHTS. Information about the heat source, time step and duration is written in to the head.fem file and the analysis is run with the same model.fem file as for regular USFOS analysis. Three result files are written:

- A visualization file, res.raf, that can be opened by the GUI
- A general result file, with information about the structure as well as calculated surface area, accumulated energy etc.
- A temperature result file, beltemp.fem, with element temperatures and heat flux for each time step. This is the input for structural analysis.

**The structure response simulation** is run in USFOS. Information about the nature of the problem, number of loads, imperfections and criteria for ending the simulation is entered in a new head.fem file. In the model.fem file, the information about the structure is written; defining nodes, beams, shell elements, material properties and the actual definition of the load cases. Three result files are written:

- A visualization file, res.raf, that can be opened and examined in the GUI.
- A general result file, with structural response to each each load step calculated.
- A result status file, containing condensed information about a few main results: First yield, first plastic hinge, first fracture

All the mentioned files are written in the same format every time, it is just the values and number of data points that change. This is convenient if many simulations are to be run, as the input can be written and output can be read automatically.

### 6.1.1 Matlab input generator

A short Matlab program "int\_placement.m" was written to generate input values for the simulations (appendix C). Sets of input values were written for both the FAHTS head, USFOS head and model file. Note that the automation process was just done for jet fire cases. The program works as follows:

Having saved data from the structural model file in a spreadsheet, for ease of reading,

the function "nodes.m" reads the spreadsheet and makes a matrix of nodal data, beam element data and group data. The group of east- west orientated beams on the topside deck is already defined in the spreadsheet.

For the FAHTS head files, data about the fire were generated. The user specifies the origin of the fire, flame length, number of flame directions wanted, direction of the first case, flame intensity and diameter, duration and time step. The program calculates end coordinates of the flames, one set for each of the directions. All the data is then written to a "fahtsparam.dat" data file, with column headers as shown in figure 6.1. This is done by the function "writefahts.m"

xinit	yinit	zinit	hinit	xend	yend	zend	hend	inD	enD	jetdir	dur	tstep	lstT
3	3	1	1.23E+06	17.14	-1.59	3	1.23E+06	2.5	2.5	342	60	1	63

Figure 6.1: FAHTS parameter data file generated by matlab program

The USFOS simulation uses the "PUSHDOWN" control sequence. This record needs to know which time step in the "beltemp.fem" result file is going to be read. The default start time step is 4 in FAHTS, so a counter is started at 3 in matlab. The last time step is then calculated on basis of the user defined fire duration and time step size. The user also specifies which functional load case to be used in the structural response analysis. The function "writeusfos.m" writes to a "usfosparam.dat" file with column headers:

Hjur	lastT	push
60	63	3

Figure 6.2: USOFS parameter data file generated by matlab program

Lastly a text file with load definition is written. This is only for the wireline operation loads. The user specifies the total weight of the equipment as well as a rectangle to be loaded. The rectangle is defined by its south-west origin, width (east-west) and a length (north-south). The function "writeload.m" take the defined rectangle and finds all the nodes that has coordinates inside its boundaries. They are stored in temporary "nodelist" vector. The beam element matrix is then run through and checked. If both nodes related to an element is represented in "nodelist", that means that the whole element is situated inside the rectagle. The element is saved in a temporary "beamlist" vector. Finally, if an element number in "beamlist" matches an element in the group of east- west directed beams it has passed the test and is saved in a "load\_ beams" vector. Depending on the size of the rectangle and total equipment weight, the load intensity will vary. Knowing that all elements on the north half of the topside deck are 0.5 [m] long, the load intensity is calculated for the distributed loading. Two text files are written. One with element numbers and load intensity ("inter.load.dat") structured as it would be in a structrual file for USFOS (figure 6.3), and one defining an element group ("inter\_group") to be able to check that all elements are included (figure 6.4)

```
#      ldCase ElemID  Xint  Yint  Zint #
BEAMLOAD  3  2882    0    0 -1.4715E+04
```

Figure 6.3: Load data for wireline distributed load

```
#      Group of loaded topside beams
Name Group          3 Intervention_load
GroupDef          3 Elem
                  2882
```

Figure 6.4: Group data for beams subjected to wireline load

The rest of the loads, extra mass definitions and group definitions were taken out of the model.fem file and saved in separate text files. The remaining model file was named "MainModel.fem" to be used later. Control files "usfoshead.fem" and "fahtshead.fem" were made where, instead of values, the column headers from "fahtsparam.dat" and "usfosparam.dat" were put in (appendix E. The headers would be switched by the bash shellscript later.

The flow of the program is shown below:

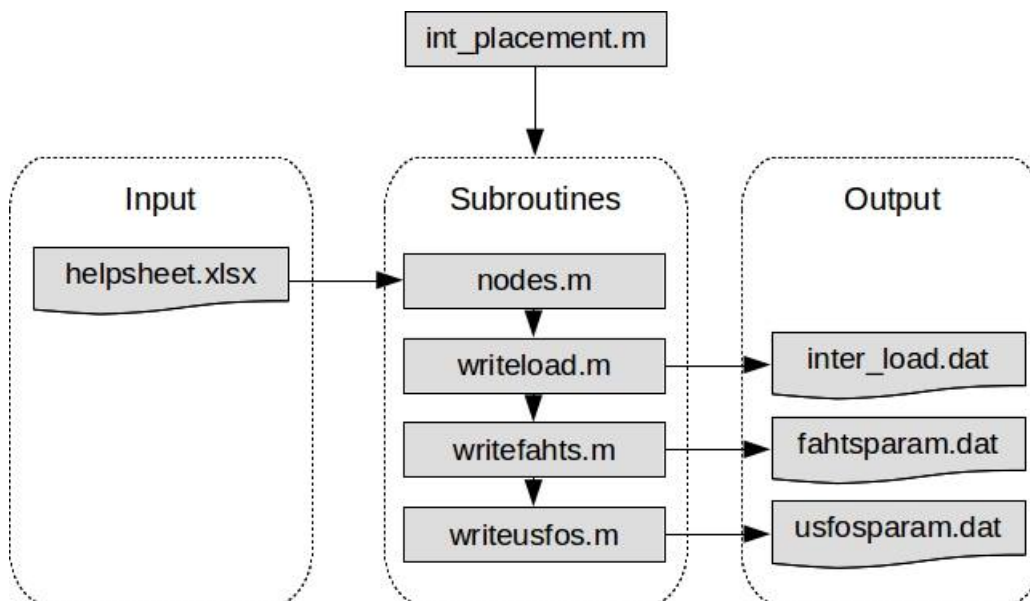


Figure 6.5: Flow chart for matlab input generator

## 6.1.2 Bash script

As mentioned before, the course "TMR4195 Design of Offshore Structures" featured a project work including automated runs of pushover analysis. This program was modified to work with the problem at hand. The script uses a feature called "xargs" to run multiple tasks in parallel and that worked when running just FAHTS simulations, but when introducing multiple USFOS analyses per FAHTS simulation,

the numerics of the USFOS analyses broke down. This has to do with the job names defined in the bash script, and is NOT a fault in USFOS. The results were fine when running single thread, so that was done for the bulk of the simulations. The job name error was later solved, but at such a late stage that it was only used for a few simulations.

**main.sh** is the runnable program that calls on the other functions (appendix D). At first the model file is assembled, copying in the text files made earlier. This way, all the information about extra element mass, loads, and groups get placed in the correct order. "fahtsparam.dat" is read line by line, creating a job- name and folder for each line. For each folder, a FAHTS control file is created and copied into the folder along with a copy of the model file. A separate "substitute" function takes care of substituting in values for the header names in the control files.

**runone** is called on by main, and is responsible for running the programs "20-usfos" and "30-fahts" in succession, using the correct job names. Instead of letting FAHTS and USFOS write output to terminal, runone writes this information into log- files

"**20-fahts.sh**" runs FAHTS with the files and paths matching the job name.

"**30-usfos.sh**" is the problem. For each job name, a set of many pushdown analyses are needed. Thus, the program "30-usfos" stops the smoothly running job name change, while reading through each line in "usfosparam.dat". Values are substituted in for the header names in the USFOS head.fem files making control files for each line. USFOS is run and for each "res.raf" result file, a utility program Fact reads pre- selected element forces for ease of post- processing.

A flow chart is tried sketched below:

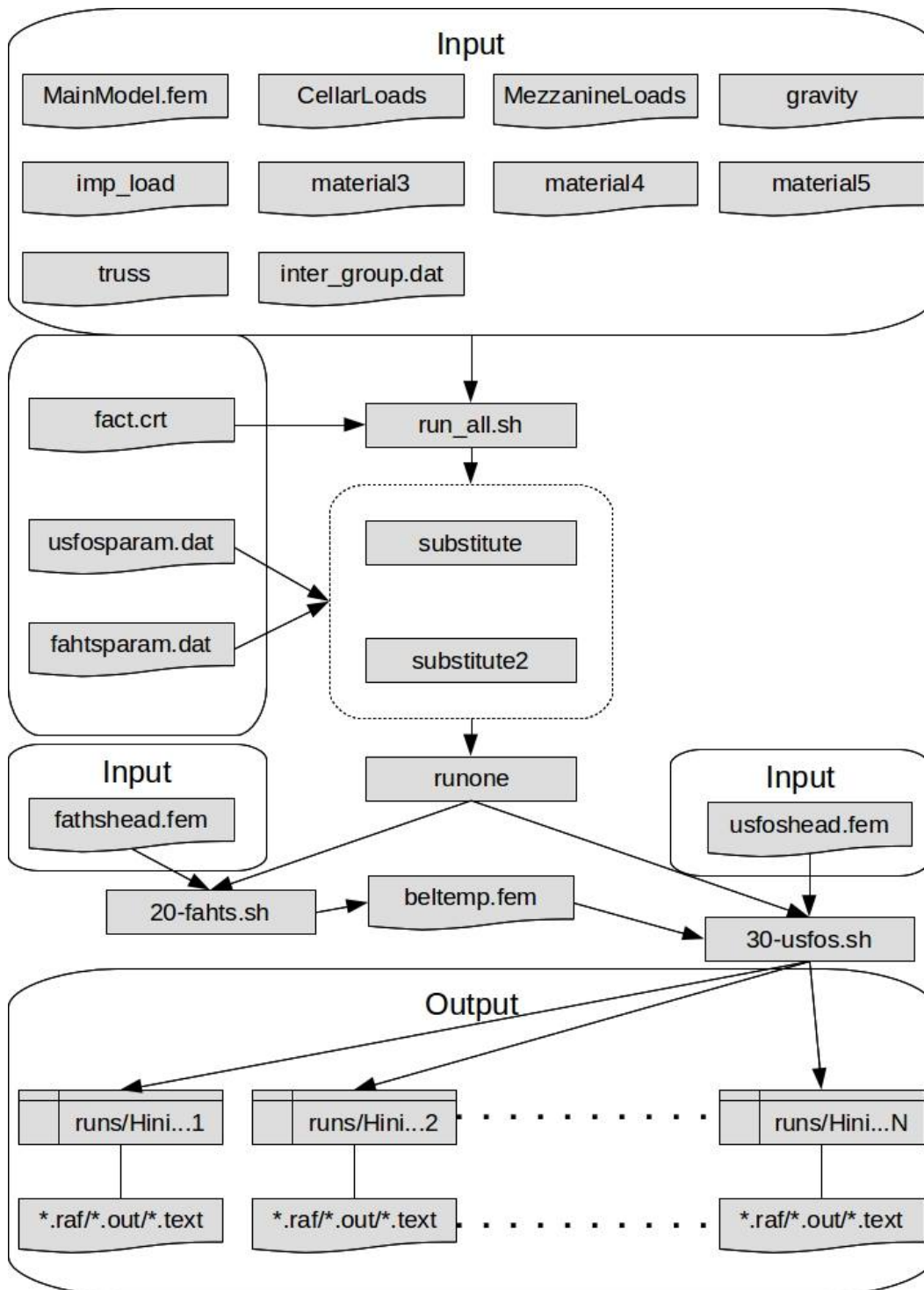


Figure 6.6: Flow chart for the shell script



## 6.2 Cantilever collapse

In the case of an accidental jack- up rig cantilever collapse, two scenarios are considered:

1. Fire on board the jack- up rig, affecting the structural integrity of the cantilever to such an extent that it creeps down and rests on top the wellhead platform topside.
2. A large jet fire originating in the well area on the wellhead platform directed towards the jack- up rig, with the same effect: the cantilever rests on the topside.

For both cases it is assumed that the distance between drilling cantilever and topside is so small, thus giving such a small impact velocity that the load can be considered static. This may be a bit non-conservative, but it is assumed that some structural resistance is left in the cantilever, slowing the decent.

The weight of the drill rig cantilever is modelled as two point loads, one of them applied in the centre of the deck, and the other on top of one of the main columns (figure 6.7).

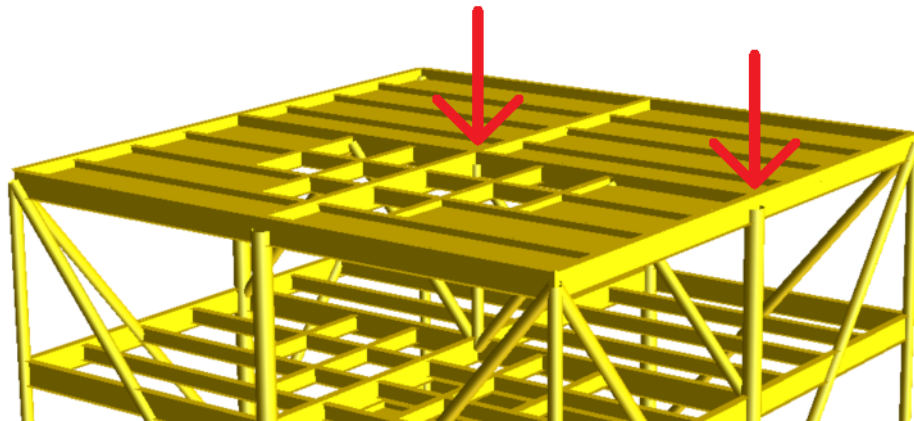


**Figure 6.7:** Cantilever weight modelled as point loads

An impact will most likely not be located exactly at the indicated nodes, and the cantilever is not shaped as two spikes at its bottom. However, due to stiffness in both the cantilever and topside, the forces will ultimately be carried by the columns. A more refined load could have been obtained by splitting it into three and loading the top of the diagonal braces (in between the two indicated loads), but considering that the shear force in the cantilever is carried by walls, the largest forces will be transferred by its edges. One improvement would have been to put restrictions on how much the impacted nodes can move in relation to each other, but that would require detailed information about the stiffness of the cantilever.

### 6.2.1 Fire on board jack- up rig

For this case, the temperature of the topside is assumed unaffected, thus a normal static simulations is performed. The functional loads are stepped together with the accidental loads until collapse is reached. This being an accidental load, the data from the simulation is considered directly, without multiplying by safety factors as they are set to 1.0 for abnormal effects (figure 2.4).

A first step is checking for yield at the expected load level. Figure 6.8 shows the distribution of von Mises stress at load level 1, referring to full gravitational pull on the structure, as well as the two point loads of  $4.905\text{ MN}$  (500 tonnes) each. The structure's weight is increased in the further stepping, as that is the procedure for pushdown analysis. This provides a reference for the simulations including heat loads. The color stress scale is set to range between 0 and  $370\text{ MPa}$ .

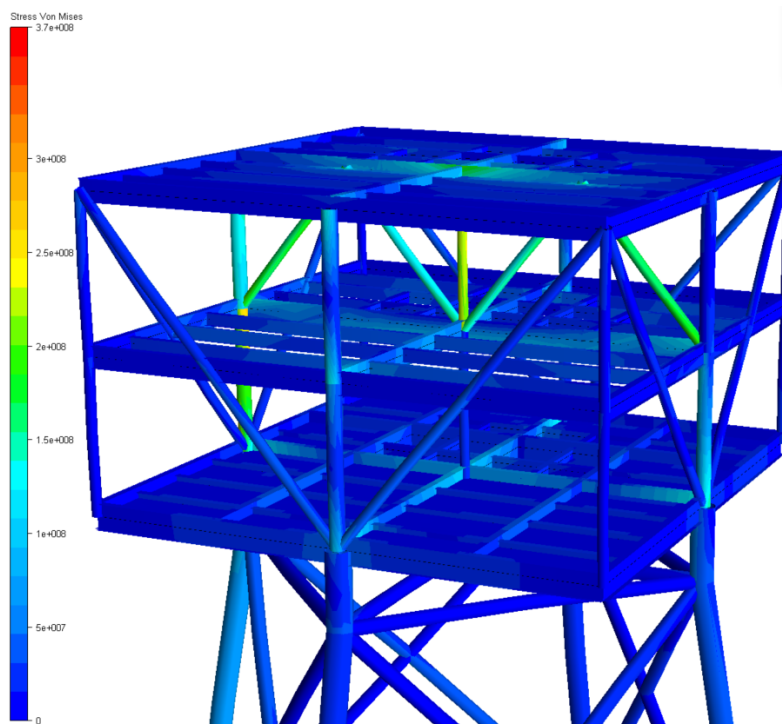


**Figure 6.8:** von Mises Stresses. JUR cantilever load. Load factor 1

See that no yielding occurs at the estimated load level. USFOS writes a result status file, with a brief summary of the simulation. The first yield is read there to be in at a load level of 1.16. Not surprising, the elements expecting high stresses are the two heavily loaded columns. The top middle column yields first, as the diagonal braces help restrict deflection in the mezzanine deck. Figures 6.9 and 6.10 shows the axial forces of the two columns as function of global load level.

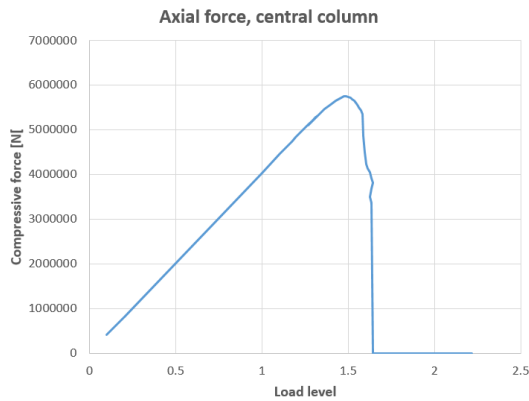


**Figure 6.9:** Axial force in central column

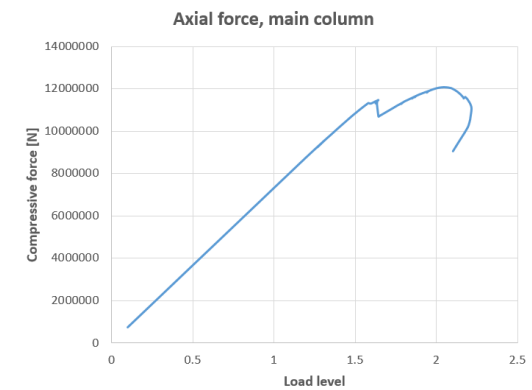


**Figure 6.10:** Axial force in main column

See a rapid unloading as the central columns buckles. This is also seen in the load curve for the main column, where a dip in the load is experienced as the structure redistributes the loads no longer carried by the buckled central column. The ultimate capacity of the structure is met when the main column buckles and the simulation no longer can find equilibrium. The peak load level is found to be **2.21**. The vertical displacements are shown as topological contour lines.

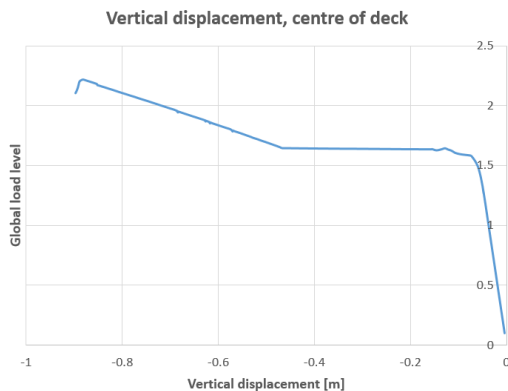


**Figure 6.11:** Vertical displacement of central node, topside deck

Figure 6.11 shows the displacement of the centre point in topside deck. See that the step right before global collapse give a deflection of almost  $0.9\text{ m}$ . Depending on the general arrangement and layout of equipment, that could be damaging for objects placed on mezzanine deck. Figure 6.12 shows the vertical displacement of the whole structure. Ignore the color of the highlighted element, it was put in to show which main column initiated the instability of the structure.

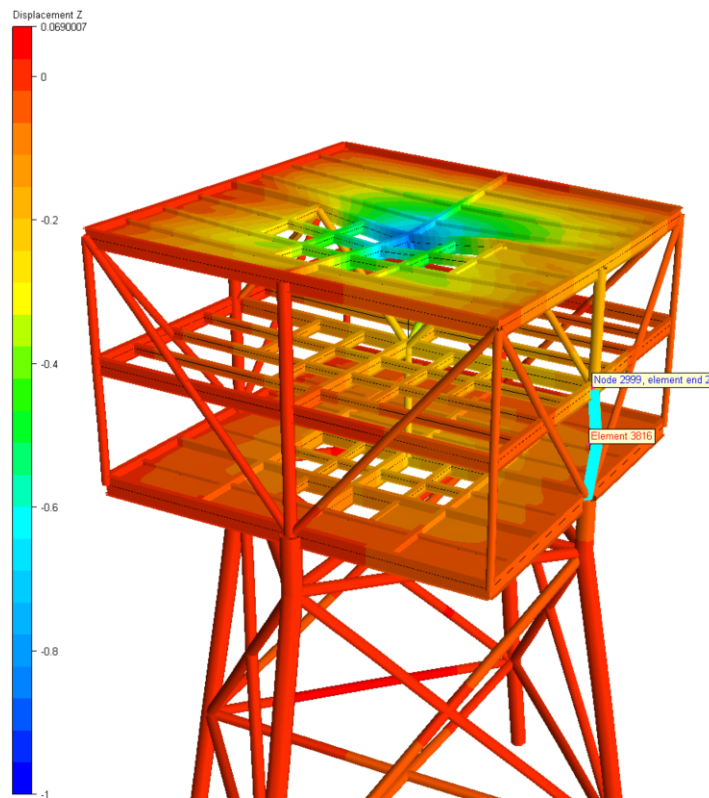


**Figure 6.12:** Cold cantilever collapse. Contour lines. Buckling main column highlighted

The dark blue color represent 1 *m* vertical displacement. See that moderate deflections are experienced on the lower decks, but if the reduced distance between topside and mezzanine deck can be accepted, no dramatic effects are shown until global instability.

### 6.2.2 Fire originating on topside

For a jet fire to reach and affect the jack- up rig, it has to originate at a point near the side the rig. Initially, one case was considered, where the fire originated in the riser sleeve closest to the edge and flared almost directly up towards the cantilever. But as this had little effect on the structural integrity of the topside, another case was defined. The origin was moved to the centre of the cellar deck and the fire directed out under the topside deck. A leak between risers and manifold could be imagined. This way, the central column would experience more heat. The two cases are visualized below, by modelling a tubular element where the jet fire will be.

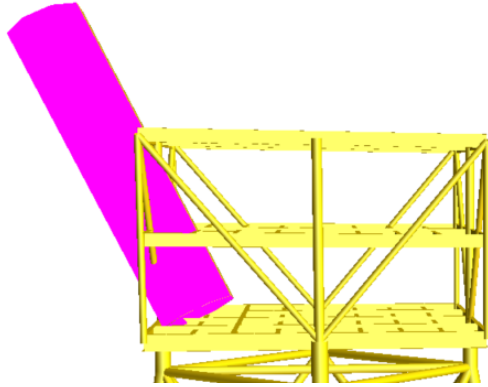


**Figure 6.13:** Initial fire case. "Outer" position

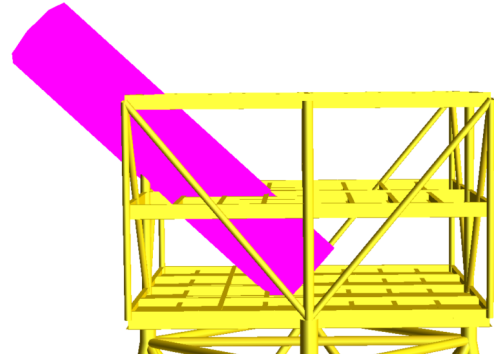


**Figure 6.14:** Fire affecting the internal columns. "Inner" position

Calculating the heat load intensity was necessary, as the loads given were max initial heat flux on the structure. An estimation was done by the derived model in section 2.5.2 and then calibrated by running FAHTS analysis to get the correct heat flux. Two assumptions were made: the maximal heat flux would be experienced by an element inside the flame's radius. And for that element, the flame length would seem infinitely long. Thus, the contributions from heat sources were integrated in the domain  $\theta \in [-\pi/2, \pi/2]$  and the distance  $\mathbf{d}$  was set to be 1 m (figure 2.19). The initial heat flux from a line source on the element will be:

$$\begin{aligned}
 q &= \int_{\theta=-\pi/2}^{\pi/2} \frac{Q_R \tau}{4\pi \frac{d^2}{\cos^2(\theta)}} \cos(\theta) d\theta \\
 &= \frac{Q_R \tau}{2\pi d^2} \int_{\theta=-\pi/2}^0 \cos^3(\theta) d\theta \\
 &= \frac{Q_R \tau}{2\pi d^2} \cdot \frac{10}{12}
 \end{aligned} \tag{6.1}$$

Rearranging, and using  $\tau = 0.8$  as instructed in section 2.5.2:

$$Q_R = \frac{12\pi d^2}{5\tau} q \tag{6.2}$$

an initial heat flux of  $350 \text{ kW/m}^2$  demands a line source of  $3297 \text{ kW/m}$ . Calibrating with a FAHTS simulation as mentioned, the final heat load was set to be  $3430 \text{ kW/m}$ . The slight deviation, may be explained by the fact that a finite length fire will have slightly less radiation than the infinite fire in the calculations.

### 6.2.2.1 "Outer" case

The fire from figure 6.13 was simulated in FAHTS, with time steps of 6 seconds over the duration of 5 minutes. Temperatures reached over  $1000^\circ \text{ C}$ , as seen in figure 6.15

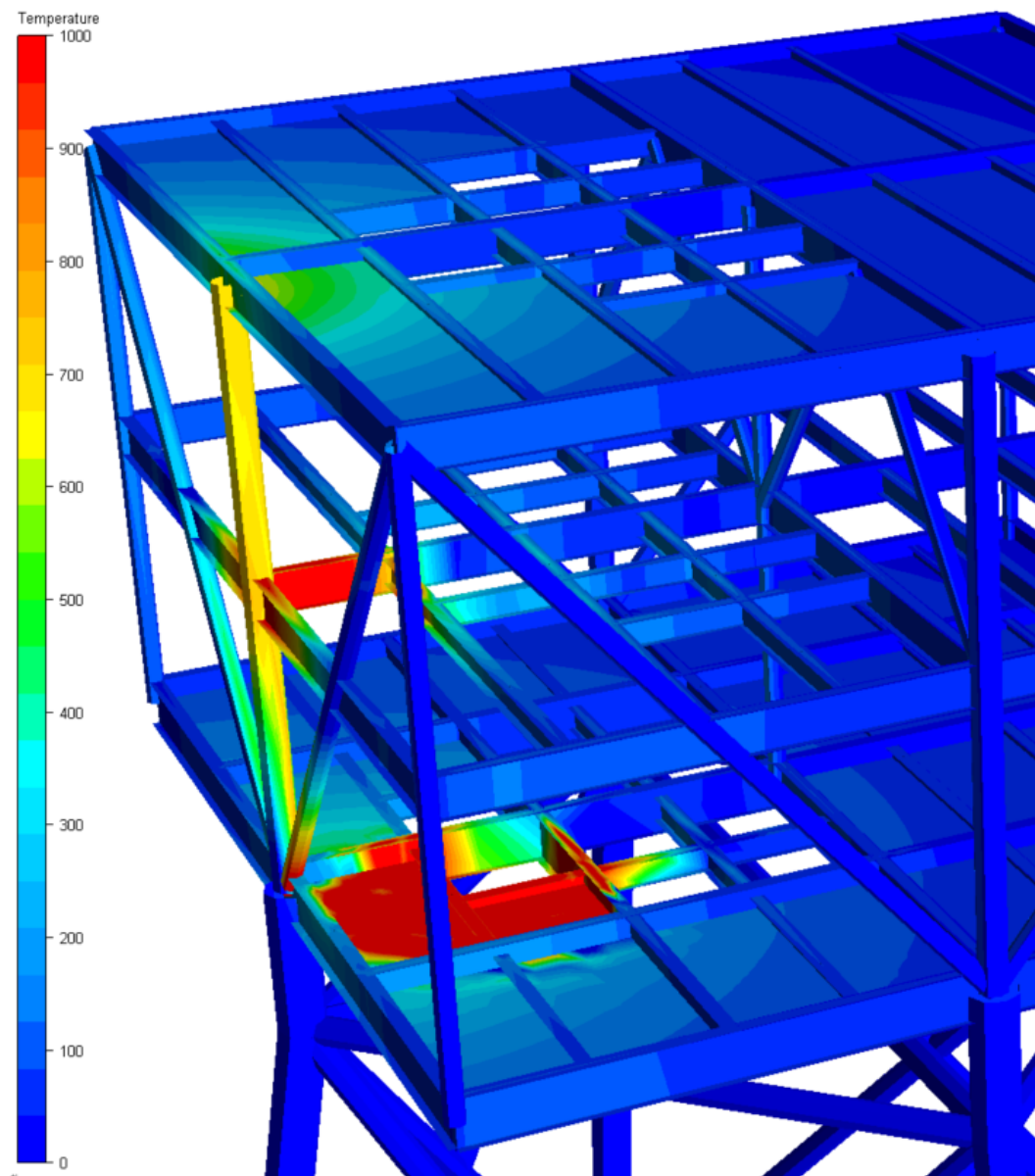


**Figure 6.15:** Temperature plot after the full 5 minute duration of the  $350 \text{ [kW/m}^2\text{]}$  fire

Pushdown analyses were run for each time step using the shell program mentioned in section 6.1, and the last time step was evaluated first, following the reasoning that if the structure withstands the temperatures at the end of the fire, it would have to have withstood the preceding steps as well.

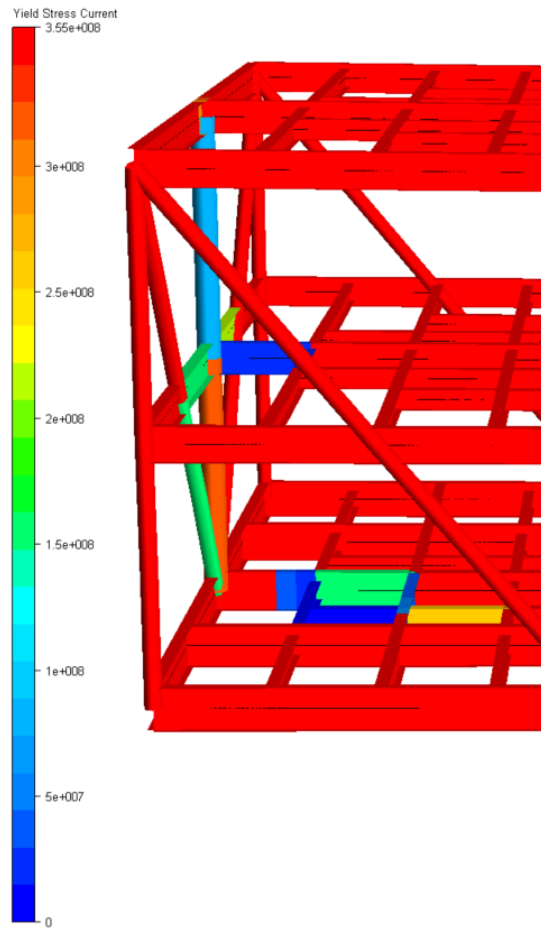


**Figure 6.16:** Updated yield strength for beam elements. JUR collapse "outer" case

The updated yield strength for the beam elements is shown here. See that the reduction is substantial for some of the elements. The pushdown analysis does not show large global differences from the cold reference case in section 6.2.1. As expected, first yield comes earlier due to the reduced material properties. The first detected yield stress is in the girder on mezzanine deck (dark blue on the figure) but the load is redistributed without big problems. The thing to notice, however, is that the unstable behaviour is now triggered in a new way. Remembering the grillage system from appendix B, and the interaction between girders, the loss of strength in one of them give a new failure mode. A loss of stiffness in one girder end means that more of the deck load has to be transferred through the other end (deck midpoint). The girder system is there supported by tensile forces in the inner diagonals. Increased tension in the tensile members give increased compression in the compressive members, thus the second member to fail is not the main column this time, but the compression diagonals in the inner truss.

Though the simulation does not end until a load level of 2.3, the large displacements of both centre point of the topside deck (figure 6.17) and girder on mezzanine deck (figure 6.18) become so large when the diagonals buckle, that equipment is in danger of being impacted. Thus, the failure load is taken to be **2.0** (the second plateau on the curves).

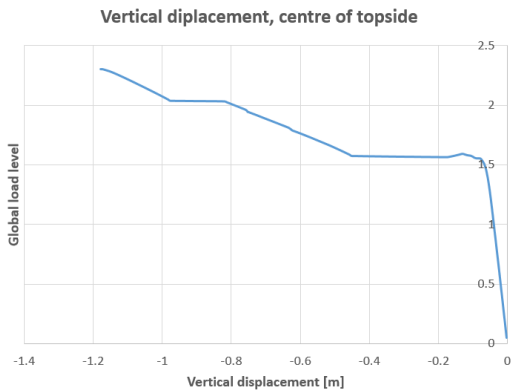


**Figure 6.17:** Vertical displacement of topside deck central node. "Outer" position

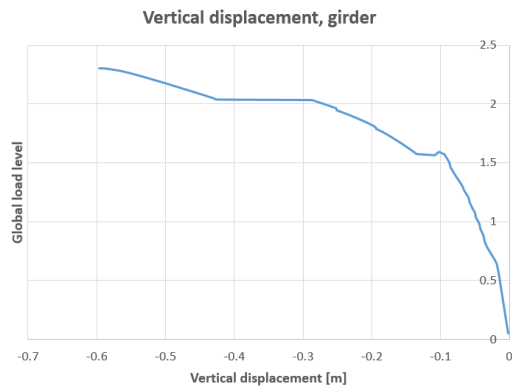


**Figure 6.18:** Vertical displacement of heated girder. "Outer" position

**Temperature domain** Judging from the pushdown analysis, the structure should be able to withstand the 5 minute duration of the powerful jet fire. A reserve strength ratio of about 2 is obtained for the last time step. Survivability will now be confirmed or refuted by a temperature simulation. The functional loads are now applied and stepped up to a load factor of 1.0. Temperature loads are then applied, increasing throughout the duration of the fire. Figure 6.21 shows the vertical displacement of the whole structure as topological contours. See that the largest deflection is less than 6 [mm].

The weakening of the structure is observed in the cellar deck, where the main girder unloads bending moment due to elevated temperature (figure 6.19) the effect causes the middle column to displace, shown as a slight dip in the vertical displacement of the central node on topside deck (figure 6.20). The long vertical line in figure 6.19 illustrates that functional loads are applied in the beginning of the simulation.

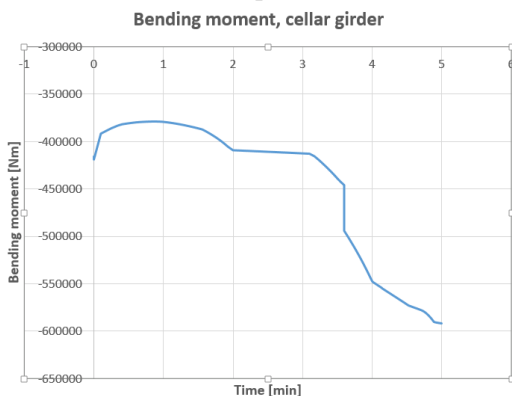


**Figure 6.19:** Bending moment in cellar deck girder. "Outer" position

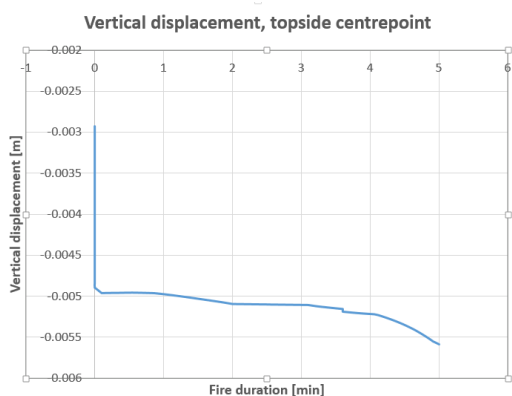


**Figure 6.20:** Vertical displacement of central topside node. "Outer" position



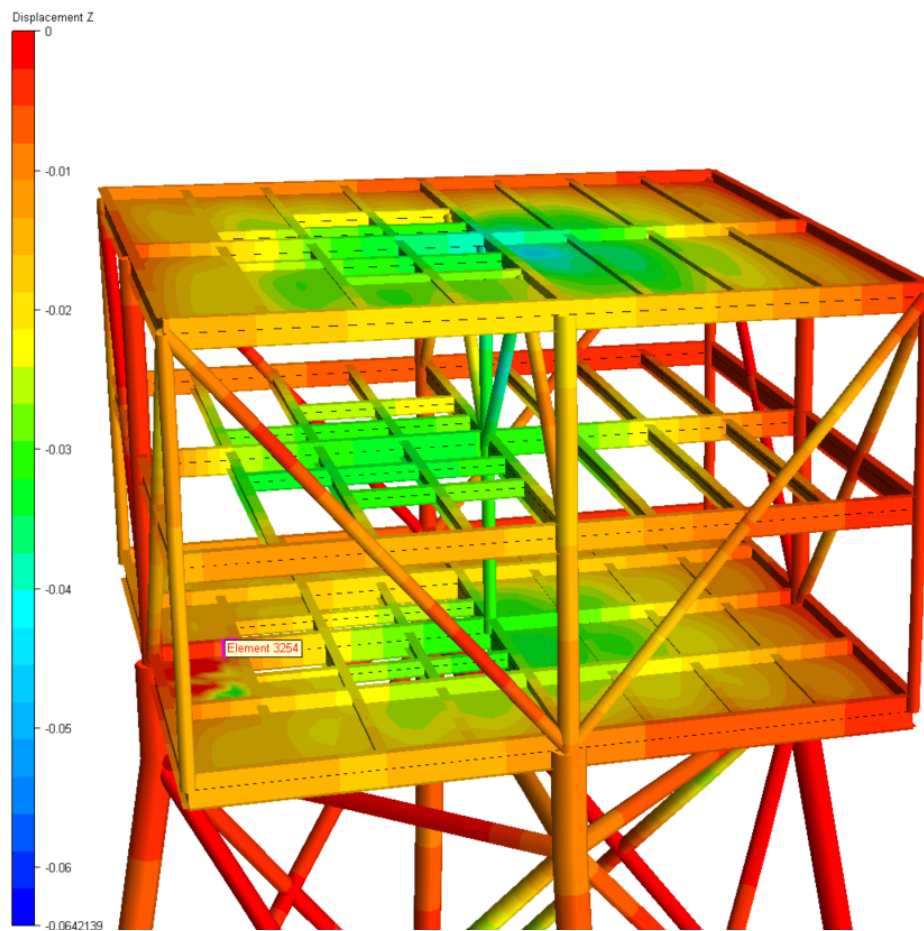


**Figure 6.21:** Vertical displacement, last time step, temperature domain simulation.

No dramatic effects are observed throughout the specified duration. However, the trend in figure 6.19 is unsettling, so a simulation over a longer duration would be interesting. It seems that the pushdown analysis may not have been sufficient for this specific case.

### 6.2.2.2 "Inner" case

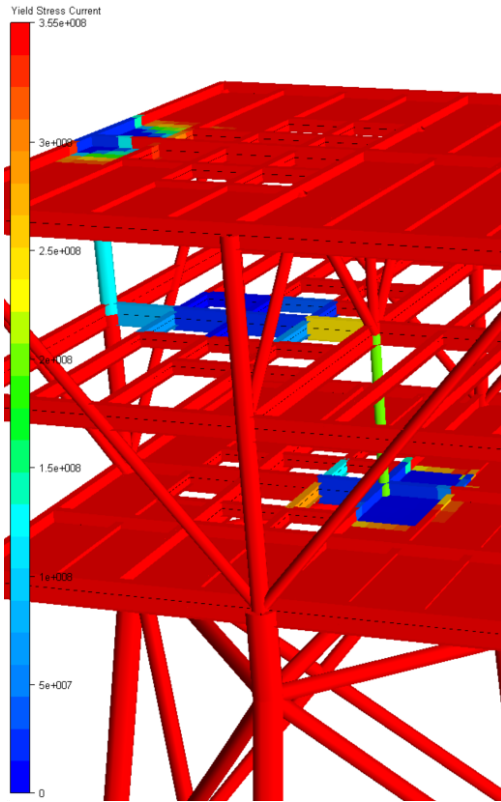


**Figure 6.22:** Updated yield strength for beam elements.  
JUR collapse "inner" case

When placing the fire further inn on the cellar deck, the heating affects a larger number of structural components. See that a several elements have reduced yield strength. This results in lower redundancy, and the collapse is more sudden.

Again, pushdown simulation of the last time step is performed, this time with considerable reduction of the reserve strength ratio. The required load of factor 1.0 is still carried without large deformations, but as a large number of beams on the mezzanine deck has reduced capacity, the increasing load leads to fracture in two deck beams forming one of the riser sleeves (appear grey in figure 6.23).

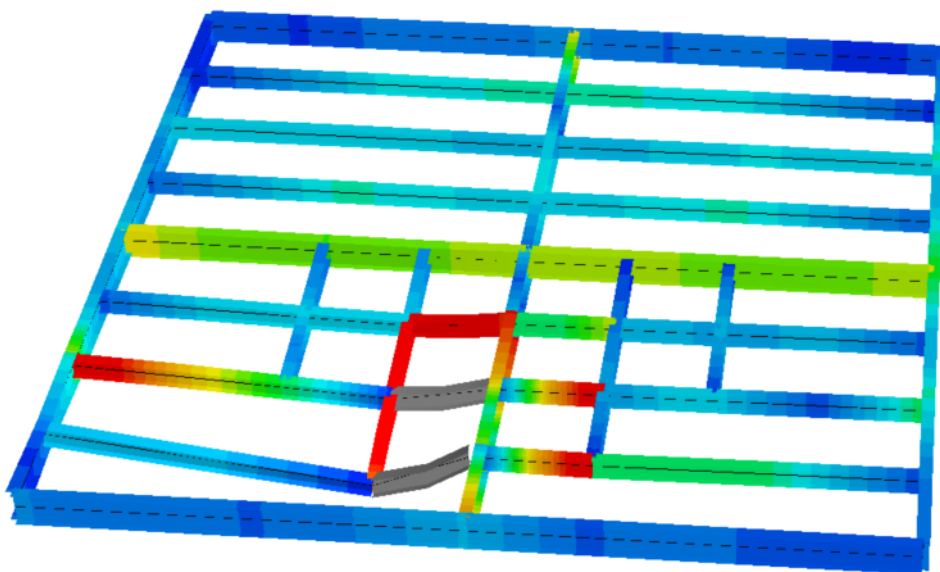


**Figure 6.23:** Fractured beams on mezzanine deck. "Inner" position

The vertical displacement of the southern most fractured element is plotted against global load in figure 6.24. See that only a small increase of the load after the first fracture makes the next beam fracture. A slight increase in load is again applied, before the third plateau, representing buckling of inner truss members. At this load level, the fractured beam has displaced 1.63 [m]. The possibility that equipment has fallen down from mezzanine to cellar deck causing further damage can not be ruled, thus the failure load is set before the first fracture occurs, at load level 1.47.

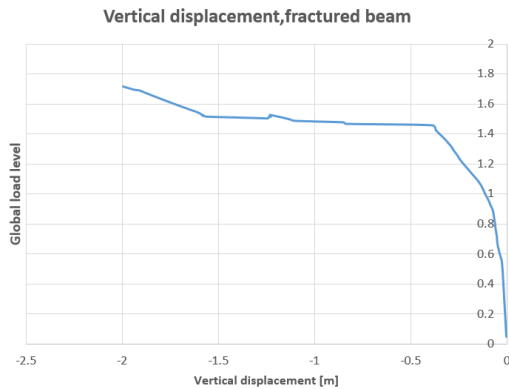


**Figure 6.24:** Vertical displacement of fractured beam. "Inner" position

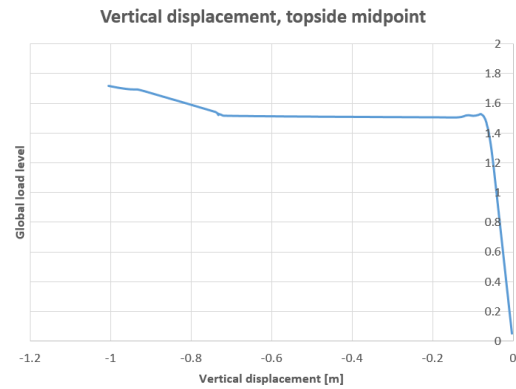


**Figure 6.25:** Vertical displacement of central topside midpoint. "Inner" position

**Temperature domain.** The vertical displacement of the southern most fractured beam from the pushover simulation is shown as function of time in figure 6.26.

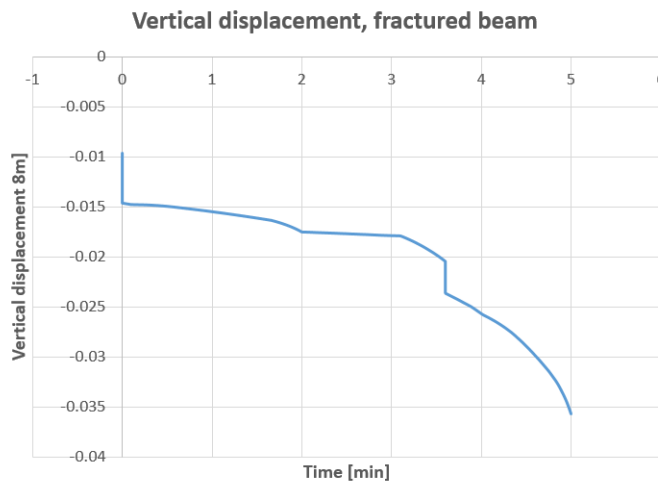


**Figure 6.26:** Vertical displacement in temperature domain of fractured beam. "Inner" position

There is reason to assume the structure survives this fire scenario as well. But again, the trend is unsettling the last minute of duration. The pushdown simulation predicts some centimeters deflection (figure 6.24), but a longer simulation in temperature domain would help determine if pushdown is adequate for this case.

## 6.3 Wireline operation

As mentioned in section 6.1.1, the load definition of the well intervention equipment weight can be user specified in the matlab program:

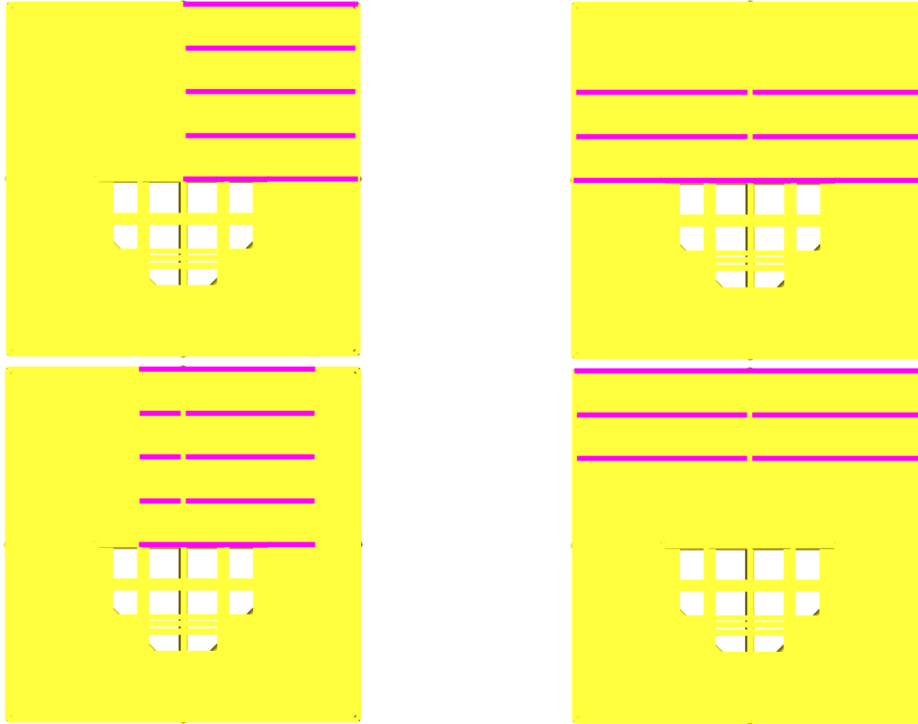


**Figure 6.27:** Different load configurations

Initially simulations were run for various configurations, but taking accessibility and practicality in to consideration, it was decided to only spread the load across the whole north area of the topside (20 m x 10 m).

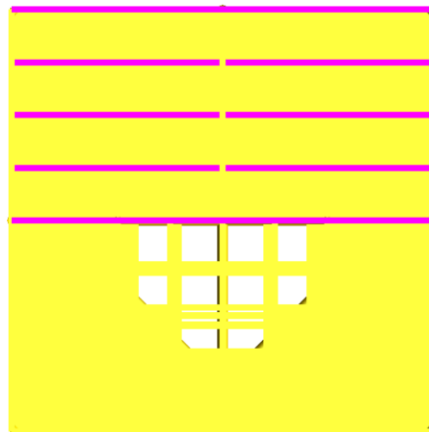


**Figure 6.28:** Wireline load configuration

### 6.3.1 Cold Pushdown Analysis

Loading the structure stepwise with functional loads and own weight simultaneously as explained in the cantilever collapse case, the topside carries the load very well. The first yield stress is detected in the north facing main column, at load level 3.17. Nothing dramatic happens before the first inner diagonal truss member buckles (figure 6.29). Vertical displacement of the midpoint of the loaded area has the largest value (figure 6.31), and is shown in figure 6.30. The removal of the buckled brace give a drop, as shown in both figures, but redistribution of the loads are carried out. The ultimate load level of **7.1** stopped the analysis, as when one additional member failed, equilibrium could not be reached. Remembering to apply the safety factor of  $\gamma_{design} = 1.5$  reduces the number to 4.7.

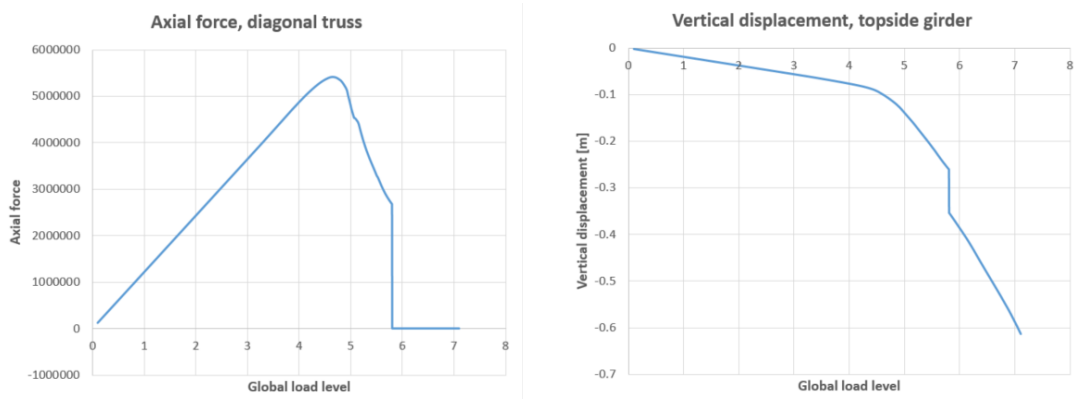


**Figure 6.29:** Buckling of diagonal truss member. **Figure 6.30:** Vertical displacement of topside girder midpoint  
Wireline load

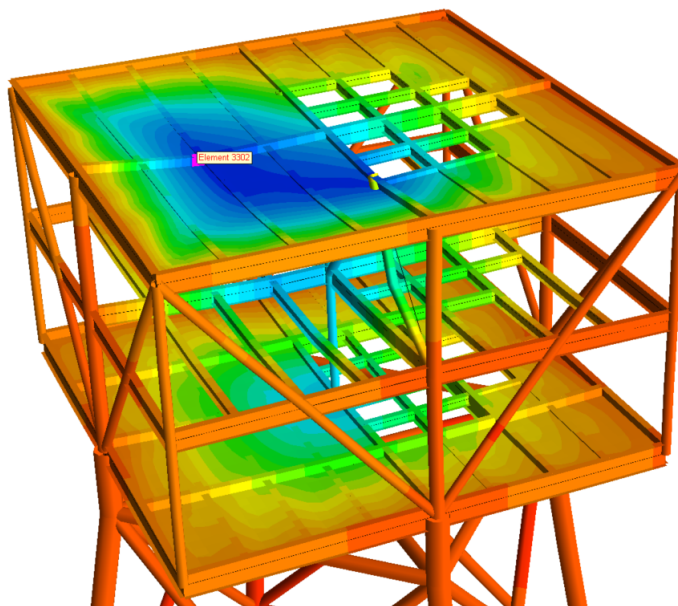
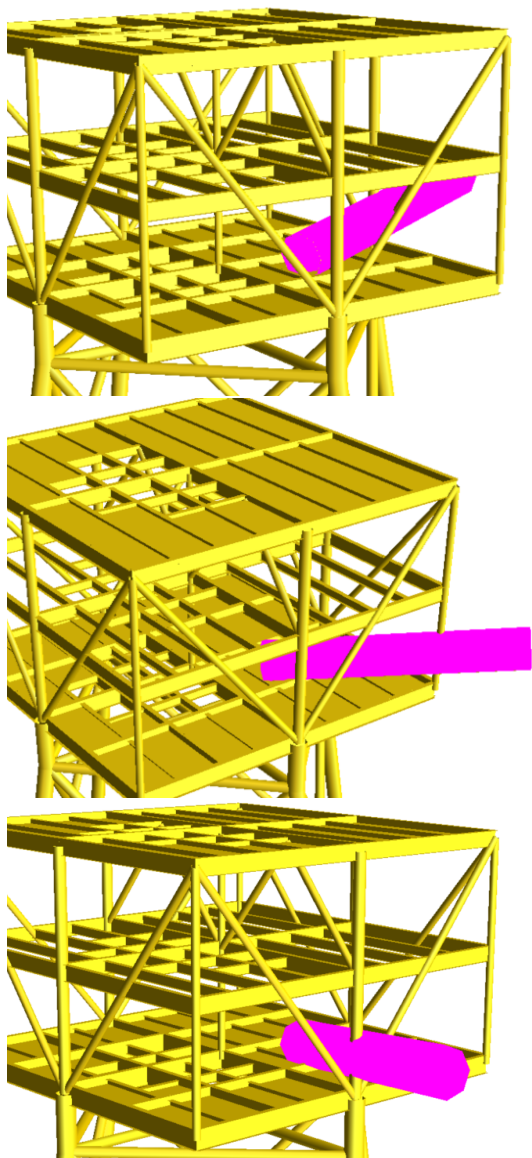


**Figure 6.31:** Vertical displacements before ultimate collapse shown as contour curves

### 6.3.2 250 kW/m<sup>2</sup> Jet Fire

The same applies as for the cantilever collapse load when exposed to fire loads. The load condition is automatically an accidental one, and safety factors are set to one. Again, the last time step is subjected to a pushdown analysis first, to see if more are necessary. Remembering, this case has an hour duration.

The fire intensity was calculated and calibrated in the same manner as in section 6.2.2, and the applied intensity is set to 1230 kW/m.



Using symmetry, three flame directions in the north-east quadrant have been investigated. The flame origin is thought to be in relation to the manifold that is to be placed on cellar deck, just north of the middle. Origin coordinates [3 m, 3 m, 1 m] is applied to be able to reach the columns.

Simulations were run with flame length 10 m, but the effects shown were small. Conferring with figure 2.14 the flame length in the tabulated guidance corresponding to an initial heat flux of 250 kW/m<sup>2</sup> is 15 m. Hence, the length is set to be 15 m for the simulations.

Two incident elevations were investigated for each direction. One where the flame was directed almost horizontal, as shown in the figures to the left, and one directed towards the elevation of the mezzanine deck.

**Figure 6.32:** Various flame directions. 108°, 45° and 342° in succession

### 6.3.2.1 Direction 108 degrees

Starting with the lowest elevation, the jet hits the main column and a diagonal directly. These two buckle first, almost simultaneously. The global instability is reached when one of the inner braces buckles a few steps after. The same girder displacement is plotted as in the previous section (figure 6.33), and the main column axial force curve is presented in figure 6.34.

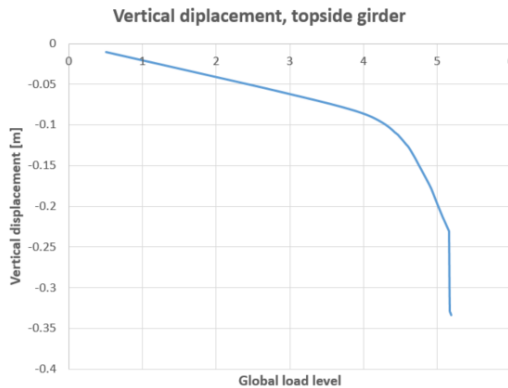


**Figure 6.33:** Low incident fire elevation. Displacement of topside girder

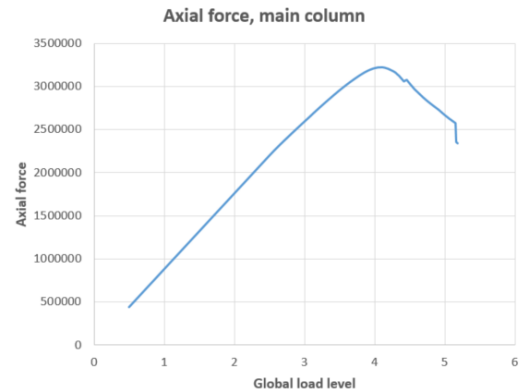


**Figure 6.34:** Axial force curve for main column

The collapse load is reached at a load level of **5.1**.

Directing the fire a little higher reverse the collapse order: the compression member in the inner truss buckles first. The collapse load is somewhat higher, all though not by much:

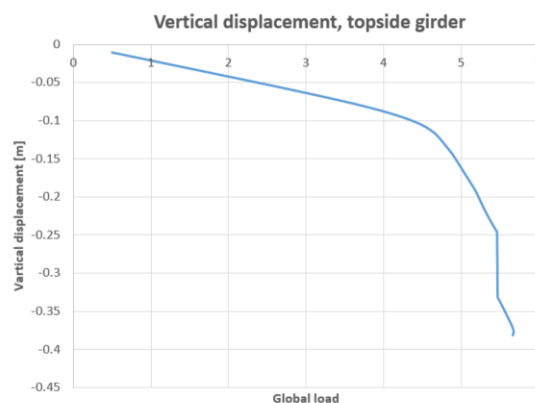


**Figure 6.35:** Vertical displacement of topside girder

Some extra resistance is mobilized as the outer diagonal is not as affected by heat as the previous case, seen in the tail of the curve. But when it buckles, the system is unstable and collapses. Maximal load level before failure: **5.65**

With such large reserve strength ratios, it is assumed concluded that the structure survives, without presenting results from temperature domain analysis.

### 6.3.2.2 Direction 45 degrees

The analyses were run up to a load level of 6 for both elevations, to save hard drive space as so many analyses were run. The structure did not experience unstable collapse before reaching load level 6. The two compression braces in the internal truss buckled, but the load was redistributed. Collapse is not expected as fast when heating the corner column, as the bulk of the topside loads are transferred through the main columns and deck girders. There is reason to conclude the structure will survive these scenarios as well.

### 6.3.2.3 Direction 342 degrees

A larger response is expected for this case, as more load is carried by the main column, though not as large as the 108° direction.

Starting with the flame burning at the low elevation, the largest deflections are now located towards the east edge. Following the vertical displacement of the top of the column, the collapse load is again easily identified at the tail of the curve.

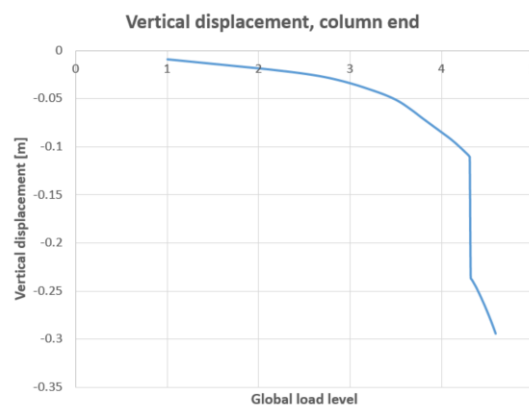


**Figure 6.36:** Vertical displacement, top of the main east column

Critical load level is **4.58**

Figure 6.37 show the collapse mechanism. As the main column buckles and is removed from the system, the girders transfer load to the outer diagonal braces. Some loading is added before they to collapse, and the system reaches instability.



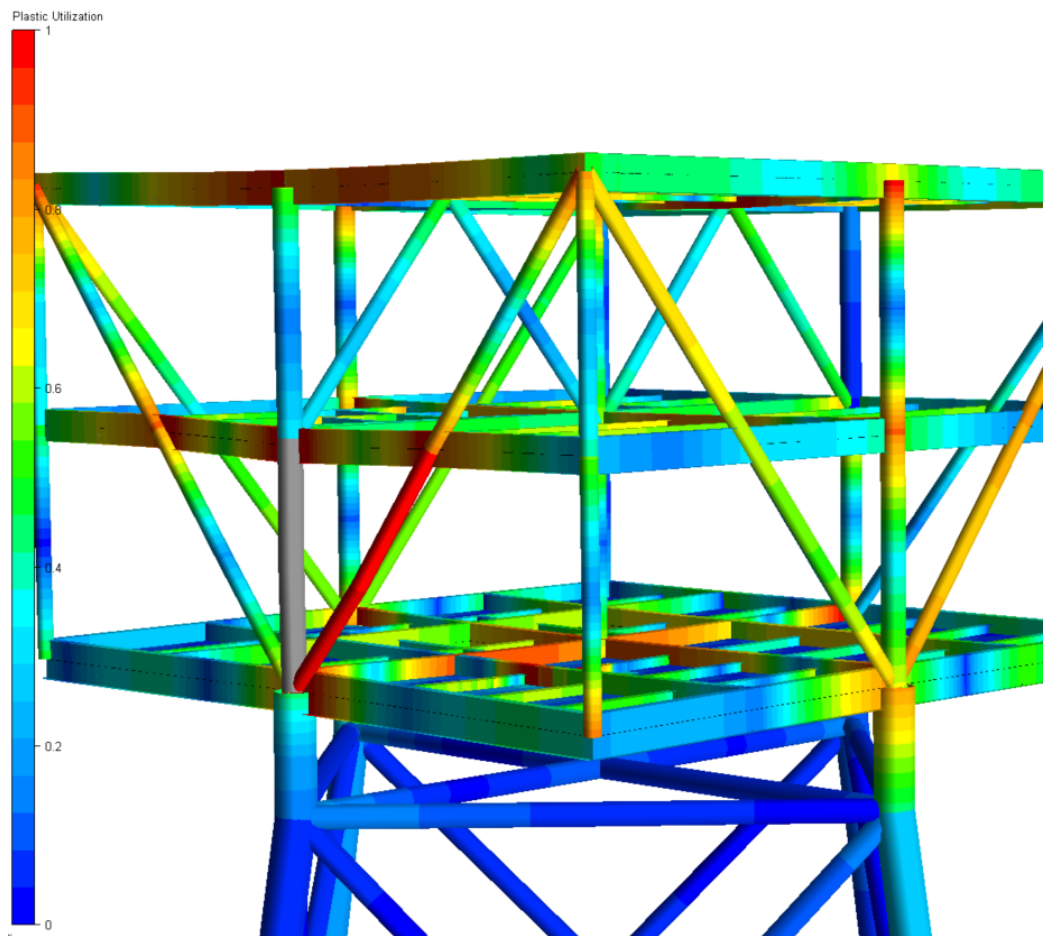


Figure 6.37: Collapse mechanism after column buckling

Directing the flame upwards to the mezzanine deck give fracture of the perimeter girder:

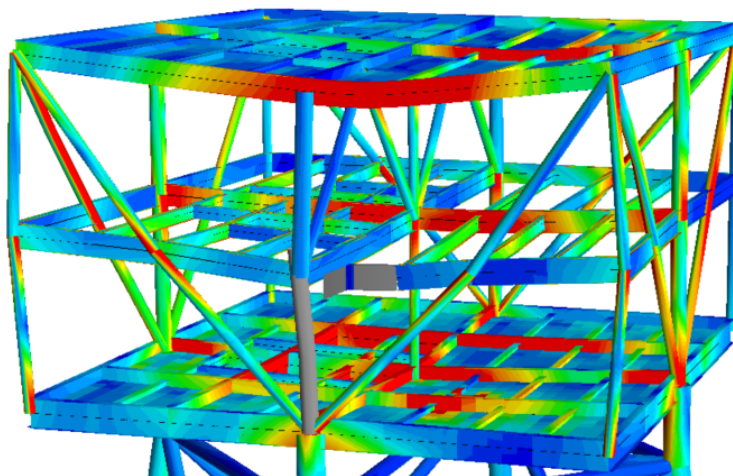
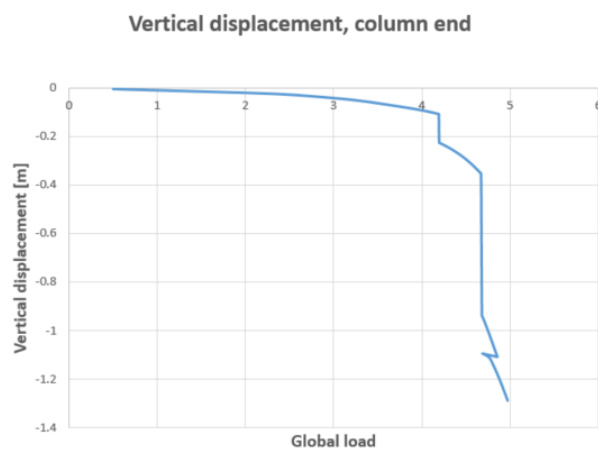


Figure 6.38: Fracture due to reduced material strength

The main column has already failed, causing extra tensile and bending stresses in the girder. Immediately, large lateral displacements occur, because the structure is loaded at the top. The risk of equipment falling down on the cellar can not be tolerated. Thus, the collapse load is set before fracture. This is indicated by the sudden increase in vertical displacement of the column top node:



**Figure 6.39:** Vertical displacement, top of the main east column during fracture

Collapse load level: **4.65**.

Anders Strand

### 6.3.3 Pool fire

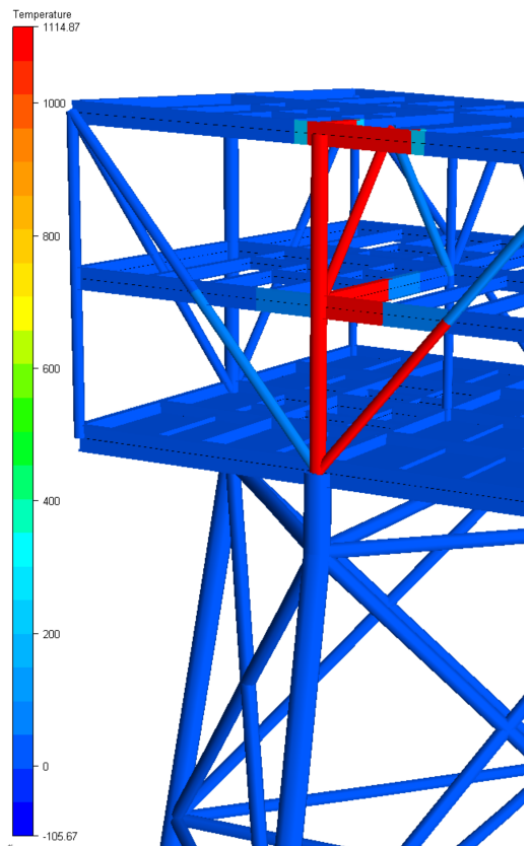
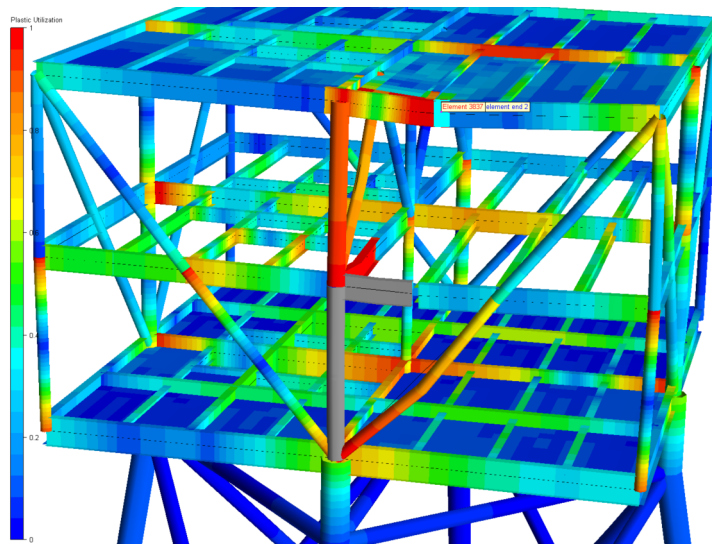


Figure 6.40: Small HC fire

No direct models are available in FAHTS for simulating pool fires. The use of a conical jetfire was discussed, but it was deemed unsatisfactory after trying it. The standard HydroCarbon temperature curve is available, and though it is often thought of as conservative, it is frequently used in simplified models. Having in mind the fracture in the last section, a small pool fire of  $3.5 [m] \times 3.5 [m]$  and a height reaching up to the topside deck is defined in the area of the east main column. See that an unrealistically small amount of heat is transferred to surrounding elements, thus giving to stiff "boundary conditions" for the heat affected elements.

The girder fractures during the half- hour pool fire as well, but now at the other end. The fracture happens at load level **2.64**, one step before the situation in figure 6.41. See that the column has failed in advance for this case as well.



**Figure 6.41:** Failure mode, 30 minutes local HC-fire

The displacement of the highlighted node is shown in figure 6.42. See that more load can be carried globally after the fracture, but the criteria of preventing further damage sets the collapse load before fracture.

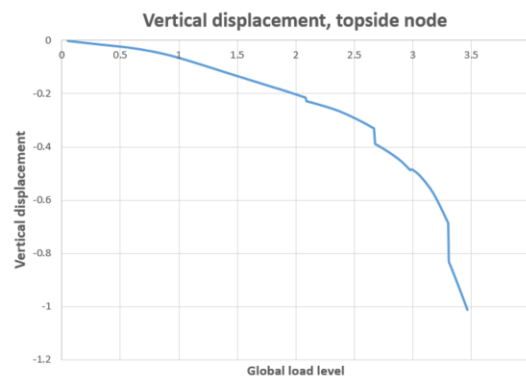


**Figure 6.42:** Vertical displacement of topside girder node

## 6.4 Simulation summary

All presented simulations display a reserve strength ratio above 1. This means the structure withstands the characteristic loads, both functional and heat loads. There is some concern, however, about the last of the cantilever collapse simulations, where the displacement curve showed an unnerving trend.

The pool fire simulation was not really that, and the results are not relied upon.

Whether or not the use of PFP is required depends on the uncertain case of the

cantilever collapse. The structure did perform well without modelling any protection for the given durations of fire scenarios.

The use of temperature- load domain method was advised against by supervisor, as it would complicate the simulations and take that much more time. The temperature domain will for most cases give more conservative results, though not as realistic.



# Chapter 7

## Conclusion

A review of current and proposed regulations regarding design against fire loads have been made, touching upon simplified methods for calculating structural response during an accidental fire. Models to predict heat loads have been presented along with their limitations.

The main structure of an unmanned wellhead platform has been designed, based on comparable structures and public information about Kværner's "Subsea On a Stick". Rough estimations have been carried out to choose reasonable steel sections for primary structural elements, choosing heavy sections to try and avoid the use of PFP.

Provided help from Granli in Kværner, a finite element model was established in GeniE and then imported to USFOS. Improving the resistance to first yield by 60 %.

A small shell program was modified to work with FAHTS and USFOS, and several hundred FAHTS and USFOS simulation was, run only to discover that 15-20 would have been sufficient for the present results.

The platform displayed robustness as expected, being over-dimensioned to some extent. It was noted that other load conditions may need the extra strength. All fire scenarios were run in load- domain (Pushdown) and the structure withstood all of them with a reserve strength ratio greater than zero.

To compare, temperature domain simulations were performed for certain load conditions. It was observed that the short 5 [min] duration of the most intense fire scenario should have been run passed the duration to confirm or debunk the trend in displacement curves.





# Chapter 8

## Further work

Several tasks have come up during the work that could still be done:

- Run the fire scenarios over a longer duration than specified. Investigating trends and predicting the behaviour in post- collapse
- Run temperature- load domain simulations to compare
- The script problems were to some extent solved. And a newer version were tested but not used in the thesis work. The files will be handed in with the thesis. Finishing the program and following post processor would give a powerful tool to run fire response in.
- Local models should be checked, with respect to joints.
- CFD simulations of fire scenarios would give more realistic response simulations.
- jet fire cases should be performed with the flame directed up towards the topside deck.
- The effect of having a plated mezzanine deck as opposed to grating.
- More work towards defining a good fracture definition for elevated temperatures.



# Bibliography

Amdahl, J. (2005), *TMR4205 Buckling and Ultimate Strength of Marine Structures*, Institutt for Marin Teknikk.

Amdahl, J. (2010), *TMR4167 MARIN TEKNIKK 2. Del 1: Konstruksjonsanalyse*, Vol. 1, Institutt for Marin Teknikk.

CNGEurope (2014), 'Fuel calorific values'.

**URL:** <http://cngeurope.com/fuel-calorific-values/>

DentSteel (2016), *buyers guide book*, fourth edition edn, Dent Steel Services ltd. Free list of profiles delivered by Dent Steel in Great Britain.

**URL:** <http://www.dentsteel.co.uk/buyersguide.aspx>

DNV-RP-C204 (n.d.), 'Dnv-rp-c204 design against accidental actions'.

EC1-1-2 (2002), 'Eurocode 1: Actions on structures. part 1-2: General actions, actions on structures exposed to fire'.

EC3-1-1 (2005), 'Eurocode 3: Design of steel structures. part 1-1: General rules and rules for buildings'.

EC3-1-2 (2005), 'Eurokode 3: Prosjektering av stålkonstruksjoner. del 1-2: Brannteknisk dimensjonering'.

FABIG (2010), 'Fabig technical note 11. fire loading and structural response'.

Fabigweb (2016), 'What is fabig'.

**URL:** <http://www.fabig.com/about/WhatisFABIG>

IMTsoftware (2012), 'Usfos scripting', Resource web page for stuents in the Department of Marine Technology.

**URL:** <http://www.ivt.ntnu.no/imt/software/usfos:scripting>

Lorentzen, M. (2015), 'Ingen kjøpere har foreløpig meldt seg: Nå fokuserer kværner på "indremedisin"', Dagens Næringsliv.

**URL:** <http://e24.no/energi/kvaerner/ordrebooken-kan-halveres-innen-nyttaar-ingen-kvaerner>

Moan, T. (2003), *Finite Element Modelling and Analysis of Marine Structures*, Institutt for Marin Teknikk.

N-001 (2012), 'Norsok n-001 integrity of offshore structures'.

N-003 (2007), ‘Norsok n-003 actions and action effects’.

N-004 (2013), ‘Norsok n-004 design of steel structures’.

OffshoreEnergyToday (2014), ‘Kvaerner selected for oseberg platform concept study’.

**URL:** <https://www.offshoreenergytoday.com/about-2/>

SINTEF (1994), *FAHTS User’s manual*.

**URL:** <http://usfos.no/manuals/fahts/theory/documents/FahtsTheoryManual.pdf>

SINTEF (2001), ‘Usfos getting started’. [Online; accessed 04-June-2015].

**URL:** <http://www.usfos.no/manuals/usfos/theory/documents/Gettingstarted.pdf>

Skallerud & Amdahl (2005), ‘Usfos user’s manual, solution strategy’. [Online; accessed 02-June-2015].

**URL:** <http://www.usfos.no/manuals/usfos/users/documents/UsfosUM04.pdf>

USFOSweb (2014), ‘Pushdown analysis in usfos’, USOFS.no.

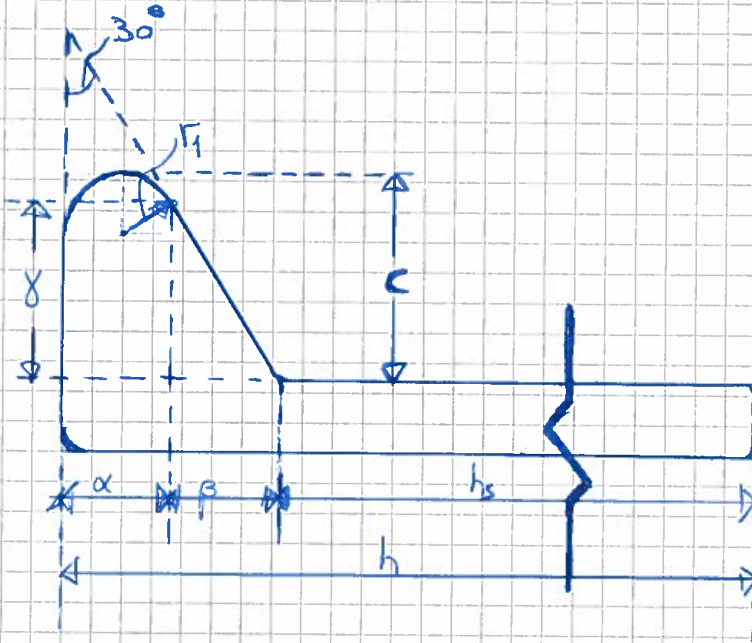
**URL:** <http://usfos.no/manuals/usfos/theory/documents/PushDownAnalysisinUsfos.pdf>



# Appendix A

## Web height of bulb flat steel

# Web height of bulb flat steel profile



$$\alpha = r_1 (1 + \cos(30^\circ))$$

$$y = c - r_1 (1 - \sin(30^\circ))$$

$$\beta = y \tan(30^\circ)$$

$$h_s = h - (\alpha + \beta)$$

	$r_1$	$c$	$\alpha$	$y$	$\beta$	$h_s$	$h_s/h$
HP 120x6	5	17	9,33	14,50	8,37	102,3	85%
HP 100x6	4,5	15,5	8,39	13,25	7,65	84,0	84%
HP 80x6	4	14	7,46	12,00	6,93	65,6	82%

# Appendix B

## Girder grillage model

A grillage beam system is solved by the unit load method in the Marin Teknisk 2 compendium (Amdahl 2010), chapter 8. This example is solved for the specific system relevant to the current platform by setting beam lengths and stiffness to be equal for both beams.

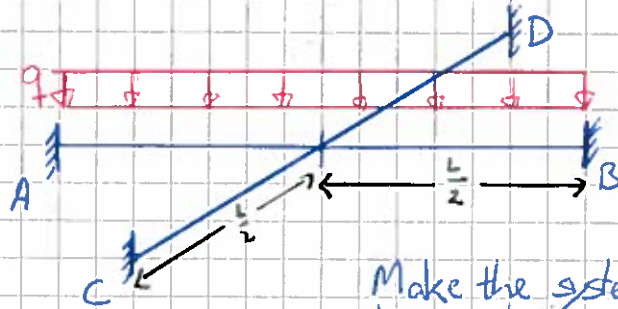


# Grillage "beams"

- Assuming deck beams transfer all deck load into one of the girders, the other one will just support the midpoint:

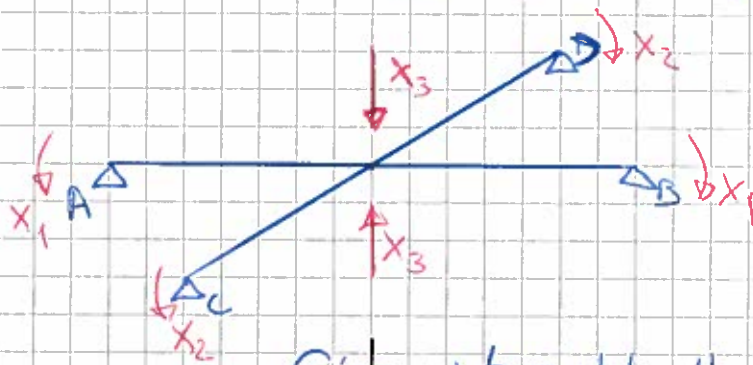
$$L_{AB} = L_{CD}$$

$$EI_{AB} = EI_{CD}$$

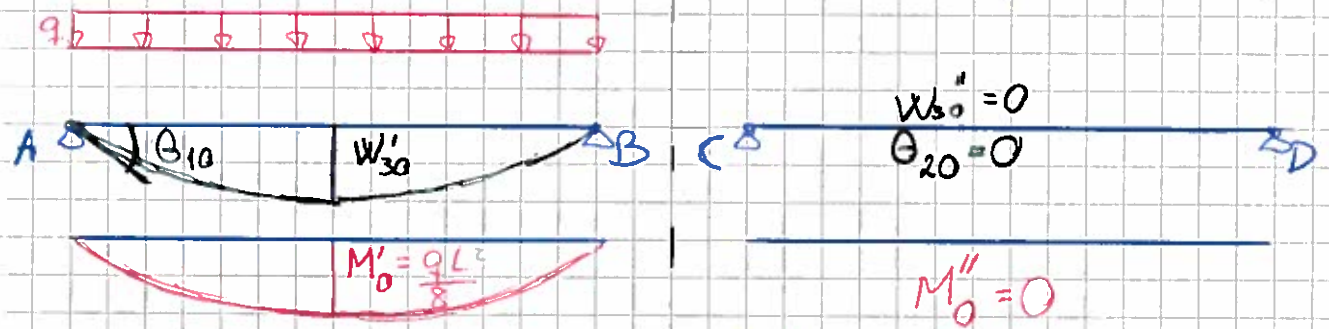


Make the system statically determined by releasing the clamped ends

Substitute "contact point" by a force  $X_3$

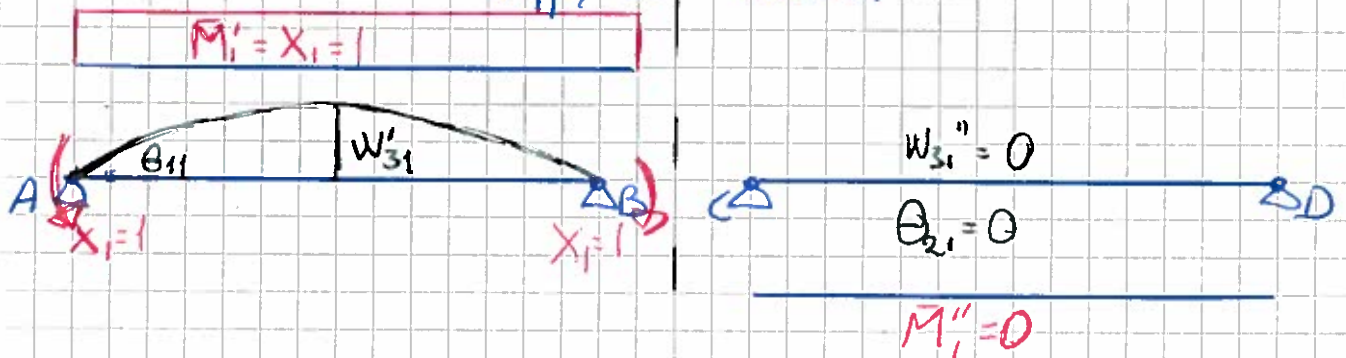


Give us two statically determined systems



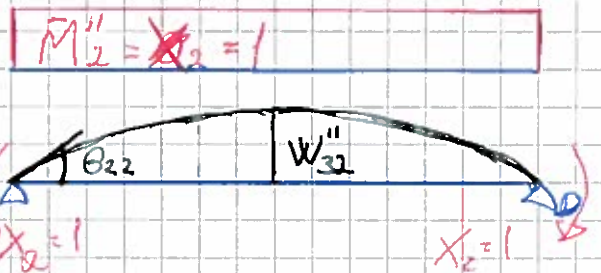
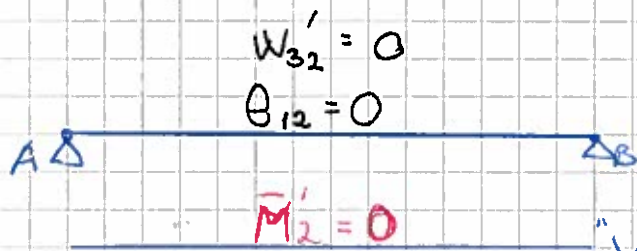
" $X_0$ -system"

Apply unit moment " $X_1$ "



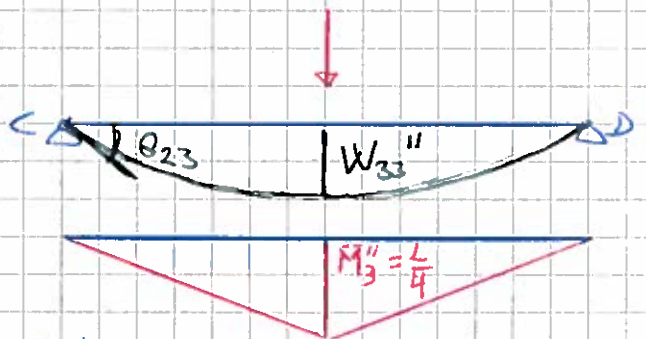
" $X_1$ -system"

Apply unit moment  $X_2$



" $X_2$ -system"

Apply unit force  $X_3$



" $X_3$ -system"

3 unknown forces:  $X_1, X_2$  &  $X_3$  requires

3 equations:

Rotation ~~at~~ of point A is zero:

I  $\theta_{10} + X_1 \theta_{11} + X_2 \theta_{12} + X_3 \theta_{13} = 0$

Rotation of point C is also zero:

II  $\theta_{20} + X_1 \theta_{21} + X_2 \theta_{22} + X_3 \theta_{23} = 0$

Compatibility in the intersection of the two beams:

III  $w_{AB} + w_{CD} = 0$ , where:

$w_{AB} = w_{30}' + X_1 w_{31}' + X_2 w_{32}' + X_3 w_{33}'$ , &

$w_{CD} = w_{30}'' + X_1 w_{31}'' + X_2 w_{32}'' + X_3 w_{33}''$

III  $w_{30}' + w_{30}'' + X_1 (w_{31}' + w_{31}'') + X_2 (w_{32}' + w_{32}'') + X_3 (w_{33}' + w_{33}'') = 0$

$\Rightarrow w_{30}' + X_1 w_{31}' + X_2 w_{32}' + X_3 w_{33}' = 0$



Rapid integration (use symmetry):

$$\theta_{10} = \int_0^L \frac{M_0 \bar{M}_1}{EI} dx = \frac{L}{EI} \frac{qL^2}{8} \cdot \left(-\frac{2}{3}\right) = -\frac{qL^3}{12EI}$$

$$\theta_{20} = \int_0^L \frac{M_0 \bar{M}_2}{EI} dx = 0 \cdot 1 = 0$$

$$W_{30} = \int_0^L \frac{M_0 \bar{M}_3}{EI} dx = \frac{L}{EI} \frac{qL^2}{8} \cdot \frac{L}{4} \cdot \left(-\frac{5}{12}\right) = -\frac{5}{384} \frac{qL^3}{EI}$$

$$\theta_{11} = \int_0^L \frac{\bar{M}_1 \bar{M}_1}{EI} dx = \frac{L}{EI} \cdot 1 = \frac{L}{EI} = \theta_{22}$$

$$\theta_{12} = \theta_{21} = 0$$

$$\theta_{13} = \int_0^L \frac{\bar{M}_3 \bar{M}_1}{EI} dx = \frac{L}{EI} \cdot \frac{L}{4} \cdot 1 \cdot \frac{1}{2} = \frac{L^2}{8EI} = W_{31}$$

By symmetry

$$\theta_{23} = \int_0^L \frac{\bar{M}_3 \bar{M}_2}{EI} dx = \frac{L}{EI} \cdot \frac{L}{4} \cdot 1 \cdot \left(-\frac{1}{2}\right) = -\frac{L^2}{8EI} = W_{32}$$

$$W_{33} = 2 \int_0^{\frac{L}{2}} \frac{\bar{M}_3 \bar{M}_3}{EI} dx = 2 \cdot \frac{L}{EI} \cdot \frac{L}{4} \cdot \frac{L}{4} \cdot \left(\frac{1}{3}\right) = \frac{L^3}{24EI}$$

$$\begin{matrix} \text{I} \\ \text{II} \\ \text{III} \end{matrix} \frac{L}{EI} \begin{bmatrix} 1 & 0 & \frac{L}{8} \\ 0 & 1 & -\frac{L}{8} \\ \frac{L}{8} & -\frac{L}{8} & \frac{L^2}{24} \end{bmatrix} \cdot \begin{bmatrix} X_1 \\ X_2 \\ X_3 \end{bmatrix} = \begin{bmatrix} 1 \\ 0 \\ \frac{5L}{32} \end{bmatrix} \frac{qL^3}{12EI}$$

$$\begin{bmatrix} X_1 \\ X_2 \\ X_3 \end{bmatrix} = \frac{1}{\text{Det}(\text{Matrix})} \begin{bmatrix} \frac{L^2}{24} & \frac{L}{8} & \frac{L}{8} \\ \frac{L}{8} & \frac{L^2}{24} & -\frac{L}{8} \\ \frac{L}{8} & -\frac{L}{8} & \frac{L^2}{24} \end{bmatrix} \begin{bmatrix} 1 \\ 0 \\ \frac{5L}{32} \end{bmatrix} \frac{qL^3}{12EI}$$

$$\begin{aligned} \text{Det}(\text{Matrix}) &= 1 \cdot \left(1 \cdot \frac{L^2}{24} - \left(-\frac{L^2}{24}\right)\right) - 0 \cdot \left(\frac{L^2}{24} \cdot \frac{L}{8} - \left(\frac{L}{8} \cdot \frac{L}{8}\right)\right) + \frac{L}{8} \cdot \left(0 \cdot \frac{L}{8} - \frac{L}{8}\right) \\ &= \frac{L^2}{24} - \frac{L^2}{64} - \frac{L^2}{64} = \frac{L^2}{96} \end{aligned}$$

$$M_{11}'' = 1 \cdot \frac{L^2}{24} - \left(-\frac{L}{8}\right)\left(-\frac{L}{8}\right) = \frac{5L^2}{192}$$

$$M_{12}'' = 0 \cdot \frac{L^2}{24} - \left(-\frac{L}{8}\right)\left(\frac{L}{8}\right) = \frac{L^2}{64}$$

$$M_{13}'' = 0\left(-\frac{L}{8}\right) - \left(\frac{L}{8}\right) = -\frac{L}{8}$$

$$M_{21}'' = 0 \cdot \frac{L^2}{24} - \left(\frac{L}{8}\right) \cdot \frac{L}{8} = -\frac{L^2}{64}$$

$$M_{22}'' = 1 \cdot \frac{L^2}{24} - \frac{L}{8} \cdot \frac{L}{8} = \frac{5L^2}{192}$$

$$M_{23}'' = 1\left(-\frac{L}{8}\right) - 0 \cdot \frac{L}{8} = -\frac{L}{8}$$

$$M_{31}'' = 0 \cdot \frac{L^2}{24} - 1 \cdot \frac{L}{8} = -\frac{L}{8}$$

$$M_{32}'' = 1 \cdot \frac{L^2}{24} - 0 \cdot \frac{L}{8} = \frac{L^2}{24}$$

$$M_{33}'' = 1 \cdot 1 - 0 \cdot 0 = 1$$

$$M'' = \begin{bmatrix} \frac{5L^2}{192} & \frac{L^2}{64} & -\frac{L}{8} \\ \frac{L^2}{64} & \frac{5L^2}{192} & -\frac{L}{8} \\ -\frac{L}{8} & -\frac{L}{8} & 1 \end{bmatrix}$$

$$\Rightarrow \begin{bmatrix} X_1 \\ X_2 \\ X_3 \end{bmatrix} = \frac{96}{L^2} \begin{bmatrix} \frac{5L^2}{192} & \frac{L^2}{64} & -\frac{L}{8} \\ \frac{L^2}{64} & \frac{5L^2}{192} & -\frac{L}{8} \\ \frac{L}{8} & -\frac{L}{8} & 1 \end{bmatrix} \frac{96}{12} \begin{bmatrix} 1 \\ 0 \\ \frac{5L}{32} \end{bmatrix}$$

$$X_1 = \frac{96}{12} \left( \frac{5L^2}{192} - \frac{L}{8} \cdot \frac{5L}{32} \right) = \frac{5}{96} p L^2$$

$$X_2 = \frac{96}{12} \left( \frac{L^2}{64} - \frac{L}{8} \cdot \frac{5L}{32} \right) = -\frac{9L^2}{32}$$

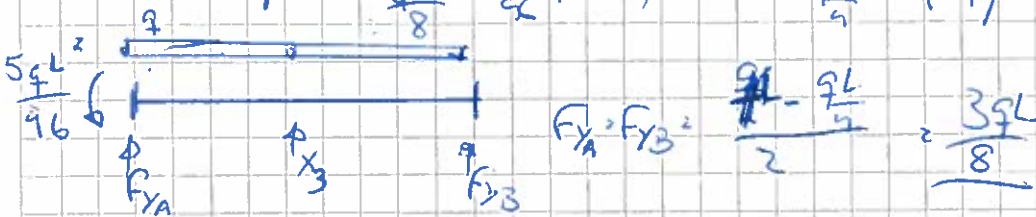
$$X_3 = \frac{96}{12} \left( -\frac{L}{8} + \frac{5L}{32} \right) = \frac{9L}{4}$$

## Girder AB

$$M' = M'_0 + X_1 \bar{M}'_1 + X_2 \bar{M}'_2 + X_3 \bar{M}'_3$$

$$M_A = 0 + \frac{5}{96} qL^2 (+1) + 0 + \frac{qL}{4} \cdot 0 = \frac{5qL^2}{96}$$

$$\text{Midpoint: } \frac{qL^2}{8} + \frac{5}{2} qL^2 (-1) + 0 + \frac{qL}{4} \cdot \left(-\frac{L}{4}\right) = \frac{1qL^2}{96}$$



$$F_{XA} = F_{XB} = \frac{qL - \frac{qL}{4}}{2} = \frac{3qL}{8}$$

## Girder CD

$$M'' = M''_0 + X_1 \bar{M}''_1 + X_2 \bar{M}''_2 + X_3 \bar{M}''_3$$

$$M_C = \frac{-qL^2}{32} \cdot (-1) + \frac{qL}{4} \cdot 0 = \frac{qL^2}{32}$$

$$\text{Midpoint: } \frac{-qL^2}{32} (+1) + \frac{qL}{4} \cdot \frac{L}{4} = \frac{1qL^2}{32}$$



$$F_{XC} = F_{XD} = \frac{qL}{2} = \frac{qL}{8}$$

$$2 \cdot \frac{3qL}{8} + 2 \cdot \frac{qL}{8} = qL$$



# Appendix C

## Matlab input generator

"int\_placement.m" is the program that runs the whole matlab program

```
1  clc
2  clear all
3  %% Finding beam elements to load during well intervention
4  %% Due to symmetry, only the North-East quadrant of the topside deck is
5  %% considered. Though the load could be moved past y<0 to get heavy loading
6  %% of the column at y=0
7
8  rectangledim= [20 10];           %Width(W-E) and length(S-S) of
9                                   %the "container rectangle"
10 sw_corner = [-10 0];           %South-west corner of rectangle
11 ne_corner = sw_corner + rectangledim; %North-east corner of rectangle
12
13 ldcase = 3;                     %loadcase number used in USFOS
14
15 equip_weight = 150*10^3;        %[kg] well intervention equipment
16 g = 9.81;                      %[N/kg] Gravitational acceleration
17 elem_l = 0.5;                  %[m] all beam elements on north-
18                                   %east quadrant are 0.5m of length
19
20 %% Calculating and writes load data to a load file.
21 disp('reading data from spreadsheet...')
22 [nodearray, beamarray, beamvector] = nodes();
23 disp('done')
24 disp('writing load- and group definition...')
25 [writing] = writeload(nodearray, beamarray, beamvector, sw_corner, ne_corner, ...
26     ldcase, g, elem_l, equip_weight);
27 disp(writing);
28
29 %% Generating FAHTS fhead.fem parameters
30 % User defined parameters
31 length = 15;                    %[m] Jet length
32 start_dir = 153;                %[deg] Anti-cl.wise from pos. x dir.
33 resolution = 189;              %[deg] Uniform distr # of directions (63)
34 coor_origin = [3 3 1];         %[m] Placement of "gas leak"
35 end_height = 2;                %[m] Vertical dist. to jet end point
```

```

36 intensity = 1.23E+06;           %[W/m] Heat intensity of jet
37 dinit = 2.5;                   %[m] Initial diameter of jet
38 dend = 2.5;                    %[m] End diameter of jet
39 end_time = 60;                  %[min] Duration of fahts analysis
40 resinc = 1;                     %[min] Time step length(no fancy step!)
41 endh = ldcase + (end_time/resinc);  %[m] Name of last temperature ldstep
42 disp('writing parameters for FAHTS head file')
43 [fahts] = writefahts(length, start_dir, resolution, coor_origin, end_height, ...
44     intensity, dinit, dend, end_time, resinc, endh);
45 disp(fahts);
46
47 %% Generating USFOS uhead.fem parameters
48 disp('writing parameters for USFOS head file')
49 [usfos] = writeusfos(ldcase, endh, resinc);
50 disp(usfos);

```

”nodes.m” reads the structure data from a spreadsheet (helpsheet.xlsx)

```

1 %% Function that reads node and beam data for topside beams
2 % used in script: int_placement.m
3
4
5 function [nodematrix, beamarray, beamvector] = nodes()
6 %% Input handling
7 fileid = 'helpsheet.xlsx';
8
9 %% Import node data from a spreadsheet
10 % All nodes with z-coordinate 12m(topside deck) are summoned
11 nodematrix = xlsread(fileid, 'topsidenodes', '');
12
13 %% Import beam data from same spreadsheet
14 % All beam elements of the model are summoned
15 beamarray = xlsread(fileid, 'beamarray', '');
16
17 %% Import beam data from same spreadsheet
18 % Only topside beams with orientation east-west are listed in this vector
19 beamvector = xlsread(fileid, 'beamvector', '');
20 end

```

”writefahts.m” writes parameters for FAHTS head.fem file

```

1 %Function that writes parameter file for FAHTS jetfire analysis on basis of
2 %user's chosen flame origin, length, direction resolution, diameter, heat
3 %intensity, duration and length of time step.
4
5 function [fahts] = writefahts(length, start_dir, resolution, coor_origin, ...
6     end_height, intensity, dinit, dend, end_time, resinc, endh)
7
8 %% Calculated parameters
9 proj_length = ...
10     sqrt(length^2-end_height^2);    %[m] Jet projected to horiz plane
11 num_dir = 200/resolution;
12
13
14 end_coor = [];                      %Empty parameter matrix,

```

```

15                                     %handy when writing to file
16 %% Opening and writing to parameter file.
17 fileID = fopen('fahtsparam.dat','w');
18 % Naming the parameters. Used by BASH script to substitute parameters
19 fprintf(fileID ,...
20         '%6s %6s %6s %10s %6s %6s %6s %10s %6s %6s %12s %4s %6s %4s\n' ,...
21         'xinit', 'yinit', 'zinit', 'hinit', ...
22         'xend', 'yend', 'zend', 'hend', 'inD', 'enD', 'jetdir', 'dur', 'tstep', ...
23         'lstT');
24 for i = 1:num_dir
25     % Coordinates and heat intensity of jet origin point:
26     end_coor(i,1) = (coor_origin(1));
27     end_coor(i,2) = (coor_origin(2));
28     end_coor(i,3) = (coor_origin(3));
29     end_coor(i,4) = round(intensity*100)/100;
30     % Coordinates and heat intensity of jet end point:
31     end_coor(i,5) = round((coor_origin(1) +...
32         proj_length*cosd(start_dir+(i*resolution)))*100)/100;
33     end_coor(i,6) = round((coor_origin(2) +...
34         proj_length*sind(start_dir + (i*resolution)))*100)/100;
35     end_coor(i,7) = round((coor_origin(3) + end_height)*100)/100;
36     end_coor(i,8) = intensity;
37     % Diameter of jet origin and end points:
38     end_coor(i,9) = dinit;
39     end_coor(i,10) = dend;
40     % Telling the header of FAHTS control file the resolution in degrees:
41     end_coor(i,11) = mod(start_dir + (i*resolution),360);
42     end_coor(i,12) = end_time;
43     end_coor(i,13) = resinc;
44     end_coor(i,14) = endh;
45     end_coor(i,15) = ldcase;
46     % Writing each row of data in parameter matrix into a row in the
47     % parameter file:
48     fprintf(fileID ,...
49         '%6g %6g %6g %10.2E %6g %6g %6g %10.2E %6g %6g %8g %6g %6g %6g\n' ,...
50         end_coor(i,:));
51 end
52 % Closing and saving the parameter file:
53 fclose(fileID);
54 fahts = 'done';
55 end

```

”writeusfos.m” writes parameters for USFOS head.fem file

```

1 function [usfos] = writeusfos(ldcase, endh, resinc)
2
3 %nstep = ceil(endh/2);
4 nstep = endh - ldcase;% - 20;
5 timestep = zeros(nstep,1);
6 time = zeros(nstep,1);
7 % a = ldcase;
8 fileID = fopen('usfosparam.dat','w');
9 fprintf(fileID ,'%3s %4s %4s\n' ,...
10         'djur', 'lastT', 'push');
11

```



```

12 for i = 1:(nstep)
13     %timestep(i) = endh - 2*(i-1);
14     %time(i) = timestep(i)*resinc;
15     timestep(i) = endh - (i-1);
16     time(i) = (timestep(i)-3)*resinc;
17
18     fprintf(fileID, '%4g %4g %4g\n', ...
19             time(i), timestep(i), ldcase);
20 end
21 fclose(fileID);
22 usfos = 'done';
23
24
25
26
27 end

```

”writeload.m” writes load- and group text files

```

1 % Function that takes data gathered from the spreadsheet, compares with the
2 % chosen "load rectangle", picks out the correct beam elements, calculates
3 % load intensity and writes to a load file. A group file is also written,
4 % to make the beam elements stand out in USFOS
5
6
7 function [writing] = writeload(nodearray, beamarray, beamvector, sw_corner, ...
8     ne_corner, ldcase, g, elem_l, equip_weight)
9
10 nodelist = []; %Empty array to be filled
11 counter = 1; %Help counter
12 ac = 0.001; %Accuracy helper.
13 % Go through the array of node data
14 for i = 1:length(nodearray)
15     % If the node has coordinates inside the lode rectangle it is stored in
16     % the "nodelist" array
17     if nodearray(i,2)>=(sw_corner(1)-ac) &&...
18         nodearray(i,2)<=(ne_corner(1)+ac) &&...
19         nodearray(i,3)>=(sw_corner(2)-ac) &&...
20         nodearray(i,3)<=(ne_corner(2)+ac)
21         nodelist(counter,:) = nodearray(i,:);
22         counter = counter+1;
23     end
24 end
25
26 beamlist = []; %Empty vector to be filled
27 counter = 1; %Help counter reset
28 % Go through the array of topside beams
29 for j = 1:length(beamarray)
30     % If BOTH end node numbers of a beam element exist in the "nodelist"
31     % the beam element number is stored in the "beamlist"
32     if ismember(beamarray(j,2), nodelist(:,1)) &&...
33         ismember(beamarray(j,3), nodelist(:,1))
34         beamlist(counter,1) = beamarray(j,1);
35         counter = counter + 1;
36     end

```

```

37 end
38
39 load_beams = []; %Empty vector to be filled
40 counter = 1; %Help counter reset
41 % Go through beamlist vector
42 for k = 1:length(beamlist)
43     % If the beam element exist in the "beamvector" it is east-west
44     % orientated, thus it gets stored in the "load_beams" vector
45     if ismember(beamlist(k),beamvector)
46         load_beams(counter) = beamlist(k);
47         counter = counter + 1;
48     end
49 end
50
51 %% Load calculation
52 % Assuming load is uniformly distributed over the loaded beams
53
54 numb_beams = length(load_beams); %Get the number of loaded beams
55 tot_length = elem_l*numb_beams; %Total length of loaded beams
56
57
58
59 force_eq = equip_weight*g; % [N] vertical force of the load
60 load_int = force_eq/tot_length; % [N/m] Uniform dist. line load
61
62 %% Write to load file
63 ldarray = zeros(numb_beams,5);
64 %% Opening and writing to parameter file.
65 ldfile = fopen('../loads/inter_load.dat','w');
66 % Naming the parameters. Used by BASH script to substitute parameters
67 fprintf(ldfile, '%-6s %6s %6s %6s %6s %6s %8s\n', ...
68     '#', 'ldCase', 'ElemID', 'Xint', 'Yint', 'Zint');
69 fprintf(ldfile, '%-8s\n', '#'); %Cheat to force a new line
70 for i = 1:numb_beams
71     ldarray(i,:) = [ldcase load_beams(i) 0 0 -load_int];
72     fprintf(ldfile, '%-8s %4g %6g %6g %6g %9.4E\n', 'BEAMLOAD', ldarray(i,:));
73 end
74 fclose(ldfile);
75
76 %% Opening and writing to group file
77 grfile = fopen('../groups/inter_group.dat','w');
78 fprintf(grfile, '%-6s %5s %2s %6s %7s %5s\n', ...
79     '#', 'Group', 'of', 'loaded', 'topside', 'beams');
80 fprintf(grfile, '%5s %6s %10g %17s\n', ...
81     'Name', 'Group', ldcase, 'Intervention_load');
82 fprintf(grfile, '%9s %13g %6s\n', 'GroupDef', ldcase, 'Elem');
83 fprintf(grfile, '%24g\n', load_beams);
84 fclose(grfile);
85
86 writing = 'done';
87 end

```



# Appendix D

## Bash shell script

"main.sh"

```
1 #!/ bin/bash
2 START_TIME=$SECONDS
3
4
5
6 # ----- PARAMETERS ----- #
7 INPUTFILE=" ./inputgen/fahtsparam.dat"      # The file containing the parameter data
8 THREADS=1                                  # The number of parallel threads (0=auto)
9 LOADFILE=" ./loads/inter_load.dat"
10 GROUPFILE=" ./groups/inter_group.dat"
11 origModel=" ./MainModel.fem"
12 # ----- #
13 #####
14 # Make modelfile based on generated loads and groups
15 modelFile=" assembledmodel.fem"
16 # Copy geometry and material data from "MainModel.fem"
17 cp -a "$origModel" "$modelFile"
18 #
19 # Adding load data from "loads" directory (imp is the imperfection dummy)
20 cat loads/CellarLoads >> "$modelFile"
21 cat loads/MezzanineLoads >> "$modelFile"
22 cat loads/TopsideLoads >> "$modelFile"
23 cat loads/gravity >> "$modelFile"
24 cat loads/imp_load >> "$modelFile"
25 #
26 # Adding the variable placement topside load
27 cat "$LOADFILE" >> "$modelFile"
28 #
29 #
30 # Adding element groups
31 cat groups/material3 >> "$modelFile"
32 cat groups/material4 >> "$modelFile"
33 cat groups/material5 >> "$modelFile"
34 cat groups/truss >> "$modelFile"
35 cat "$GROUPFILE" >> "$modelFile"
```

```

36 #####
37 # Define a function used to initialize modules
38 function initialize {
39     # Run all all scripts
40     for MOD in ./programs/*
41     do
42         if [ -f $MOD -a -x $MOD ]; then
43             $MOD init >> ./logs/init.log
44         fi
45     done
46 }
47
48 # Define function used to find what files that is going through substitution
49 function findfiles {
50     # Run all all scripts
51     for MOD in ./programs/*
52     do
53         if [ -f $MOD -a -x $MOD ]; then
54             $MOD files $1 | grep -v '^$' # The grep command is to remove empty lines
55         fi
56     done
57 }
58
59 # Do the postprocessing
60 function postp {
61     # Go through all scripts
62     for MOD in ./programs/*
63     do
64         if [ -f $MOD -a -x $MOD ]; then
65             $MOD postp2 >> ./logs/postp2.log
66         fi
67     done
68 }
69
70 # Make a folder for the contents of the terminal logs
71 if [ ! -d logs ]; then
72     mkdir logs
73 else
74     rm logs/*.log
75 fi
76
77 # Do the initialization
78 echo -n "Initializing folders..."
79 initialize
80
81 echo "Done."
82 echo -n "Assembling input files..."
83
84 # Reads the first line of the input file to get the column headers
85 read -r FIRSTLINE < $INPUTFILE
86
87 # Finds the number of columns
88 FIELDS='echo $FIRSTLINE | awk '{ print NF }''
89
90 # Make an array with the column/field names

```

```

91 for i in `seq 1 $FIELDS`
92 do
93     FIELD[$i]='echo $FIRSTLINE | awk '{ print $c }' c=$i`
94 done
95
96 # Reads the parameter file line by line
97 LINE=0
98 COMMAND=""
99 while read INPUTLINE
100 do
101     # Do not process the first line
102     LINE=`expr $LINE + 1`
103     if [ $LINE -eq 1 ]; then
104         continue
105     fi
106
107     # Construct the case name/filename
108     CASENAME=""
109     ARRAY=(4 10 11)
110     for i in ${ARRAY[*]}
111     do
112         VALUE=`echo $INPUTLINE | awk '{ print $c }' c=$i`
113         CASENAME="${CASENAME}_${FIELD[$i]:0:4}_$VALUE"
114     done
115     CASENAME=${CASENAME:1}
116
117     # Do the substitution process for all files returned by the modules
118     while read INPOUT
119     do
120         # If empty string , continue loop
121         if [ ${#INPOUT} -lt 3 ]; then
122             continue
123         fi
124
125         # Define file names
126         INPUT=`echo -n $INPOUT | awk '{ print $1; }'`
127         OUTPUT=`echo -n $INPOUT | awk '{ print $2; }'`
128
129         # Create folder for output file if it not exist
130         OUTDIR=`dirname $OUTPUT`
131         if [ ! -d $OUTDIR ]; then
132             mkdir $OUTDIR
133             mkdir $OUTDIR/pushdown
134             cp fact.ctr $OUTDIR/pushdown/factcont.ctr
135         fi
136
137         # Copy original file to destination
138         cp $INPUT $OUTPUT
139         cp substitute2 $OUTDIR
140         #cp substitute $OUTDIR/pushdown
141
142         # pushdir="/runs/${CASENAME}/pushdown"
143         # if [ ! -d "$pushdir" ]; then
144         #     mkdir "$pushdir"
145         # else

```

```

146 # rm "$pushdir"
147 # fi
148
149 # Substitution process for each field
150 for i in `seq 1 $FIELDS`
151 do
152     VALUE=`echo $INPUTLINE | awk '{ print $c }' c=$i`
153
154     # Substitute in header and model file
155     ./substitute ${FIELD[$i]} $VALUE $OUTPUT
156 done
157 done <<< " `findfiles $CASENAME` "
158
159 # Putting the job in the command string
160 COMMAND="$ {COMMAND} $ {CASENAME} \0"
161 done < "$ {INPUTFILE}"
162
163 # Find the number of threads your computer can run
164 if [ $THREADS -lt 1 ]; then
165     THREADS=`cat /proc/cpuinfo | grep processor | wc -l`
166 fi
167
168 # Executing the commands in parallel
169 echo "Done."
170 echo "Running multiple analyses with $THREADS threads in parallel..."
171 echo -e $COMMAND | xargs -0 -n 1 -P $THREADS ./runone analyze
172 #var_path=`pwd`
173 echo $var_path
174
175
176
177 # Running postprocessing
178 echo "Parallel processing done."
179 echo "Running postprocessing tasks..."
180
181 # No parallell run of postprocessing
182 echo -e $COMMAND | xargs -0 -n 1 -P 1 ./runone postp1
183
184 # Final postprocessing
185 echo -n "Running final postprocessing..."
186 postp
187
188 rm "$modelFile"
189 ELAPSED_TIME=$(( $SECONDS - $START_TIME ))
190 echo "$ELAPSED_TIME"
191 echo "USFOS Done" .

```

"20-fahts.sh"

```

1 #!/ bin / bash
2 #
3 #Trouble using alias inside script , so reference the ful path to
4 #execute usfos and fahts
5 upath = ` ./ . / . / . / USFOS / bin / `
6 fahts = ` / cygdrive / c / Users / Eier / Documents / project _thesis / USFOS / bin / . / fahts . exe `

```

```

7
8 # Define the input variables
9 if [ $# -eq 1 ]; then
10     ACTION=$1
11 elif [ $# -eq 2 ]; then
12     ACTION=$1
13     CASENAME=$2
14 else
15     echo "20-usfos: Invalid number of argumens supplied."
16     exit
17 fi
18
19
20 # The initialization
21 if [ $ACTION == "init" ]; then
22     # Make a folder for USFOS analysis files
23     echo "20-analyse: Creating analysis folders."
24     if [ ! -d runs ]; then
25         mkdir runs
26     fi
27
28
29 # Return the files to look for substitutions in
30 elif [ $ACTION == "files" -a $# -eq 2 ]; then
31     echo "fahtshead.fem runs/$CASENAME/fhead.fem"
32     # echo "usfoshead.fem runs/$CASENAME/uhead.fem"
33     echo "assembledmodel.fem runs/$CASENAME/model.fem"
34
35
36 # Do the individual analyzes
37 elif [ $ACTION == "analyze" -a $# -eq 2 ]; then
38     echo "20-usfos: Running analysis in Usfos."
39
40 ### # Go to analysis folder
41     casepath='C:/Users/Eier/Documents/project_thesis/TopsideModel/Analyses/stepped/'
42     #casepath='/runs/$CASENAME/'
43     cd ${upath}
44     #C:/Users/Eier/Documents/project_thesis
45     pathanalysis='./../../TopsideModel/Analyses/stepped/runs/'
46     #
47
48     # Run the FAHTS program
49     ./fahts.exe<<EndIn
50     ${pathanalysis}$CASENAME/fhead
51     ${pathanalysis}$CASENAME/model
52
53     ${pathanalysis}$CASENAME/fresult
54     EndIn
55
56 fi

```

"30-usfos.sh"

```

1 #!/bin/bash
2 #

```



```

3 upath = '../..../USFOS/bin/'
4 pathanalysis = '../..../TopsideModel/Analyses/stepped/runs/'
5 UINPUT="./inputgen/usfosparam.dat"
6
7 # Define the input variables
8 if [ $# -eq 1 ]; then
9     ACTION=$1
10 elif [ $# -eq 2 ]; then
11     ACTION=$1
12     CASENAME=$2
13 else
14     echo "30-usfos: Invalid number of argumens supplied."
15     exit
16 fi
17
18
19 # The initialization
20 if [ $ACTION == "init" ]; then
21     echo "30-usfos: No initialization tasks done."
22     exit
23
24
25 # Return the files to look for substitutions in
26 elif [ $ACTION == "files" -a $# -eq 2 ]; then
27     echo "usfoshead.fem runs/$CASENAME/uhead.fem"
28 # exit
29
30 # Do the individual analyses
31 elif [ $ACTION == "analyze" -a $# -eq 2 ]; then
32     echo "30-usfos: Running analysis in Usfos."
33
34 read -r FIRSTROW < $UINPUT
35 COLUMNS='echo $FIRSTROW | awk '{ print NF }''
36 ROWS='awk 'END {print NR}' "$UINPUT"
37 for i in `seq 1 $COLUMNS`
38 do
39     COLUMN[$i]='echo $FIRSTROW | awk '{ print $c }' c=$i
40 done
41
42
43 cd runs/$CASENAME/
44 LINE=0
45 for j in `seq 1 $ROWS`
46 do
47     read a
48     # Do not process the first line
49     LINE='expr $LINE + 1'
50     if [ $LINE -eq 1 ]; then
51         continue
52     fi
53
54     # Copy the usfos head file into the pushdown folder
55     ORIG="uhead.fem"
56     COPY="pushdown/pushhead_$LINE.fem"
57

```

```

58         cp $ORIG $COPY
59
60         # Substitution process for each field
61         for k in `seq 1 $COLUMNS`
62         do
63             VALUE=`echo $a | awk '{ print $c }' c=$k`
64             # Substitute in header and model file
65             ./substitute2 ${COLUMN[$k]} $VALUE $COPY
66         done
67
68     done < "$../../${UINPUT}"
69
70
71
72     cd -
73
74     MYDIR="runs"
75
76     DIRS=`ls -l $MYDIR | egrep '^d' | awk '{print $9}'`
77
78
79
80     cd ${upath}
81     for DIR in $DIRS
82     do
83         # Run the USFOS analysis
84         for l in `seq 2 $ROWS`
85         do
86             ./usfos.exe<<EndIn
87                 ${pathanalysis}${DIR}/pushdown/pushhead.$l
88                 ${pathanalysis}${DIR}/model
89                 ${pathanalysis}${DIR}/fresult.beltemp
90                 ${pathanalysis}${DIR}/pushdown/${l}_uresult
91             EndIn
92             ./fact.exe<<EndIn
93                 ${pathanalysis}${DIR}/pushdown/${l}_uresult.raf
94                 ${pathanalysis}${DIR}/pushdown/factcont.ctr
95                 ${pathanalysis}${DIR}/pushdown/elemforces-${l}
96             EndIn
97         done
98     done
99     # done
100    # Return to base folder (previous folder)
101    #cd -
102    #done < "${UINPUT}"
103
104    # Do postprocessing after individual run (for example to extract results)
105    elif [ $ACTION == "postp1" -a $# -eq 2 ]; then
106        echo "30-usfos: No postprocessing tasks done."
107        exit
108
109
110    # Do postprocessing after all individual runs (for example to do statistics)
111    elif [ $ACTION == "postp2" ]; then
112        echo "30-usfos: No postprocessing tasks done."

```

```

113     exit
114
115
116 # Else , do nothing
117 else
118     echo "30-usfos: Invalid action argument supplied , or missing case name."
119     exit
120 fi

```

”runone”

```

1 #!/bin/bash
2 #
3 # Script that run all analyze scripts in proper order.
4 #
5 # This script is designed to be run in parallel. It's only argument is
6 # the analysis/folder name, witch is passed directly to the individual
7 # analysis scripts.
8 #
9 # Written by HÅYkon Strandenes , hakostra@stud.ntnu.no, 2011–2012.
10 #
11 # This file is licensed under the GNU General Public License ,
12 # version 3, or later. Please see file LICENSE for details.
13 #
14
15
16 # Do some basic check on input
17 if [ ! $# -eq 2 ]; then
18     exit
19 elif [ ${#2} -lt 4 ]; then
20     exit
21 fi
22
23
24 # Go through all scripts
25 for MOD in ./programs/*
26 do
27     if [ -f $MOD -a -x $MOD ]; then
28         echo "    Running '$MOD $1 $2'";
29         $MOD $1 $2 >> ./logs/$1-$2.log
30     fi
31 done

```

”substitute”

```

1 #!/bin/bash
2
3 sed "1,$ s/$1/$2/g" $3 > subst_string.temp
4 mv subst_string.temp $3

```

# Appendix E

## Simulation control files

Examples of the control files used in FAHTS and USFOS, with the values ready to be substituted in for header names from the parameter files

```
1 HEAD          JetFire
2   flame pointing jetdir degrees
3   anticlockwise from positive x-axis
4   '
5   '
6   '
7   '
8   TimeUnit    Min
9
10  '           end-time (min)  nstep      resinc
11  TEMPSIM     dur             200         tstep          ! Simulation Param
12  '
13  ' timehist  x1      y1      z1      pow1      x2      y2      z2      pow2      D1      D2
14  USERJET    0        xinit  yinit  zinit   hinit   xend  yend  zend   hend   inD   enD
15  '
16  '           id      rho(kg/m3)  c (J/kgK)  k (W/mK)  emiss  convection
17  THERMPAR   1        7850.0    600.0     45.0      0.8    10.0
18  THERMPAR   2        7850.0    600.0     45.0      0.8    10.0
19  THERMPAR   3        7850.0    600.0     45.0      0.8    10.0
20  THERMPAR   4        7850.0    600.0     45.0      0.8    10.0
21  THERMPAR   5        7850.0    600.0     45.0      0.8    10.0
22  THERMPAR   6        7850.0    600.0     45.0      0.8    10.0
23  '
24  'Limit the "HC-firebox" to 0.5 meter outside of the main frame
25  'center lines
26  '           type     x1      y1      z1      x2      y2      z2
27  LIMTFIRE   1      -16.5   -16.5   -0.5   16.5    16.5    16.5
28  '

```

```
1 HEAD          USFOS Pushdown analysis
2   Jet fire jetdir degrees anti clockwise
3   from x-axis. Timestep=lastT, Duration=djur min.
4   '
5   '

```

```

6      ,      Keyword  Value      'Pushdown analysis
7  PUSHDOWN      LoadCase  lastT      'for the last beltemp ldcase
8      ,
9  SteelTDep
10     ,
11     ,
12     ,      Size      Pat      LoadCase  'Initial imperfections
13  cInidef      Euro3_C  MembLoad   2      'EC_3curve c. Diagonal dir
14     ,
15     ,      nloads  npostp  mxpstp  mxpdis
16  CUSFOS      15      30      680     3
17     ,      lcomb    lfact    mxld    nstep    minstp
18     ,      1      1      1      1      1E-1
19     ,      push    0.5     1      100     1E-2
20     ,      push    0.05   6      600     1E-2
21     ,
22     ,      ListType  CritType  Criterion  IDList
23  USERFRAC    Mat      Strain    0.15     1 3 4 5 6
24     ,
25     ,
26  cnodes 1
27     ,      782 3 1
28     ,
29  cSave 0 1

```